UCTEA Turkish Chamber of Civil Engineers

Teknik Dergi

Technical Journal

Volume 29 Issue 2 March 2018

Teknik Dergi is indexed by

- Science Citation Index Expanded
- Scopus
- Journal Citation Reports / Science Edition
- Engineering Index
- Concrete Abstracts (American Concrete Institute)
- National Technical Information Service (US NTIS)
- CITIS
- Ulrich's International Periodical's Directory
- TÜBİTAK / ULAKBİM

TEKNİK DERGİ PUBLICATION PRINCIPLES

Teknik Dergi is a scientific and technical journal indexed by the Science Citation Index Expanded. Annually six issues are published, three in Turkish in the months of January, May and September, three in English in March, July and November. Its main principles of publication are summarized below:

1. Articles reporting original scientific research and those reflecting interesting engineering applications are accepted for publication. To be classified as original, the work should either produce new scientific knowledge or add a genuinely new dimension to the existing knowledge or develop a totally new method or substantially improve an existing method.
2. Articles reporting preliminary results of scientific studies and those which do not qualify as full articles but provide useful information for the reader can be considered for publication as technical notes.
3. Discussions received from the readers of the published articles within three months from publication are reviewed by the Editorial Board and then published together with the closing remarks of the author.
4. Manuscripts submitted for publication are evaluated by two or three reviewers unknown to the authors. In the light of their reports, final decision to accept or decline is taken by the Editorial Board. General policy of the Board is to get the insufficient manuscripts improved in line with the reviewers' proposals. Articles that fail to reach the desired level are declined. Reasons behind decisions are not declared.
5. A signed statement is taken from the authors, declaring that the article has not been published as a "journal article or book chapter". In case the Editorial Board is in the opinion that the article has already been published elsewhere with minor changes or suspects plagiarism or a similar violation of ethics, then not only that article, but none of the articles of the same authors are published.
6. Papers reporting works presented as conference papers and developed further may be considered for publication. The conference it was presented to is given as a footnote in the first page.
7. Additionally, a document signed by all authors, transferring the copyright to UCTEA Chamber of Civil Engineers is submitted together with the manuscript.

Printed by: Lotus Life Ajans Rek.Tan.Bas.Yay.Org.Amb.İth.İhr.San.ve Tic.Ltd.Şti.
Sokullu Cd. Perçem Sk. No: 9/A Çankaya / Ankara - Tel: 0.312.433 23 10

Date of Print: 01 March 2018 / Number of copies: 2.000

Distributed to İMO members free of charge. / Local periodical.

UCTEA Turkish Chamber of Civil Engineers

Teknik Dergi

Technical Journal

Volume 29 Issue 2 March 2018

UCTEA Turkish Chamber of Civil Engineers

Teknik Dergi *Technical Journal*

Publisher:
Cemal GÖKÇE
On behalf of UCTEA Turkish Chamber of Civil Engineers

Administrative Officer:
Hüseyin KAYA

Correspondence:
Teknik Dergi
Chamber of Civil Engineers
Necatibey Cad. No:57
Kızılay 06440 Ankara, Turkey
Tel : +90 (312) 294 30 00
Faks: +90 (312) 294 30 88
Web: www.imo.org.tr
E-mail:teknikdergi@imo.org.tr

Publication Frequency:
Bimonthly

Editor in Chief:
Tuğrul TANKUT

Co-Editors:
Ender ARKUN
İsmail AYDIN
Özer ÇİNİCİOĞLU
Metin GER
Gürkan Emre GÜRCANLI
Alper İLKİ
Kutay ORAKÇAL
İsmail ŞAHİN

English Proof Reader:
Ender ARKUN

Secretary:
Cemal ÇİMEN

ISSN : 1300-3453

Reviewers:
This list is renewed each year and includes reviewers who served in the last two years of publication.

Emine AĞAR
Sami Oğuzhan AKBAŞ
Özge AKBOĞA KALE
M. Vefa AKPINAR
Zuhal AKYÜREK
Hilmi Doğan ALTINBİLEK
Davit ARDITI
Deniz ARTAN İLTER
Cem AYDEMİR
Yusuf AYVAZ
Selim BARADAN
Bekir Oğuz BARTIN
Bilge BAŞ
Zerrin BAYRAKDAR
İdris BEDİRHANOĞLU
Serkan BEKİROĞLU
Niyazi Özgür BEZGİN
İlknur BOZBEY
Zafer BOZKUŞ
Zekai CELEP
Halim CEYLAN
Barlas Özden ÇAĞLAYAN
Özgür ÇAKIR
Necati ÇATBAŞ
Erkan ÇELEBİ
Kutay ÇELEBİOĞLU
Oğuz Cem ÇELİK
Hilmi Berk ÇELİKOĞLU
Ender DEMİREL
Fatih DİKBAŞ
Seyyit Ümit DİKMEN
Ahmet Anıl DİNDAR
Emrah DOĞAN
Nilay ELGİNÖZ KANAT
Murat Altuğ ERBERİK
E. Mete ERDEMGİL
Ercan ERDİŞ
Esin ERGEN PEHLEVAN
Ayşen ERGİN
Gökmen ERGÜN
Güngör EVREN
Ergun GEDİZLİOĞLU
Haluk GERÇEK
Mustafa GÖĞÜŞ
Ilgın GÖKAŞAR
M. Halis GÜNEL
Mehmet Şükrü GÜNEY
Aslı Pelin GÜRGÜN
Soner HALDENBİLEN
Zeki HASGÜR
Zeynep IŞIK
Recep İYİSAN
Murat KARACASU
Engin KARAESMEN
Erhan KARAESMEN
Halil KARAHAN
Mustafa KARAŞAHİN
C. Melek KAZEZYILMAZ ALHAN
Engin KEYDER
Veysel Şadan Özgür KIRCA
Niyazi Uğur KOÇKAL
Özgür KURÇ
Hilmi LUŞ
Yetiş Şazi MURAT
Sepanta NAIMI
Dilek OKUYUCU
Mehmet Hakkı OMURTAG
Engin ORAKDÖĞEN
Akın ÖNALP
Aybike ÖNGEL
Bihrat ÖNÖZ
Halit ÖZEN
Hakkı Oral ÖZHAN
Hulusi ÖZKUL
Beliz ÖZORHON ORAKÇAL
Turan ÖZTURAN
Gül POLAT TATAR
Altuğ SAYGILI
Hasan SAYGIN
Serdar SELAMET
Osman SİVRİKAYA
Serdar SOYÖZ
İbrahim SÖNMEZ
Ayşe Filiz SUNAR
Özkan ŞENGÜL
Aykut ŞENOL
Ali Ünal ŞORMAN
Ergin TARI
Erhan TEKİN
H. Onur TEZCAN
Onur Behzat TOKDEMİR
Nabi Kartal TOKER
Mustafa TOKYAY
Tamer TOPAL
Cem TOPKAYA
Ahmet TORTUM
Ahmet TÜRER
Handan TÜRKOĞLU
Mehmet UTKU
Alper ÜNLÜ
Tanvir WASTI
Mert Yücel YARDIMCI
Ufuk YAZGAN
Emine Beyhan YEĞEN
Osman YILDIZ
Koray Kamil YILMAZ
M. Tuğrul YILMAZ
M. Semih YÜCEMEN
Yeliz YÜKSELEN AKSOY
Nabi YÜZER

Teknik Dergi is a peer reviewed periodical publishing papers of original research and interesting practice. It addresses both the research community and the practicing engineers.

UCTEA Turkish Chamber of Civil Engineers

Teknik Dergi

Technical Journal

Volume: 29 Issue: 2 March 2018

CONTENTS

Comparison of Blast Analysis Methods for Modular Steel Structures 8253
Bülent ERKMEN

An Efficient Contact Tank Design for Potable Water Treatment 8279
Ender DEMİREL, Mustafa M. ARAL

Classification of Construction Accidents in Northern Cyprus 8295
Kemal D. TÖZER, Tahir ÇELİK, G. Emre GÜRCANLI

Modeling Laminated Orthotropic Plate-Foundation Interaction Subjected to Moving Load Using Vlasov Model 8317
Korhan ÖZGAN

Foreword, March 2018

THE FIRST ISSUE IN ENGLISH

The journal in your hand is the first issue of Teknik Dergi in English. As explained in detail in the foreword of the July 2017 issue, Teknik Dergi has adopted a bi-lingual publication policy starting from the beginning of 2018. As announced earlier, Teknik Dergi has decided to publish January, May and September issues fully in Turkish and March, July and November issues fully in English from this year on.

Initially the Editorial Board has been concerned about the difficulty of creating a sufficient and sustainable inflow of manuscripts in English. Teknik Dergi has been accepting English manuscripts in the last six months. Observations in this period are somewhat encouraging. Statistics indicate approximately equal number of Turkish and English manuscripts received. Presently, reviewers do not appear to be very satisfied with the content and quality of the manuscripts in English, consequently the decline rate is a little higher for the English manuscripts. However, this higher rate of decline is not considered alarming and not expected to cause a serious problem. It seems that a sufficient number of papers of acceptable scientific quality can be produced. The Editorial Board therefore maintains its optimism and hopes that such difficulties will gradually fade away.

Another concern of the Editorial Board is related to the quality of manuscript language. Some of the manuscripts are not written in correct, clear and understandable English, although their scientific content is satisfactory. Such manuscripts require a thorough revision and editing. To this end, one of the Teknik Dergi co-editors has been appointed as the "English Proof Reader" to review the manuscripts accepted for publication.

We wish the bi-lingual Teknik Dergi starting today to last long and be successful.

With kind regards,

Tuğrul Tankut, Editor-in-Chief
On behalf of the Editorial Board

İMO Teknik Dergi, 2018 8253-8277, Paper 498

Comparison of Blast Analysis Methods for Modular Steel Structures

Bülent ERKMEN[1]

ABSTRACT

Two blast analysis methods widely used are three-dimensional finite element (FE) and uncoupled equivalent single degree of freedom (ESDOF) methods. The uncoupled equivalent ESDOF method, which is the most common blast analysis method, provides considerable advantages and simplicity in analysis and design stages. However, the inherent assumptions and simplifications involved but especially neglecting member's dynamic interactions can significantly affect accuracy of analysis results. In this study, blast performance of a prototype two-module steel blast-resistant building is evaluated using uncoupled ESDOF and FE methods. The results are compared to evaluate adequacy of uncoupled ESDOF method for blast analysis of the structure.

Keywords: Blast loads, blast-resistant steel modular buildings, equivalent single degree of freedom, dynamic interaction.

1. INTRODUCTION

Due to growing terror threat and accidental explosions, blast performance of structures is becoming an important structural design consideration for not only military structures but also for structures at petrochemical industry and industrial plants to ensure safety and protection of the workforce. Blast loads, which are typically ignored in the design of structures, have effects including but not limited to structural damage, personal casualties, and social and economic impacts. Especially, the terror attacks on the Oklahoma City Federal and World Trade Center buildings, which resulted in total building collapse and massive loss of lives, have attracted the attention of many researchers to improve blast resistance of structures [1,2,3]. Although blast events are increasingly encountered in Turkey [4] (as well as the rest of the world), there is no regulation or guideline that concerns design principles and guides for engineers on the blast design and analysis.

The primary design objective for structures subjected to blast loading is to ensure structural integrity and thereby preventing or limiting loss of lives [2,5,6]. Unless the structure is very critical, it is not economical and practical to ensure that the deformations and structural

Note:
- This paper has been received on July 23, 2016 and accepted for publication by the Editorial Board on January 30, 2018.
- Discussions on this paper will be accepted by May 31, 2018.

• DOI: 10.18400/tekderg.389954

1 Ozyegin University, Department of Civil Engineering, İstanbul, Turkey - bulent.erkmen@ozyegin.edu.tr

damage remain within elastic limits for an unlikely blast event. Therefore, deformations occurring in structural components under blast loads are allowed to be beyond linear elastic limits (i.e., plastic deformation) to minimize the cost. Therefore, blast damage is typically measured in terms of deformations instead of internal loads (e.g., shear, moment) as would be done in seismic design. Different blast damage levels and corresponding deformation limits are given by FEMA [2], ASCE [5], and US Army Corps of Engineer [7].

For blast analysis, there are two widely used nonlinear dynamic analysis methods. These are three-dimensional (3D) finite element (FE) and uncoupled equivalent single degree of freedom (ESDOF) analysis methods. In addition, there are also tools consisting of simple graphical solutions, empirical formulas, and closed-form solutions [3]. However, these simple methods are generally based on the ESDOF analysis method, applicable for special conditions, and provide limited information for blast performance of structural members [2,5]. The 3D finite element method is the most suitable and reliable analysis method for determining blast performance of structural members. With FE analysis method, the overall structural behavior under blast loads can be determined since the whole structural system is modeled. In addition, the dynamic interaction of structural members, the effects of geometric nonlinearity (e.g., membrane action and second order effects), and nonlinear material behavior can be included. With this method, the progressive formation of plastic hinges, their location, and plastic hinge propagation along structural members can be captured, and their effects on deflection, ductility, and support plastic rotation can be included. Mass and mass distribution over the structure are other important parameters that affect blast analysis results. Because all structural members are included in the FE model, achieving realistic mass distribution within the structure is possible. Blast loads are surface pressures acting on outer surfaces of structures, and hence with realistic FE models it is possible to achieve more realistic blast load distribution over the structure. In conclusion, FE blast analysis method is a reliable and powerful approach, and it has been shown that blast performance of structural members (damage level, ductility, and support plastic rotations) determined using FE approach is reliable and consistent with experimental results [5,8,9]. However, the need for high-performance computers to solve millions of equilibrium equations, high costs of FE software, and the need for well-trained and experienced engineers to build models, select and perform the appropriate analysis method, and interpret the results are significant disadvantages of the FE method for blast analysis.

Because of the disadvantages of the FE method, the uncoupled equivalent single degree of freedom blast analysis method is usually preferred at the preliminary design stage and for structures with simple lateral and vertical load resisting systems, or structures that are not considered to be critical in terms of blast performance. The ESDOF analysis method is also known as simplified spring analysis method, and it is commonly used because of its simplicity and relatively modest computational resources required. Because the ESDOF method is easy and simple compared to the FE method, it is widely used to determine structural damage due to blast loading [1,5,10]. For example, the ESDOF method is used by the United States Army Corps of Engineers in blast design and evaluation of critical military structures. In addition, the blast software SBEDS developed by this army unit is based on the ESDOF method, and it is widely used by representatives of U.S. Government Agencies and their contractors as a reliable blast analysis tool [7].

The ESDOF blast analysis method is a dynamic analysis method that gives approximate results [5,8,11]. The ESDOF method provides considerable advantages and simplicity in blast analysis and design of structures. However, the assumptions and simplifications involved can significantly affect the accuracy of analysis results. In the ESDOF analysis, the dynamic interaction of structural members is ignored (i.e., uncoupled). In other words, the deformation compatibility of structural members and internal force balance at their connections are neglected and violated. Biggs [12] showed that the dynamic interaction of structural members can be neglected when the ratio of natural vibration frequencies of interconnected elements is at least two. However, the study was performed on a rather limited number of structural element, boundary condition, and blast loading. Baker et al. [13] showed that the ESDOF analysis is an approximate but on the safe side analytical method based on the work performed on two-degree of freedom systems with a limited number of parameters.

Although the ESDOF method is widely used throughout the engineering community, and it is considered to yield conservative results compared to the FE blast analysis method, there is no comparative detailed study on the accuracy and reliability of the ESDOF blast analysis method. In this study, damage levels of vertical and lateral load-resisting systems of a two-module blast-resistant steel-framed structure were determined using three-dimensional FE and ESDOF blast analysis methods. The analysis results are compared to evaluate the adequacy of the uncoupled ESDOF blast analysis method.

2. PROTOTYPE MODULAR STEEL STRUCTURE

Figure-1 shows a typical three-module blast-resistant modular steel-framed (BMS) structure during and after installation. The BMS structures are recognized as an economical and practical solution to minimize blast effects and are valuable assets for protection of personnel involved in activities located near potential explosion sites [5,6]. These structures are widely used as control rooms, office buildings, and living quarters in areas with a high risk of explosion, fire, or danger from toxic materials in petrochemical industry, and temporary living shelters in military areas.

Figure 1. Blast-resistant modular steel-framed (BMS) building with three modules

The prototype BMS structure studied consists of two modules, each with a length of 12 m, width of 3 m, and 3.5 m height. The building floor and elevation plans are given in Figure-2 through 4. The joints and connections are designed to develop full plastic capacities of the connected members. In addition, the connection between the modules is assumed to be strong enough to ensure full load transfer between the modules under blast loads. The vertical openings between the steel frame members (i.e., column and beam) are closed with crimped wall panels as shown in Figure-3 and Figure-4. Flat steel plates supported by the roof and floor joists are used to cover the roof and floor openings. In addition, diaphragm struts are used at two bays both on the roof and floor to strengthen their diaphragms as shown in Figure-2.

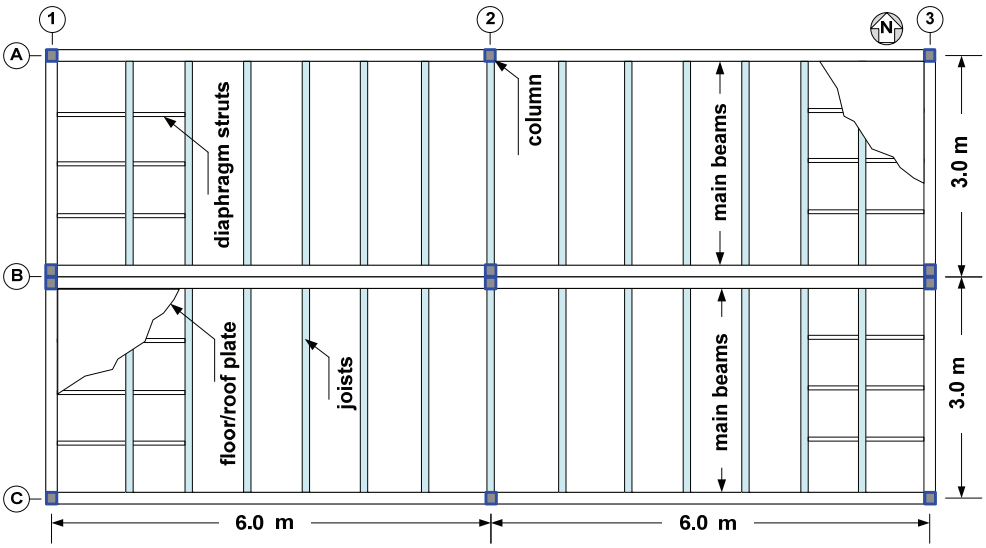

Figure 2. Prototype building floor and roof plans

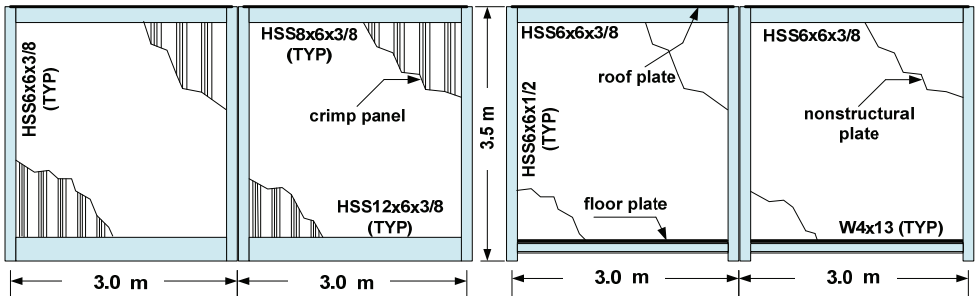

Figure 3. Prototype building elevation views at (a) column axes 1 and 3 (b) column axis 2

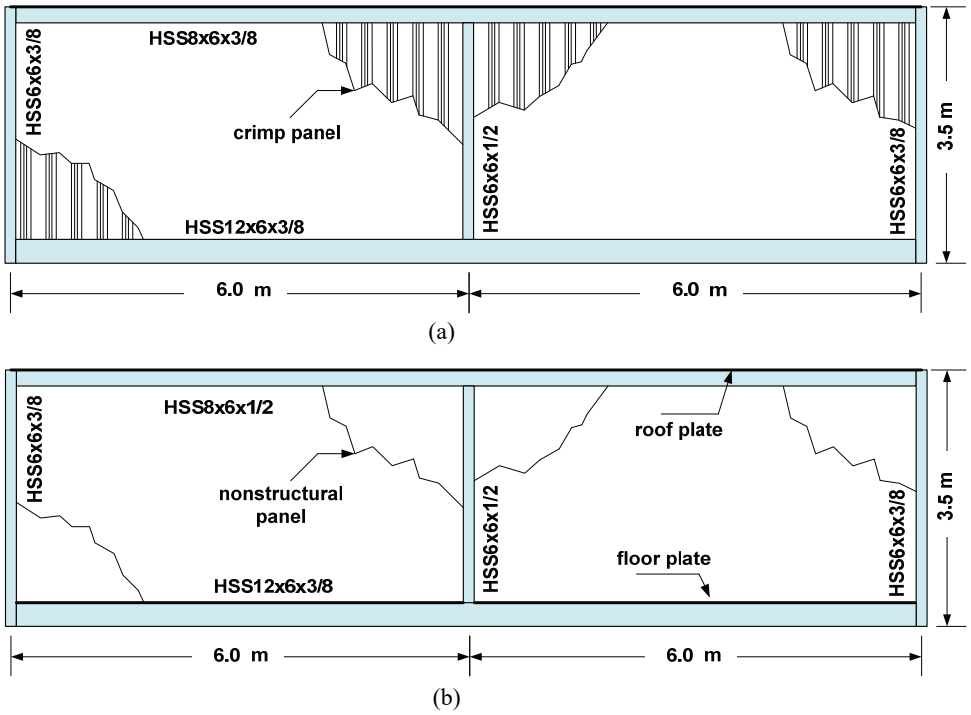

Figure 4. Prototype building elevation views at (a) column axes A and C (b) column axis B

All structural sections used for the prototype building are AISC-360 (American Institute of Steel Construction) [14] hollow structural sections (HSS). The only exception is the W4x13 I-beam section, which is used for floor and roof joists. The structural elements were selected to be seismically compact per AISC-341 [15] about both their weak and strong bending axes to ensure that local buckling and instability failures do not occur before the full plastic bending capacity of the sections is achieved. The connections between the structural sections are assumed to be continuous weld type and strong enough to develop the full capacities of the connected members. The wall, floor, and roof plates are assumed to be attached to the frame members by continuous welds as well.

The prototype building wall panels are crimped (trapezoidal cross-section) steel plate while the floor and roof are covered with flat steel plates. The wall panels are generally the most critical structural elements for blast loading because the blast load is the largest on the surfaces directly facing the blast. Despite the ease of connecting flat steel wall panels to the frame elements, these panels are not generally preferred due to their limited ductility capacity. Crimped steel wall panels, which have much higher ductility, are therefore preferred for the walls. The sections of steel frame elements used for the prototype building and the associated AISC steel grades are given in Table-1.

Table 1. Prototype building steel frame members, steel grades, and sections

Frame Member	**Steel Grade**	**Section**
Corner columns (total of 8)	A500 Gr. B	HSS6x6x3/8
Other columns (total of 4)	A500 Gr. B	HSS6x6x1/2
Top perimeter longitudinal main beams (total of 2)	A500 Gr. B	HSS8x6x3/8
Top intermediate longitudinal main beams (total of 2)	A500 Gr. B	HSS8x6x1/2
Top perimeter transverse main beams (total of 4)	A500 Gr. B	HSS8x6x3/8
Top intermediate transverse main beams (total of 2)	A500 Gr. B	HSS6x6x3/8
Bottom longitudinal main beams (total of 4)	A500 Gr. B	HSS12x6x3/8
Bottom transverse main beams (total of 4)	A500 Gr. B	HSS12x6x3/8
Roof and floor joists	A992 Gr. 50	W4x13
Roof and floor diaphragm struts at module ends	A500 Gr. B	HSS3x2x3/16
Roof and floor steel plate	A36	5 mm thick
Crimped steel wall plate	A36	5 mm thick and 100 mm deep

2.1. Blast Damage Levels and Deformation Limits

Blast performance of structures is generally expressed in terms of damage experienced by its structural members. Under blast loading, the structural members are allowed to deform beyond their elastic limit and yield point to achieve an economic design. In other words, the structural members are expected to exhibit plastic behavior with significant post-yielding deformations but without failure. Therefore, the maximum stress levels experienced by the structural members are not good indication of blast damage. In blast design and evaluation of structural members, their adequacy is judged based on the maximum deformation and support rotation (i.e., hinge rotation) [1,5]. Generally, the maximum deformation of structural members is expressed in terms of ductility ratio (μ). Ductility, which is defined as the ratio of maximum displacement experienced by the member to the displacement corresponding to its elastic limit, is a good indication of plastic deformations and structural damage. Support rotation (θ) is another measure of structural damage, and it is a good indication of instability present in critical areas of frame members [5]. However, the support rotation is not directly the joint rotation at the support, but rather it is defined as the angle formed between a line connecting the supports and a line between the support and the point of maximum deflection [5].

The structural damage caused by blast loading is usually characterized as low, medium, or high damage. At the low damage level, the building is expected to remain functional with some local damage, but moderate repairs are expected to restore the integrity of the structure envelope. At medium damage level, widespread building and component damage is expected with significant cost of repair before the building can be reoccupied. At high damage level, significant damage is permitted up to the point of failure, but the structure is expected to remain intact. The allowable response (i.e., ductility and support rotation) of individual frame components for these three damage levels are given in Table-2 for the prototype building. The limits on maximum ductility and support rotation are based on the type of frame element,

construction material, location of frame element within the structure, and the selected damage level.

Table 2. Damage levels and corresponding maximum ductility and support rotations [5]

Structural Element Type	Blast Response Range					
	Low Damage		Medium Damage		High Damage	
	μ	θ	μ	θ	μ	θ
Crimped wall panel	2.5	1.5	5.0	3.0	10.0	6.0
Floor and roof steel flat plates	5.0	3.0	10.0	6.0	20.0	12.0
Primary steel frame members	1.5	1.0	2.0	1.5	3.0	2.0
Other beams (joists)	3.0	2.0	10.0	6.0	20.0	12.0

2.2. Material Behavior at High Strain Rates

To determine damage levels for structures and structural elements under rapidly applied loads such as blast loading, the mechanical behavior of construction materials at high strain rates should be employed. The static properties of steel grades available from standards and codes are the minimum mechanical properties. However, in practice, the average yield strength of steel used for structural elements is approximately 25% greater than the specified minimum values [5,16]. A strength increase factor (SIF) is used to account for this extra static strength to reduce conservatism and make use of section full available capacity for blast loading. The SIF values used for the structural elements of the prototype building are given in Table-3 for different stress types and steel grades.

Table 3. Strength and dynamic increases factors and dynamic yield strength [5]

Steel Grade	Static Yield Stress, F_y (MPa)	Min. Tensile Strength, F_u (MPa)	SIF	Stress Type	DIF	Dynamic Yield Stress, F_{dy} (MPa) (1)
ASTM A-36 Gr. 36	248	400	1.1	Bending and Shear	1.29	352
				Axial	1.19	325
ASTM A500 Gr. B	317	400	1.21	Bending and Shear	1.10	422
				Axial	1.10	422
ASTM A992 Gr. 50	345	448	1.1	Bending and Shear	1.19	452
				Axial	1.12	425

(1) $F_{yd} = F_y$ (*SIF* x *DIF*)

Under dynamic loads such as blast loading, concrete and steel materials cannot respond at the same rate at which the load is applied to the structure. The yield strength of these materials increases under rapidly applied blast loads due to high strain rate. This increase in the yield

strength can be significant for lower strength materials and decreases as the material static yield strength increases [2,5,10,12,13]. To incorporate the effect of strain rate on material mechanical behavior, a dynamic increase factor (DIF), which is simply the ratio of dynamic material strength to its static strength, is typically applied to the static strength values. The appropriate DIF values are functions of material type, strain rate, and type of stress [5,16]. The DIF values recommended for the prototype building and the corresponding dynamic yield strength values used in the blast analyses are given in Table-3 for different loading conditions. In the performed dynamic analyses, elastic-perfectly plastic material models were used with yield strength equal to the dynamic yield strength.

3. BLAST LOADS FOR THE PROTOTYPE BUILDING

Blast loads that are mentioned here are explosion loads occurring in the petrochemical industry due to vapor cloud and dust explosions, and do not include blast and fragment dissipations caused by bombs, mortars and rockets. At the time of explosion, a sudden release of energy in the form of atmospheric shock or pressure wave occurs [3]. The explosive material is converted to very hot, dense, and high-pressure gas expanding at very high speeds. Depending on the type of explosive material, two characteristic shapes of blast waves known as shock waves and pressure waves are distinguishable. The shock and pressure waves are generated when the explosive material is a condensed material (liquid or solid) or vapor cloud, respectively. The shock waves cause an almost instantaneous rise from atmospheric pressure to a peak pressure known as free-field, peak side-on or incident, overpressure (P_{so}). As the wave front expands, the pressure starts to decrease rapidly with distance and time to ambient pressure, and a negative pressure phase occurs as shown in Figure-5 [1]. The wave has a very brief span of existence, measured typically in thousandths of a second. When the explosive material is vapor cloud, the blast creates pressure waves. The pressure waves increase ambient pressure relatively slowly, reach the ambient pressure more slowly, and do not create a negative pressure wave as shown in Figure-5.

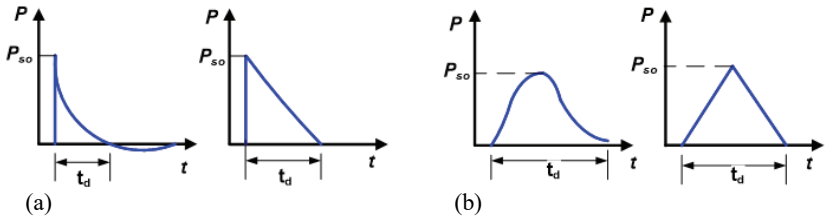

Figure 5. Characteristic and idealized shapes of (a) shock waves (b) pressure waves

Blast load pressure-time data resulting from common explosions in the petrochemical industry are difficult to precisely determine due to uncertainties regarding type and quantity of the explosive material and location of explosion. In addition, the interaction of blast wave with topography and structure geometry is quite complex [5,17]. Although the interaction between the blast wave and structures can be incorporated using computational fluid

dynamics (CFD), such analyses are quite complex and not economical. Therefore, usually simpler closed-form solutions are preferred to determine blast loads acting on different sides of structures if the structure geometry is not complex, and the structure is not very critical [5].

Typical blast peak side-on overpressure due to explosions occurring in petrochemical industry is between 10-100 kPa with a positive phase duration (t_d) between 20-200 ms [5]. In this study, two different explosion scenarios corresponding to moderate and high damage levels of the prototype building were selected. These are blast loading with a free-field overpressure of 50 kPa (BL-50) and 80 kPa (BL-80) corresponding to medium and high damage levels of the building, respectively. It was assumed that the positive duration of both blast scenarios is 140 ms, and the explosion source is on the north side of the building with the pressure wave approaching the building from its broadside.

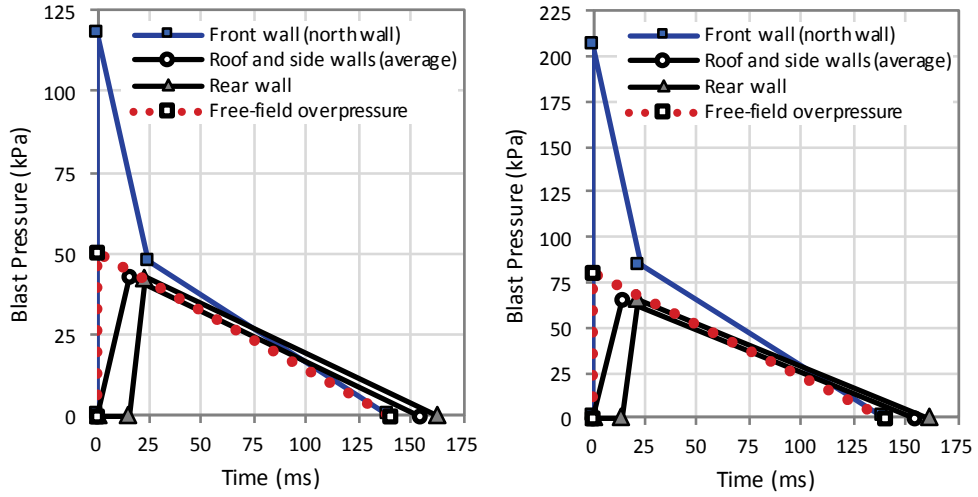

Figure 6. Free-field and local pressures on walls for (a) blast BL-50 and (b) blast BL-80

When the incident pressure wave impinges on a structure, it is reflected and reinforced, producing what is known as reflected pressure (P_r). The reflect pressure is always greater than the incident pressure and varies with the angle of incidence of the blast wave. In other words, the reflected blast pressure is different for each surface of the building such as front wall, side walls, rear wall, and roof. For example, the reflected pressure on a surface that is perpendicular to the direction of the blast wave will experience the maximum reflected pressure, which is approximately twice the free-field overpressure. In this study, a simplified method proposed by ASCE [5] was used to determine pressure-time blast curves acting on different surfaces of the prototype building for each blast scenario. In other words, free-field overpressure was converted into local pressure loads for the prototype building front, side walls, rear wall, and roof by approximating the complex interaction between the blast

pressure wave and building geometry. For the two blast scenarios, time-pressure curves acting on the walls and roof of the building are given in Figure-6. As the explosion wave propagates along the roof and side walls, the pressure on these surfaces decreases. However, the change in pressure along the side walls and roof was not taken into consideration since the prototype structure width is small compared to the speed of the blast wave.

4. BLAST ANALYSIS METHODS

Blast performance of the prototype building under the blast scenarios was determined using finite element (FE) and uncoupled equivalent single degree of freedom (ESDOF) analysis methods. With the FE method, the overall blast performance of the structure was determined including dynamic interaction of structural members. Because the FE method is a standard structural dynamic analysis method, it is briefly summarized in the following section for the prototype building. The fundamentals of ESDOF blast analysis method and how to apply the method to determine blast performance of individual structural members is given in the following sections with several examples.

4.1. Finite Element Blast Analysis Method

ABAQUS 6.14 general-purpose program was used for the FE blast analysis of the building. The developed three-dimensional (3D) building FE model, which is shown in Figure-7, consisted of approximately 40,000 nodes and 38,500 elements. All beams and columns were modeled using the B31 beam element, which is suitable for thick (stout) as well as slender beams. The element is a Timoshenko (shear flexible) beam allowing transverse shear deformation. The S4R shell element, which is a 4-node, quadrilateral element with reduced integration and large-strain formulation, was used for roof and floor plates and wall crimped panels. A nominal mesh size of 300 mm was used for all elements. The building was assumed to be anchored to its foundation at nine anchorage points located under the columns as shown in Figure-7. The anchorage points were represented by pinned boundary condition. Elastic-perfectly plastic material model was used in the analysis, and both material SIF and DIF factors were considered for the dynamic yield stresses. Both material and geometric nonlinearities (membrane action) were considered. The bending stiffness of the plates (roof, floor, and walls) is very small since plates thickness is very small. Therefore, the loads are mainly resisted by in-plane membrane action of the plates [18]. This mechanism was included in the model by including effects of geometric nonlinearity for the shell elements. The only loads considered for the analysis are the building self-weight and the blast loads. The building blast performance was computed in two analysis steps, namely static and subsequent implicit dynamic analysis steps, in which building self-weight and blast loads were applied, individually.

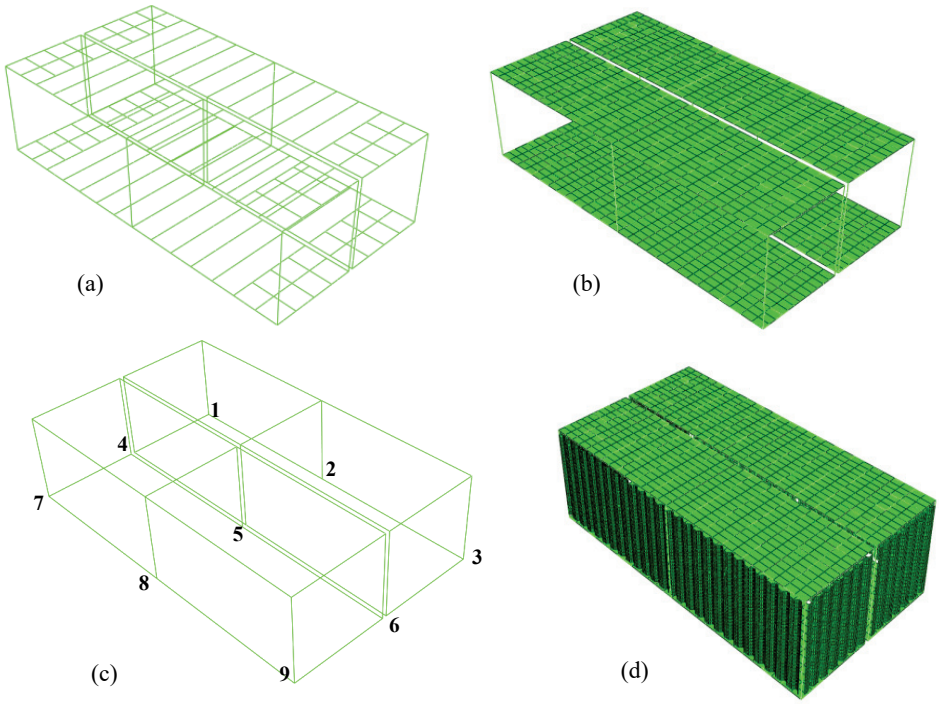

Figure 7. Prototype building FE model (a) beams and columns, (b) floor and roof plates, (c) anchors and (d) whole model

4.2. Uncoupled Equivalent Single Degree of Freedom Blast Analysis Method

The uncoupled equivalent single degree of freedom system is also known as simplified spring model since the point mass can only move along one axis. Because of its simplicity, being user friendly and requiring few input parameters, the ESDOF method is widely used to determine dynamic behavior of structural members subjected to blast loads. The ESDOF method is usually favorable because of its simplicity however this simplicity also leads to inaccurate analysis results. Therefore, the ESDOF analysis method is considered as a blast analysis method that gives approximate but also conservative results [5,8,12].

Because the dynamic behavior of structural elements is computed independently (i.e. uncoupled) in the ESDOF analysis, the dynamic interaction of interconnected elements (e.g., columns, beams, and plates) is neglected. In other words, the deformation compatibility and internal dynamic load equilibrium at member joints are neglected in the ESDOF analysis. Studies on effects of dynamic interaction of interconnected structural elements on ESDOF results are very limited. Biggs [12] showed that dynamic interaction of interconnected structural members could be neglected for two degrees of freedom systems where the ratio of natural vibration frequencies of the connected elements is at least two. However, the systems studied were rather simple with an elastic beam supported by elastic girders at each support. Blast loads were considered only for the beam while no direct blast load was

considered for the girders. Baker et al. [13] performed dynamic analysis on two-degree of freedom systems with limited range of variables and showed that the ESDOF approach is conservative. Lawver et al. [11] using experimental results on individual steel columns showed that the ESDOF method is unable to predict blast performance of steel columns for close or large blast charges. However, in the developed ESDOF models, the effects of local bending of column web and flanges were neglected, and this is the main reason for the reported observations. Krauthammer [8] attributes the greatest weakness of the ESDOF to lack of information on the treatment of fully nonlinear systems by the ESDOF simulations.

In any elastic-perfectly plastic ESDOF model, there are four parameters controlling the dynamic behavior and results of the analysis. These are blast load, system damping force, capacity of plastic hinges (yielding level or resistance), and natural vibration period, which depends on spring stiffness and concentrated point mass. The blast load applied to the ESDOF system of a structural member is determined as the product of blast pressure and its tributary surface area. The tributary blast surface area is defined as the area computed by dividing the total static load carried by the member to the uniform static pressure applied to the building side (wall or roof) where that member is located. Typically, good engineering judgment is required in lieu of rigorous mathematical procedures to determine tributary area and blast load for each individual structural member.

Another important parameter for the ESDOF blast analysis is the spring load-deflection relationship, which is also known as the resistance-curve. Because the ESDOF system has only one displacement degree of freedom, this displacement is selected to correspond to the displacement of the structural member at the point of maximum response such as a plastic hinge location. To determine load-deflection relationship for the ESDOF system, the location of maximum deflection, plastic hinge locations, its formation sequence, and capacities should be determined for the structural member. For example, the ESDOF systems corresponding to the beam shown in Figure-8 with fixed support condition will have the maximum deflection at the mid-span when subjected to uniform blast loading. The corresponding resistance-curve will have three different stiffness values. The location of plastic hinges, stiffness values, and the corresponding loads (resistance) can be determined by applying a distributed static load with the same distribution as the blast load and increasing it until failure. Readily available tables defining resistance-curves for beams with different boundary conditions, column, and plates are available in the literature [12].

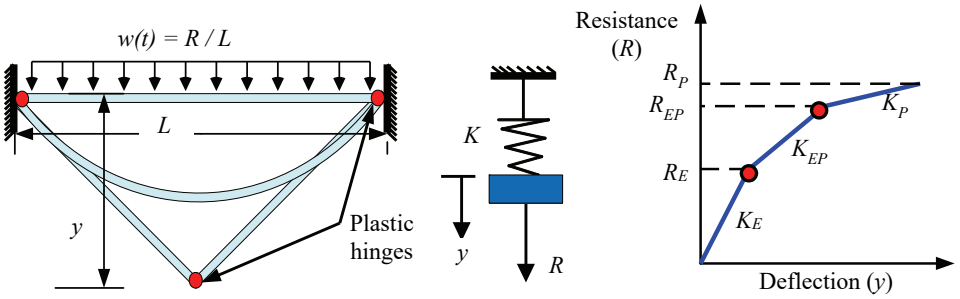

Figure 8. Plastic hinges for a beam with fixed supports and force-displacement relationship for the corresponding ESDOF system

Another parameter affecting the dynamic behavior of ESDOF system is the point mass attached to the spring. This mass includes the self-weight of the structural member, weight of permanently attached equipment if any, and an estimate of the mass located over the tributary blast area and riding along with the member. However, the concentrated mass of ESDOF system is actually distributed over the tributary blast area of the structural member, and the velocity, acceleration, and displacement histories are different for any point on the tributary area. Additional error is introduced into the ESDOF analysis results by assuming that the blast load is a concentrated load applied at the point of maximum deflection. Therefore, ESDOF systems set up as described does not have the same work, strain and kinetic energies at any given time as the actual structural member, and it cannot be used to accurately predict the blast performance (i.e., displacement) of the structural member. In order to match the displacement histories computed using the ESDOF and actual structural member, effective mass, force, and resistance terms are used for the ESDOF system [12]. The dynamic motion of an ESDOF system is given by

$$M\ddot{y}(t) + c\dot{y}(t) + Ky(t) = F(t) \tag{1}$$

where M is the total mass associated with the structural element, c is the viscous damping constant, K is the stiffness of structural element at the point of maximum deflection, and $\ddot{y}(t)$, $\dot{y}(t)$ and $y(t)$ are acceleration, velocity and displacement of the ESDOF system, respectively. The total blast load on the tributary blast area is applied to the ESDOF system, and it is $F(t)$. The damping is usually neglected for blast analysis since the structure reaches its maximum deflection in a very short time, in which the damping has negligible effects on the peak displacement. For the structural elements that the mass and blast load is concentrated at the point of maximum deflection, the ESDOF system described by Equation (1) yields sufficiently accurate results. The error due to actual mass and blast load being distributed over the tributary area is fixed by using load or stiffness transformation factor K_L and mass transformation factor K_M [5,12]. These transformation factors are commonly referred as Biggs' Factors. The values of these transformation factors are determined so that the ESDOF system and the actual systems will have the same total work and strain and kinetic energies at any given time. The updated equation of motion for the ESDOF system is given as

$$(K_M M)\ddot{y}(t) + min[K_L K y(t), K_L R_u] = K_L F(t) \tag{2}$$

where R_u is the ultimate resistance capacity of the member. An alternative and convenient way of writing Equation (2) is obtained by denoting the ratio of mass and load transformation factors as K_{ML}

$$(K_{ML} M)\ddot{y}(t) + min[Ky(t), R_u] = F(t) \tag{3}$$

The values of load and mass transformation factors depend on mass distribution, structural element support conditions, blast load distribution, and deformed shape of structural element (elastic, elastic-plastic, and plastic) under blast loads. The values of transformation factors for simply-supported and clamped beams subjected to uniformly distributed blast load are given in Table-4 [5,12].

Table 4. Transformation factors for simply supported and uniformly loaded beams

Clamped beams				**Simply supported beams**			
Deflection	K_L	K_M	K_{ML}	Deflection	K_L	K_M	K_{ML}
Elastic	0.53	0.41	0.77	Elastic	0.64	0.50	0.78
Elastic-Plastic	0.64	0.50	0.78				
Plastic	0.50	0.33	0.66	Plastic	0.50	0.33	0.66

The general equations for computing transformation factors are given by Biggs [10,12] as

$$K_M = \frac{\int_0^L m\emptyset^2(x)\,dx}{mL} \tag{4}$$

$$K_L = \frac{\int_0^L w\emptyset(x)\,dx}{wL} \tag{5}$$

where L and m are beam span length between the supports and mass of the beam, respectively; w is the distributed static load that has the same distribution as the blast load, and ϕ is the assumed-shape function for the beam deflection when it is subjected to the blast. The shape function is in fact the deflected shape of the beam, where the maximum deflection is set to be unity. Because the shape of deflection curve changes depending on the deflection being elastic, elastic-plastic or plastic, the values of transformation factors change accordingly as given in Table-4. However, in practice it is common to use a constant value for the transformation factors throughout the analysis. The appropriate values depend on the predominant displacement response of the structural member. In the following section, the details of prototype building roof joist and plate ESDOF systems are given as sample cases.

The ESDOF system for prototype building roof joists

The roof joists (W4x13) span length (L) is 2.9 m and its tributary area for blast loading and mass calculation is 0.8 m, which is the nominal spacing between the joists. The section self-weight (W) 190 N/m, moment of inertia about strong axis (I_x) 4703415 mm^4, strong axis plastic section modulus (Z_x) 102911 mm^3, and modulus of elasticity (E) 200000 MPa were obtained from AISC steel construction manual [14]. The section dynamic yield stress values are 452 MPa and 425 MPa for bending/shear and axial stresses, respectively as given in Table-3. For the blast analyses performed, the bending dynamic yield stress value (452 MPa) was used since the main response of the joists will be in bending rather than axial deformations. The boundary conditions for the joist were assumed to be fixed on both ends. For beams with fixed ends and subjected to uniform distributed load, the plastic hinges form first at the supports, and as the load increases a third plastic hinge forms at the mid-span as shown in Figure-8 and 9.

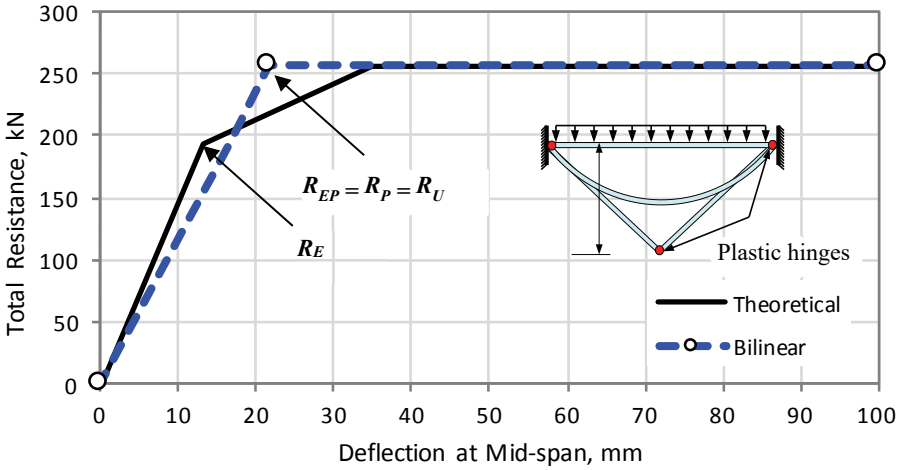

Figure 9. Roof joists resistance-curves

The beam load versus displacement curve (resistance-curve), which is needed to define the spring resistance for the ESDOF system, has three regions namely elastic, elasto-plastic, and plastic regions as given in Figure-9. The stiffness equations for mid-span deflection (location of maximum deflection) of the beam for each region are given as

$$K = \begin{cases} K_E = 384EI_x/L^3\,, & \text{elastic} \\ K_{EP} = 384EI_x/5L^3\,, & \text{elasto-plastic} \\ K_P = 0\,, & \text{plastic} \end{cases} \tag{6}$$

The stiffness values K_E and K_{EP} are 14.81 kN/mm and K_{EP} 2.96 kN/mm, respectively. Resistance values, which are needed to define the resistance-curve are given as

$$R = \begin{cases} R_E = 12M_{PS}/L\,, & \text{elastik} \\ R_{EP} = 8(M_{PC} + M_{PS})/L\,, & \text{elasto-plastic} \\ R_P = 8(M_{PC} + M_{PS})/L\,, & \text{plastic} \end{cases} \tag{7}$$

where R_E, R_{EP}, and R_P are the elastic, elasto-plastic, and plastic resistance capacities of the roof joists for the given blast load distribution, and M_{PC} and M_{PS} are the ultimate moment capacity of the section at mid-span and supports, respectively. Because the section of the joists is constant along its span, M_{PC} and M_{PS} are equal and given as the product of plastic section modulus and dynamic yield stress (Z_xF_{dy}). In general, the resistance-curves are assumed to be bilinear (elastic-perfectly plastic) to simplify dynamic analysis as shown in Figure-9. The stiffness of elastic part of the bilinear curve is called effective stiffness (K_{EQ}), and it is selected so that the areas under the actual and bilinear resistance-curves are equal. The effective stiffness of the roof joist is given as $307EI_x/L^3$, and it corresponds to an elastic stiffness of 11.84 kN/mm for the joists.

The last parameters that are needed for the ESDOF system are the mass associated with the joist and the initial static load (self-weight) carried by the joist. The dynamic mass of joist is 146.7 kg, and it includes 56.2 kg of joist self-mass and 90.5 kg for roof plate mass over the joist tributary area. Therefore, the initial static load associated with this mass and carried by the joist is 1439 N. The theoretical and bilinear deflection versus resistance-curves for the roof joist are given in Figure-9. The bilinear curve with K_{EQ} = 11.84 kN/m, ultimate resistance R_u = 256.6 kN, transformation factor K_{ML} = 0.78, and mass of 146.7 kg were used for the joist ESDOF system.

The ESDOF system for prototype building roof plate and crimped wall panels

Roof and wall plates load versus deflection relationship (i.e., resistance-curves) need to be established to develop the corresponding ESDOF systems. Because the panels are only 5 mm in thickness, the blast load applied perpendicular to their planes is carried primarily by the membrane action rather than the bending action. Although there are readily available tables and closed form equations for predicting load versus deflection relationship for flat plates, such tools typically ignore the membrane action, and they do not exist for crimped wall panels. Therefore, the resistance-curves for the panels were developed using local 3D FE models to capture effects of membrane action and geometric nonlinear behavior. Moreover, using FE local model to establish plate's ESDOF resistance-curves minimizes analysis errors associated with the resistance-curve. The developed local roof panel model had a span length equal to the spacing between the roof joists and a width equal to half of its span length. The edges of the panel supported by the roof joists were assumed to be fixed (restrained for all degrees of freedom) along the panel width, and free support condition (all degrees of freedom released) was assumed for other two edges along the span length. The assumed boundary conditions are compatible with the roof panels acting as one-way slab between the roof joists.

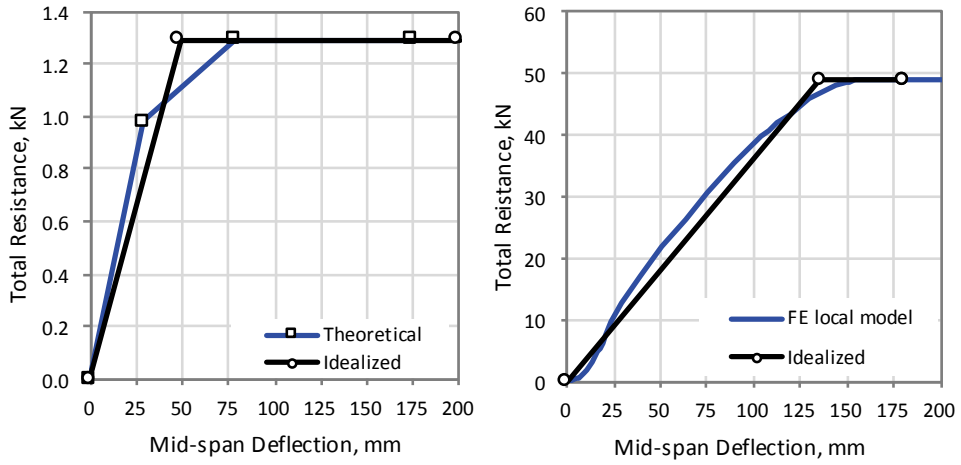

Figure 10. Resistance-curves for roof plate (a) bending mechanism only (b) bending plus membrane mechanisms

The theoretical and idealized load versus displacement curves per 25 mm roof panel width are given in Figure-10 for cases with and without membrane action. The results show that roof plate carries the blast load mainly by the membrane action as expected, and the bending mechanism has negligible contribution to plate's resistance. In addition to the ESDOF, two FE models were used to evaluate blast performance of the roof panels. These are the FE prototype building model, where the entire building was modeled, and the local FE model used to determine roof panels resistance-curve. For the crimped wall panels, developing the resistance-curve is challenging due to trapezoidal cross-section and geometric nonlinearity. Therefore, the resistance-curve for the crimped wall panels given in Figure-10 was established by loading a local FE model of the entire wall panel spanning between the columns and floor and roof beams under uniformly distributed static load.

5. RESULTS AND DISCUSSSION

Maximum deflection, the corresponding Von-Mises stresses and effective plastic strain (PEEQ) for the prototype building are shown in Figure 11 and 12 for blast loads BL-50 and BL-80, respectively. For low damage level blast loading BL-50, the crimped wall panel facing direct blast loading developed plastic hinges in the vicinity of its connection to the floor and roof beams as well as at its mid-span. However, the stress levels remained below the yielding for other wall and roof plates due to much smaller blast load acting on them. Yielding in the north module roof joists occurred at their north supports only, while yielding in the south module joists occurred at their mid-span only as shown in Figure-11. In other words, the observed yielding patterns of roof joists in the north and south modules contradict the expected and assumed deformation shape function for the corresponding ESDOF systems. Due to joists having fixed support condition, yielding was expected to occur first over the supports and then at their mid-span. For the main frame beams and columns of the building, yielding occurred only in the middle column facing direct blast loading. Because the connections between the structural members (i.e., full penetration welds) were assumed to be strong enough to develop their full plastic capacity, their full plastic capacity is reached when three plastic hinges (over each support and at the mid-span) are formed. The only structural elements with three plastic hinges are the crimped wall panels facing direct blast loading (Figure-11c). Therefore, building blast damage level is not significant under BL-50 loading and consistent with low damage level.

For high damage level blast loading BL-80, significant yielding was observed for the structural members including wall and roof panels, columns, and roof and floor beams as shown in Figure-12. Especially, the frame members of the north module experienced significant plastic deformation and damage. The roof and floor joists and beams also experienced significant plastic deformations. The roof plate damage was mostly limited to building north module, but the prototype building experienced significant damage overall under BL-80 blast loading, and the observed deflections and damage levels were consistent with high damage level response.

Roof joists deflection histories under blast loads BL-50 and BL-80 are given in Figure-13 for ESDOF and FE analyses. The reported deflections are relative deflections at the point of maximum deflection, and they are corrected for the support deflection. The maximum roof joist displacements computed from the ESDOF and FE analyses were 16 mm and 30 mm

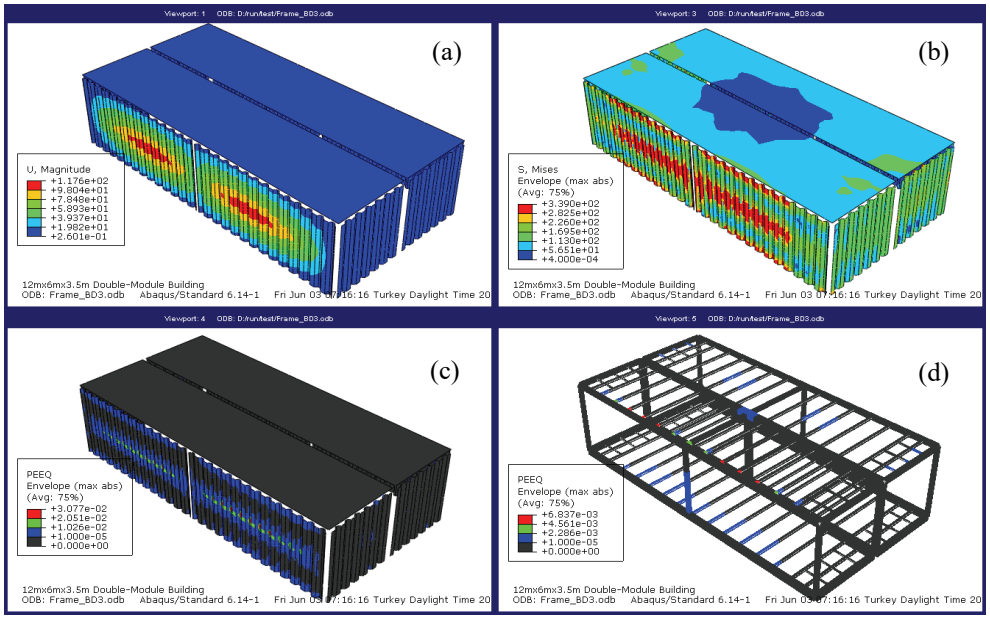

Figure 11. Under blast load BL-50 (a) maximum deflection in wall panels, (b) Von-Mises stresses, and (c &d) effective plastic strain (units in mm and MPA)

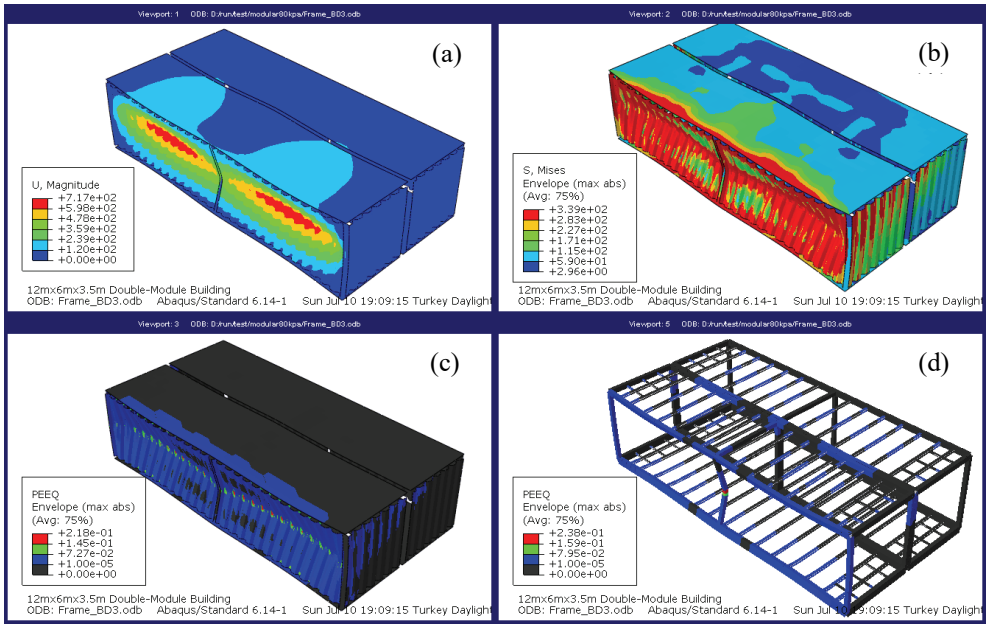

Figure 12. Under blast load BL-80 (a) maximum deflection in wall panels, (b) Von-Mises stresses, and (c &d) effective plastic strain (units in mm and MPA)

under blast load BL-50 and 26 mm and 38 mm under blast load BL-80, respectively. For both blast loads, the roof joist deflection history predicted using the ESDOF analysis was always smaller than that predicted using FE analysis. The maximum roof joist deflections computed using the ESDOF analysis correspond to a ductility of 0.7 and 1.2 for blast loading BL-50 and BL-80, respectively. However, FE analysis results given in Figure-11 and 12 show significant roof joist plastic deformation for both loadings. In other words, the ESDOF blast analysis results are on the unconservative side for the roof joists.

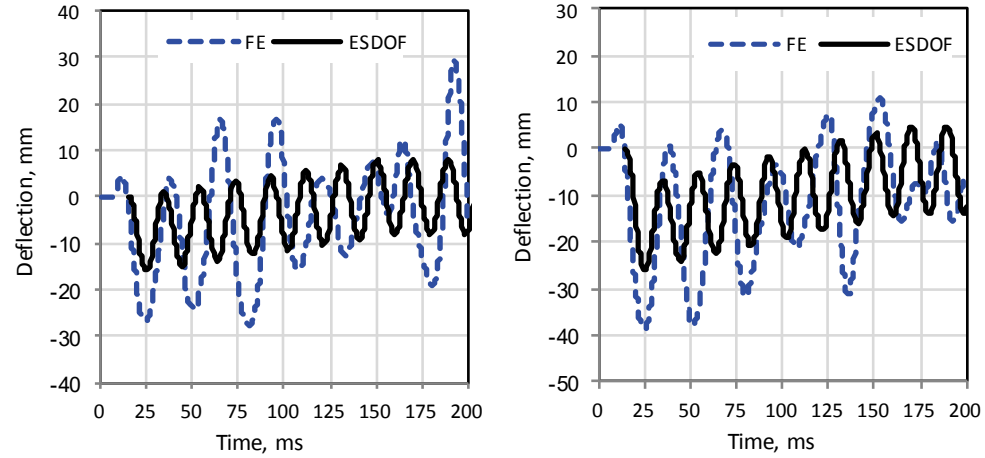

Figure 13. Displacement versus time histories for roof joists subjected to (a) BL-50 and (b) BL-80 blast loads

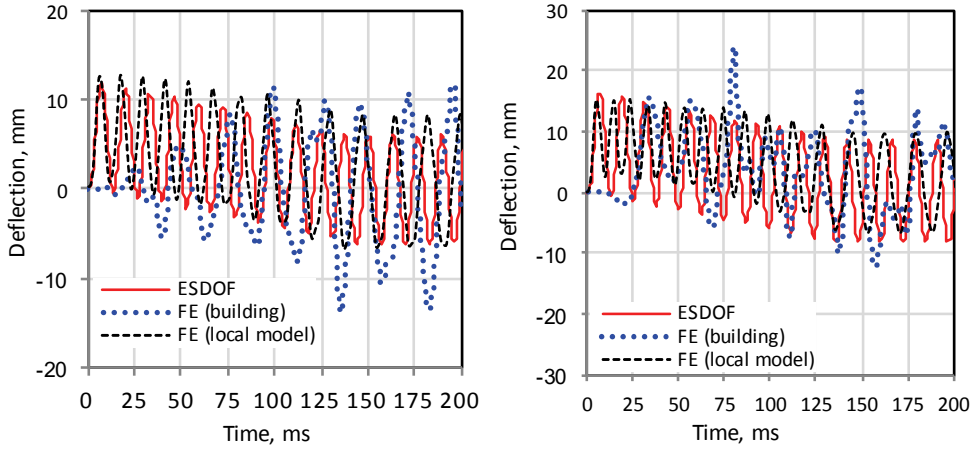

Figure 14. Roof plate displacement histories under (a) BL-50 and (b) BL-80 blast loads

The time versus deflection curves for roof panel calculated using the ESDOF and two FE analyses for blast loads BL-50 and BL-80 are given in Figure-14. In addition to the building FE model, the local roof plate FE model used to develop the ESDOF resistance-curve was also employed for roof plate blast analysis. This local model is useful to further verify the ESDOF analysis results and distinguish the effects of dynamic interactions.

The initial discrepancy between roof plate deflection histories in Figure-14 predicted with the ESDOF and building FE models is due to the time required for the blast wave to reach the location on the roof with the plate maximum deflection. The deflection histories of roof plate predicted with the ESDOF and local FE models exhibit good agreement for both blast loads BL-50 and BL-80 in terms of maximum deflections and vibration periods as shown in Figure-14. Therefore, roof plate ESDOF model is suitable to predict its uncoupled blast performance. However, roof plate FE results indicate that the ESDOF blast analysis results are on the unconservative side mainly due to dynamic interaction of structural members, which is neglected in the ESDOF and local FE analyses. The computed roof plate maximum deflections, which were corrected for the support deflections, under blast load BL-50 were 12 mm, 13 mm, and 14 mm for the ESDOF, plate local FE, and building FE models, respectively. Under blast load BL-80, the roof plate maximum deflections were 17 mm, 16 mm, and 24 mm from the ESDOF, local FE, and building FE models, respectively.

Table 5. Summary of performance of prototype building members under blast load BL-50

Structural Element	Location	Maximum deflection, mm and (μ) [1]		Maximum support rotation θ (degree) [2]		ESDOF Error [3] (%)
		ESDOF	Building FE	ESDOF	Building FE	
Roof joists	Roof	16 (0.7)	30 (1.3)	0.3	1.2	-47
Roof strut	Roof	<1 (0.1)	2 (1.7)	<0.1	0.5	-67
Roof plate	Roof	12 (0.1)	14 (0.1)	1.7	2.0	-14
Top intermediate long. beam HSS 8x6x1/2	Roof (column line-B)	60 (1.2)	48 (1.0)	1.2	0.9	25
Top intermediate transverse beam HSS 8x6x3/8	Roof (column line-2)	2 (0.2)	13 (1.2)	0.1	0.5	-85
Column HSS 6x6x1/2	column line-A&2	30 (1.8)	37 (2.2)	1.1	1.4	-19
Wall panel	column line-A	41 (1.3)	105 (3.3)	2.3	5.8	-61

[1] Ductility = [(maximum deflection / ESDOF yield deflection]

[2] Support rotation = [(Maximum deflection)/minimum distance to the support from max. deflection point]

[3] Error = [(ESDOF- Building FE)/ Building FE]100; (applied to maximum deflections)

Table 6. Summary of performance of prototype building members under blast load BL-80

Structural Element	Location	Maximum deflection, mm and (μ) [1]		Maximum support rotation θ (degree) [2]		ESDOF Error [3] (%)
		ESDOF	Building FE	ESDOF	Building FE	
Roof joists	Roof	26 (1.2)	38 (1.8)	1.0	1.5	-32
Roof strut	Roof	<1 (0.1)	3 (2.5)	<0.1	0.6	-67
Roof plate	Roof	17 (0.1)	24 (0.2)	2.4	3.4	-29
Top intermediate long. beam HSS 8x6x1/2	Roof (column line-B)	194 (4.0)	132 (2.7)	3.7	2.6	47
Top intermediate transverse beam HSS 8x6x3/8	Roof (column line-2)	4 (0.4)	31 (2.8)	0.2	1.2	-87
Column HSS 6x6x1/2	(column line-A&2)	375 (22)	396 (23)	13.8	14.6	-5
Wall panel	(column line-A)	198 (6.2)	665 (20.1)	10.8	32.6	-70

[1] Ductility = [(maximum deflection / ESDOF yield deflection]

[2] Support rotation = [(Maximum deflection)/minimum distance to the support from max. deflection point]

[3] Error = [(ESDOF- Building FE)/ Building FE]100; (applied to maximum deflections)

Blast performance of other structural members of the prototype building predicted using the ESDOF and building FE analyses are given in Table-5 and Table-6 for blast loads BL-50 and BL-80, respectively. The results show that blast performance of the prototype building (i.e., deflection, ductility, support rotation) predicted with the ESDOF method were on the unconservative side by 19% to 85% for the blast load BL-50 and by 5% to 87% for the blast load BL-80. The only exception was the top intermediate longitudinal beam, of which blast performance was over predicted by 25% and 47 % in terms of maximum deflection using the ESDOF analysis. This main roof beam is supporting the roof joists and plate, and it is connected to the adjacent building module through the roof plate. Therefore, the dynamic interaction of this beam with the rest of the structure is complicated, and this interaction is considered to be significant on its dynamic response.

The main reason for the ESDOF blast analysis results of the prototype building being on the unconservative side is the inherent assumption that members' dynamic interaction does not affect their dynamic response. The accuracy of the ESDOF depends on how well the deformed shape of the element is predicted and blast loads are applied. The dynamic interaction affects the member behavior by changing the assumed deformed shape for the ESDOF analysis and consequently affecting the values of Biggs' transformation factor and location and sequence of plastic hinge formation. For example, in the ESDOF analysis of roof joists, the support condition was assumed to be fixed, and Biggs' transformation factors were accordingly determined. However, the effective plastic strain (PEEQ) counters in Figure 11 and 12 show that plastic hinges formed at only one end of the joists over the support

under blast load BL-50. However, the assumption of fixed-end support condition for the joists requires formation of two plastic hinges over the two supports at the same time. Therefore, the observation shows that dynamic interaction between the roof joist and other members affects roof joists' support condition and their shape function. A similar observation can be done for the intermediate column on the north wall under blast load BL-80. For the ESDOF analysis, the boundary condition was assumed to be fixed for two ends, and therefore the assumed deformed shape is based on formation of plastic hinges over the supports and then at the mid-span. However, the effective plastic strain counters given in Figure 11 and 12 show that yielding occurred over the column base support and mid-span while the rest of the column remained elastic including the top support region.

6. SUMMARY, CONCLUSIONS AND RECOMMENDATIONS

In this study, the blast performance of a two-module blast-resistant modular steel-framed building was determined in terms of deflection, ductility, and support rotation demands using uncoupled equivalent single degree of freedom (ESDOF) and detailed 3D finite element (FE) blast analysis methods. Two blast loads corresponding to building "low damage" and "high damage" response levels were considered. The blast loads prescribed for the building in terms of free field overpressure and duration were converted into local pressure loads for the building walls and roof to investigate effects of dynamic interaction of structural members under blast loading. The developed building FE model included effects of dynamic interaction of structural members, blast load distribution within the structural elements, and structural mass distribution as well as initial static load to due to gravity. On the other hand, the ESDOF analysis method is an approximate dynamic approach based on the assumption that the dynamic interaction of the structural members can be neglected, and their dynamic behavior can be represented with simple spring-mass models. Although the ESDOF blast analysis method is widely used in blast analysis, a detailed verification of the approach including dynamic interaction of structural elements is not available.

Based on the analysis results presented for the structural members of the building under the given blast loads, the following conclusions are made:

- The ESDOF blast analysis method is a powerful simple tool for predicting blast response of structural members. However, the ESDOF blast analysis is an approximate analysis method with the basic assumption that dynamic interaction of interconnected structural elements can be neglected.
- The accuracy of ESDOF analysis depends on engineering judgment needed to estimate structural member deformed shape, mass, tributary blast area, and its resistance-curve for the considered blast loads.
- The predicted blast damage levels (maximum deflections) for the prototype building structural members with the ESDOF analysis were on the unconservative side by 19% to 85% for the blast load BL-50 and by 5% to 87% for the blast load BL-80 compared to those predicted using building detailed FE model. Therefore, dynamic interaction of structural members is significant, and it should not be neglected. This finding contradicts with the literature; however the studies considering the ESDOF analysis being conservative are limited to the studies performed with limited

parameters in terms of the number of structural members dynamically interacting (typically a main beam supported by two beams at supports), boundary conditions, and blast loading.

- The dynamic interaction of structural members affects the member blast performance by changing the assumed deformed shape for the ESDOF analysis and consequently affecting the values of Biggs' transformation factors and location and sequence of plastic hinge formation.

The following recommendation can be made based on the results and findings presented:

- ESDOF blast analysis is an approximate method requiring crucial engineering judgment regarding the expected deformed shape, boundary conditions, mass, and blast loads. Sufficient accurate results can be obtained where the dynamic interaction of structural members is negligible. However, for the cases that dynamic interaction is significant or high accuracy results are needed, more sophisticated finite element tools including member dynamic interaction effects should be used.
- The ESDOF blast analysis method is a powerful tool to determine blast performance of structural members. It is especially recommended at the preliminary design stage to determine size of structural members. However, there is a need for additional studies to incorporate the dynamic interaction of structural members in the ESDOF blast analysis method.

Symbols

c : Viscous damping constant
F : Dynamic blast load
F_{dy} : Dynamic yield stress
F_u : Minimum tensile strength
F_y : Static yield stress
I_x : Moment of inertia about strong axis
K : Spring stiffness
K_E : Member stiffness for elastic region
K_{EP} : Member stiffness for elasto-plastic region
K_L : Load or stiffness transformation factor
K_M : Mass transformation factor
K_{ML} : The ratio K_L / K_M
K_P : Member stiffness for plastic region
K_{EQ} : Effective stiffness
L : Member span length
m : Mass per length
M : Total dynamic mass
M_{PC} : Ultimate moment capacity at midspan

M_{PS} : Ultimate moment capacity at support
ms : Micro second
P : Blast pressure
P_{so} : Peak side-on, or incident, overpressure
R : Structural member resistance
R_E : Elastic resistance capacity
R_{EP} : Elasto-plastic resistance capacity
R_p : Plastic resistance capacity
R_U : Ultimate resistance capacity
t : Time
t_d : Duration of positive phase of blast pressure
w : Uniformly distributed load
y : Displacement
Z_x : Plastic section modulus
μ : Ductility
θ : Maximum support rotation
Φ : Assumed shape function for beam deflection

References

[1] "Reference Manual to Mitigate Potential Terrorist Attacks against Buildings (FEMA 426)," Washington, D.C., 2003

[2] "Primer for Design of Commercial Buildings to Mitigate Terrorist Attacks (FEMA 427)," Washington, D.C., 2003.

[3] Ngo T., Mendis P., Gupta A., and Ramsay J., "Blast Loading and Blast Effects on Structures – An Overview," Electronic Journal of Structural Engineering, Special Issue: Loading on Structures, 7, 76-91, 2007.

[4] Comert M., and Ilki A., "The Explosion Performance of a Ball Powder Production Facility," Journal of Performance of Constructed Facilities, 24, 326-336, 2010.

[5] "Design of Blast Resistant Buildings in Petrochemical Facilities," American Society of Civil Engineers (ASCE), New York, 1997.

[6] Summers P., "Design of Modular Blast-Resistant Steel-Frames Buildings in Petrochemical Facilities," Structures Congress, Vancouver, Canada, 2008

[7] "Methodology Manual for the Single-Degree-of-Freedom Blast Effects Design Spreadsheets," U.S. Army Corps of Engineer, Omaha, 2008.

[8] Krauthammer T., "Blast Mitigation Technologies: Developments and Numerical Considerations for Behavior Assessment and Design," Proceedings of International Conference on Structures under Shock and Impact, Computational Mechanic Publications, Southampton, 1998.

[9] Conrath E. J., Krauthammer T., Marchand K. A., and Mlakar P. F., Structural Design for Physical Security: State of the Practice, American Society of Civil Engineers, Reston, Virginia, 1999.

[10] Yokoyama T., "Verification and Expansion of Single-Degree-of-Freedom Transformation Factors for Beams using a Multi-Degree-of-Freedom Non-Linear Numerical Analysis Method," MS Thesis, California Polytechnic State University, 2011.

[11] Lawver D., Daddazio R. Vaughan D., Stanley M., and Levine H., "Response of AISC Steel Column Sections to Blast Loading," ASME Pressure and Vessels and Piping Conference, Cleveland, Ohio, 2003.

[12] Biggs J.M., Introduction to Structural Dynamics, McGraw-Hill, New York, 1964.

[13] Baker W. E., Cox P.A., Westine P.S., Kulesz J.J., and Strehlow R.A., Explosion Hazard and Evaluation, Elsevier, Amsterdam, Netherlands, 1983.

[14] "Specification for Structural Steel Buildings (AISC 360-10)," American Institute of Steel Construction, Chicago, Illinois, 2010.

[15] "Seismic Provisions for Structural Steel Buildings (AISC 341-16)," American Institute of Steel Construction, Chicago, Illinois, 2016

[16] "Structures to Resist the Effects of Accidental Explosions, Army TM 5-1300, Navy NAVFAC," U.S. Department of the Army, Washington, DC., 1990.

[17] Committee for the Prevention of Disasters Due to Dangerous Substances, "TNO Green Book, Method for the Determination of Possible Damage to People and Objects Resulting from Releases of Hazardous Materials (CPR 16E)," The Director-General of Labor, Netherlands, 1992.

[18] Feldgun V. R., Yankelevsky D., and Karinski Y.S., "Study of the Blast Response of Beams and Thin Rectangular Plates Using a Nonlinear SDOF Model," the 16th ISIEM, Destin, FL, 2015.

İMO Teknik Dergi, 2018 8279-8294, Paper 499

An Efficient Contact Tank Design for Potable Water Treatment

Ender DEMİREL[1]
Mustafa M. ARAL[2]

ABSTRACT

In this study, a second order accurate Large Eddy Simulation (LES) model is used to simulate three-dimensional turbulent flow and disinfectant transport in a contact tank. The hydraulic and mixing indexes of the tank are evaluated based on computational tracer studies. It is shown that the energy consumption rates of the contact tank can be reduced by the use of the proposed slot-baffle design instead of the conventional baffle system that is used in these facilities. The proposed slot-baffle design improves the hydraulic efficiency by 44%, mixing efficiency by 42% and reduces the energy required to drive the flow through the system by 43%. The outcome reported in this study shows that the energy consumption in water treatment plants can be significantly reduced when the novel baffle design is implemented on existing contact tanks without expensive infrastructure modifications.

Keywords: Contact tank, treatment of potable water, CFD, turbulence, LES.

1. INTRODUCTION

Contact tanks are critical infrastructures that are used in water treatment facilities that treat potable water with chlorine or ozone. Historically, as a design criteria, the design of these facilities are not based on minimum energy consumption during the operation of the contact tank. The contact tank design is based on plug flow assumptions where viscous effects are not considered and more emphasis is placed on sufficient treatment. This design approach may over or under estimate the mixing condition and the disinfectant use without much consideration given to energy consumption during treatment. In large population centers where high volumes of water are treated and consumed daily, high energy consumption rates have now become a critical impediment for water treatment at these facilities. In modern cities and municipalities, parallel to the population growth, the energy intensive treatment methods such as ozone treatment is also becoming more popular. Accordingly, improvement of hydraulic and mixing efficiency of contact tanks that would also reduce the energy demand is now in the forefront of academic research and applications. An efficient contact system

Note:
- This paper has been received on June 23, 2017 and accepted for publication by the Editorial Board on January 30, 2018.
- Discussions on this paper will be accepted by May 31, 2018.

• DOI: 10.18400/tekderg.322491

1 Eskisehir Osmangazi Uni., Department of Civil Engineering, Eskişehir, Turkey - edemirel@ogu.edu.tr
2 Bartın University, Department of Civil Engineering, Bartın, Turkey - mustafaaral@bartin.edu.tr

design that addresses effective water treatment while using less energy is now important and is the topic of this study.

In most Turkish cities, potable water is treated with chlorine. Ozone treatment is an energy intensive treatment process which is mostly used in developed countries with a gradual trend of moving to ozone treatment in developing countries as well. Ozone treatment is a more effective water treatment process and an eco-friendly application, but it is an expensive process. Thus, an efficient contact tank system is more important for ozone treatment since ozone cannot be dissolved in water as much and as quickly as cholorine. In a classical contact tank design, baffles are placed at specific locations inside the tank to increase the contact time of water and the disinfectant. In Turkey contact tanks are designed based on the assumption of plug-flow conditions which maintain the contact time for about 20 minutes [1]. However, recirculating dead zones that form in the vicinity of the corners of baffles due to the viscous and turbulent effects and the formation of high velocity jet zones in the remaining area of the mixing chamber cause the injected concentration of the disinfectant to leave the contact tank without reaching the effective disinfection contact time. This undesirable condition is identified as short-circuiting. Short-circuiting effects reduce the hydraulic and mixing efficiency of the contact tank and may yield high residual chlorine concentrations in water at the outlet. This is a risky condition for both human health and also for the environment. The short-circuiting effects also increases the energy consumption rates in water treatment plants where energy intensive treatment methods such as ozone and ultraviolet are used. It is important to remember that almost 90% of the total energy consumption in an ozone treatment plant is used for ozone generation [2]. Thus, significant importance is given to research and development studies where specific designs are considered to reduce energy consumption in ozone treatment through improved mixing more than the chlorine treatment facilities.

Hydraulic and mixing efficiency of contact tanks can be evaluated using the indexes that can be obtained from the Residence Time Distribution (RTD) and cumulative RTD plots. These distributions are obtained from tracer studies, where the injected concentration of the disinfectant at the inlet is monitored at the outlet of the tank to obtain RTD and the cumulative RTD plots. The cumulative RTD plot is the integral of the RTD plot with respect to time. Tracer studies can be conducted experimentally by monitoring the concentration of a tracer such as the fluorescent dye (Rhodamine B) by using fluorometer at the outlet [3, 4]. More recently, developments in computational methods made it possible to design contact tanks using Computational Fluid Dynamics (CFD) methods more economically than the conventional experimental methods [5, 6, 7, 8] where a tracer study can be conducted numerically. In these studies the motion of the injected tracer with the turbulent flow is numerically simulated to obtain the RTD and cumulative RTD plots which show the variation of concentration and cumulative concentration of the tracer at the outlet, respectively [7, 8]. Finally, hydraulic and mixing efficiency of the contact tank is evaluated using the indexes which are obtained from the RTD and cumulative RTD plots.

Turbulence model employed in numerical simulations have significant effect on the results obtained. To reduce computation time, RANS based turbulence models such as k-ε, k-ω and low Reynolds number models [4] have been extensively used in the design of large scale treatment plants. Recently, LES models in which the unsteady variation of large turbulent fluctuations can be evaluated, have gained significant attention with the development of

computer technologies that reduce computational time [6, 9]. It has been reported in the literature that the recirculation zones that form in the vicinity of the corners of the baffles could not be detected when the RANS based turbulence models are used, while those recirculation zones could be simulated with LES on a fine resolution computational mesh. Moreover, turbulence induced mixing of the disinfectant with the flow could only be simulated with LES models [6, 9], which is critical for the present problem.

In this study, turbulent flow in the contact tank with four chambers is simulated using a second order accurate computational model in space and time. LES turbulence model is employed in order to calculate the unsteady variation of turbulent eddies near the corners of the baffles. Mixing of the disinfectant with the the turbulent flow is simulated by solving the Advection-Diffusion equation with the momentum equations simultaneously. Accuracy of the present numerical model is evaluated based on the comparison of the numerical results with the previously reported results in the literature. It is shown that the hydraulic and mixing efficiencies of the contact tank can be increased with the proposed slot-baffle design and energy consumptions in water treatment plants can be reduced by implementing the proposed design in existing water treatment plants without costly infrastructure modification.

2. PROBLEM DEFINITION

Schematic view of the flow in the contact tank is shown in Figure 1. Water enters to the tank with constant flow rate Q=0.2 *lt/s* and the depth of the flow is maintained at h=0.21 *m* when the mass conservation is achived inside the domain after a certain time. Height of the baffles are selected as 0.18 *m* and the horizontal spacing between the baffles is w=0.113 *m*. Flow properties and dimensions of the tank are selected to be the same as previous studies

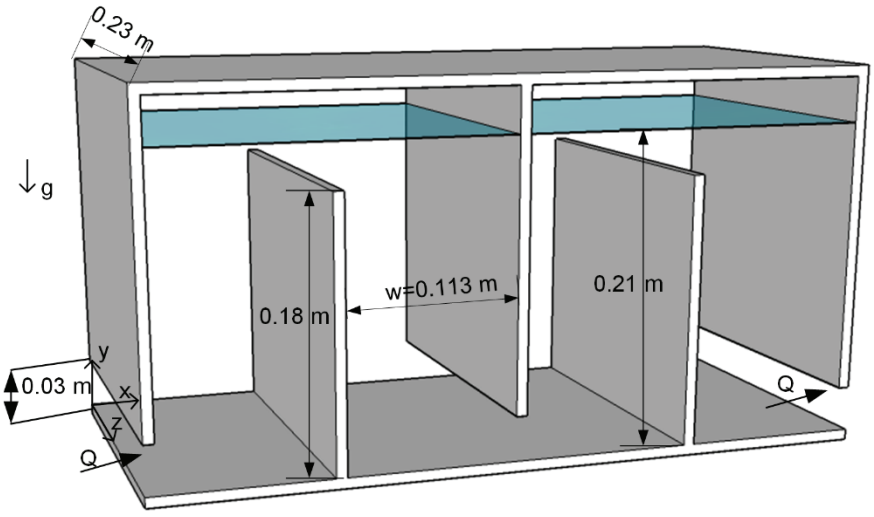

Figure 1. Three-dimensional schematic view of the flow inside the contact tank

in order to compare the numerical results with the previously reported results [6, 10]. In this study, a truncated version of the contact tank is used applying periodic boundary conditions at the inlet and outlet even though experimental studies were conducted using the same tank having 12 chambers. Prescribing inlet boundary condition for turbulence at the inlet requires a cumbersome process for the simulation of turbulent flows. Boundary conditions for the turbulence quantities at the inlet do not need to be prescribed in this study since periodic boundary conditions are used for all flow variables at the inlet and outlet of the computational domain.

The Reynolds number of the flow is calculated based on the average velocity at the inlet and the equivalent hydraulic radius as $Re = U_{av}R/\vartheta$=2740. Here $R = \sqrt{4A/\pi}$ and A is the area of the cross-section at the inlet. No-slip boundary conditions are imposed at solid walls and symmetry boundary condition is used at the free-surface based on the assumption of no-shear since the surface waves can be neglected [2, 6].

3. COMPUTATIONAL MODEL AND VALIDATION

Reyndols-averaged Navier-Stokes (RANS) models such as $k-\varepsilon$, $k-\omega$ and low Reynolds closure models have been extensively used in the literature for the simulation of the turbulent flow in the contact tank. However, recent studies in the literature have postulated that the time-varying turbulent eddies in the vicinity of the baffle corners affect not only the mean flow structure inside the tank but also the mixing of the disinfectant with the flow [6, 9]. Time variation of turbulent eddies cannot be simulated accurately using RANS based turbulence models due to the fact that only time-averaged values of the flow are considered in RANS applications. Thus, in this study numerical simulation of the turbulent flow inside the contact tank is performed employing LES turbulence model, which is the main difference from the previously published study of the authors [17]. Governing equations for the LES will not be repeated here since conventional equations of LES can be found in the literature [6, 9].

In the numerical simulation of fluid flow using LES, large eddies are resolved directly by the computational mesh and the small eddies are modeled using a sub-grid scale (SGS) model. Thus, the resolution of the computational mesh should be fine enough to capture the turbulence structure. The most classical SGS model is Smagorinsky SGS model in which the C_s Smagorinsky coefficiency is kept constant at 0.1. Some drawbacks may occur when this coefficient is kept constant in the computational domain throughout the numerical simulation. This coefficient may take smaller values near the solid walls depending on the flow properties. In addition, C_s coeficient should take negative values to calculate the backscattering effects due to energy transfer from small to large scales. Fixing the Smagorinsky coefficient at a specific value may reduce the accuracy of the computational model. In this study, Dynamic Smagorinsky LES [11] approach is employed in which the Smagorinksy coefficienct is calculated dynamically from the interior solution of the domain at every time step of simulation in order to exclude the exsessive dissipation near the walls and to consider the energy backscattering effects.

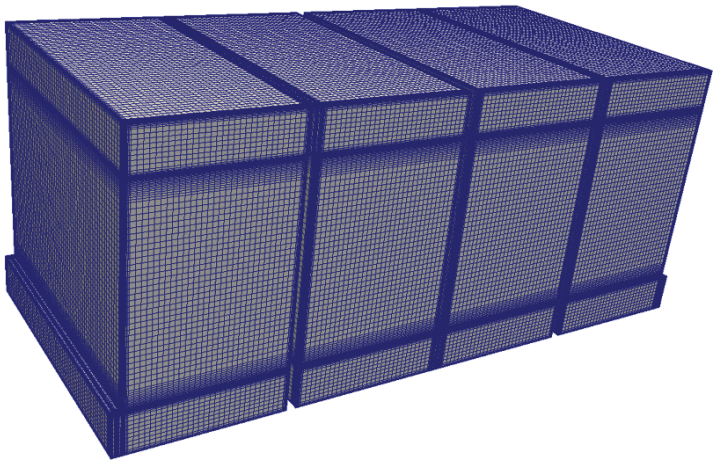

Figure 2. Three-dimensional view of the structural mesh

An open source CFD code OpenFOAM is used in numerical simulations conducted in this study [12]. In the numerical solution, convective and diffusive terms in the governing equations are discretized using second order accurate *LinearUpwind* and *linear* methods, respectively, unsteady terms are discretized using second order accurate *backward* method. Thus the numerical model employed in this study is second order accurate in space and time to reduce the truncation errors that arise from the discretization of the partial differential equations. A structured grid system is used in the numerical simulations clustering the computational mesh near the walls and free-surface where temporal and spatial variations of flow variables are to be significant. About 1.8 million computational cells are used in the computational mesh shown in Figure 2 ensuring that the dimensionless wall distance adjacent to the solid wall is $y^+ < 3$. Thus, the viscous sub-layer is resolved in the LES accurately without using wall functions, which may reduce the accuracy of the LES solutions near the walls.

Time step size Δt in the unsteady solution of the governing equations is selected according to the Courant-Friedrichs-Lewy (*CFL*) stability condition such that *CFL*=0.5 during the numerical simulation. High-resolution numerical solutions in space and time are performed in parallel on the resources of *TRUBA* (Turkish Academic Network and Information Center) with 112 computational nodes within the *OpenFOAM* on the domain decomposition approach. In parallel computing, computational domain is decomposed into the same number of available nodes calculating each sub-domain on different processor and enabling messaging of the processors with each other during the simulation. At the end of the parallel computing, decomposed solution domains are reconstructed to obtain the solution in the overall domain. Implementing parallel computing strategy allowed us to simulate the problem with high-resolution numerical solution at acceptable computational times.

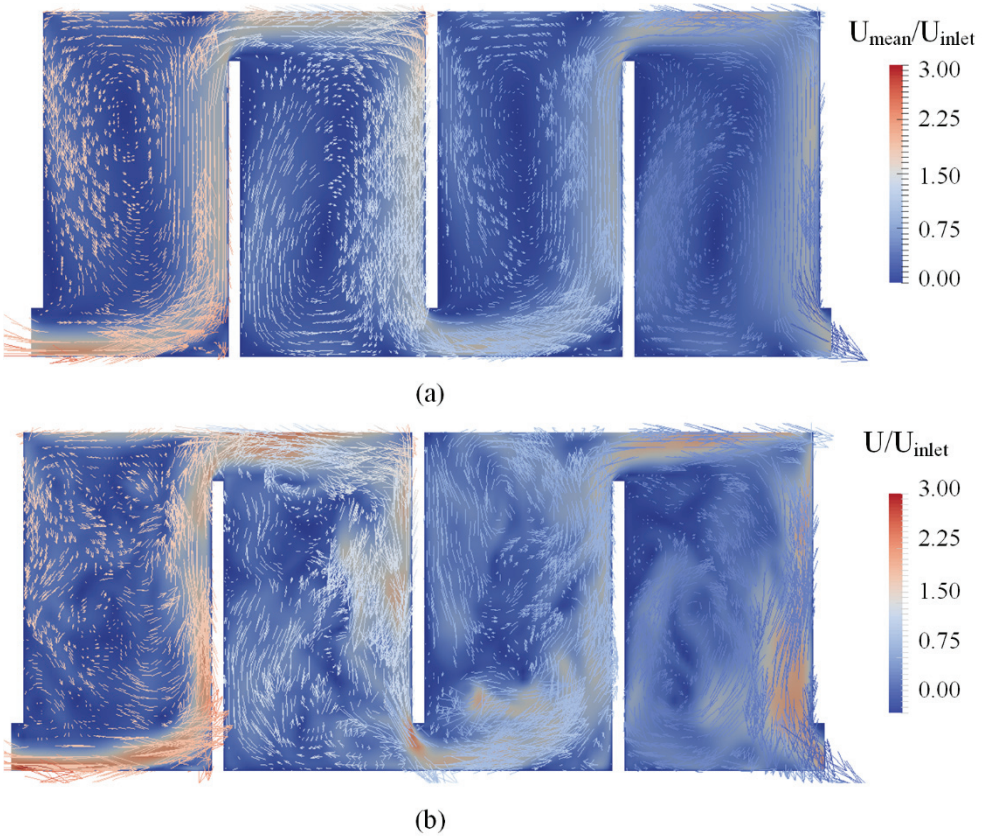

Figure 3. Velocity magnitudes and vectors at the vertical plane passing at the center of the tank (*z=b/2*); (a) Time-averaged velocity; (b) Instantenous velocity

Instantenous flow properties are used to calculate the time-averaged value of a variable during the simulation of turbulent flows using LES. It is required to simulate the flow long enough to obtain time-averaged flow field excluding the severe variations in flow properties that occur during the initial stage of the simulation [13]. In order to exclude the effects that arise from the initial conditions, time-averaging was performed starting from *t*=200 s to 600 s. Velocity magnitudes and vectors at the vertical plane passing at the center of the tank are shown in Figure 3 for both time-averaged and instantenous flow fields. As seen in Figure 3, large recirculation zones occur due to wall effects near the baffles and this also forms a jet zone with increased velocity especially at the inlet of the chambers extending towards the opposite wall. Magnitude of the flow velocity in the jet zone is decreasing along the flow direction due to viscous and turbulence effects. Turbulence fluctuations near the baffles form small recirculation zone at the inlet of each chamber. Demirel and Aral [13] showed that the recirculation and jet zones could be separated using the vorticity field and the definition of Lamb vector to define a volumetric efficiency coefficient for the evaluation of hydraulic efficiency of the contact tank. Short-circuiting in the tank causes the injected concentration

of disinfectant at the inlet to advect with the high velocity parcels and to leave the contact tank without effective disinfection. This reduces the overall efficiency of the contact tank. Viscous and turbulence induced short-circuiting effects connot be predicted for the contact tanks where the design is based on the plug-flow assumption. Thus, high-resolution numerical models should be employed for the design of contact tanks that include viscous and turbulence effects. As will be discussed at the latter part of the study, proposed slot-baffle design increases both hydraulic and mixing efficiency of the contact tank while reducing the momentum of the jet zones.

As seen in Figure 3b, unsteady effects in turbulence field significantly alter the flow field. LES turbulence models should be used in order to simulate large eddies in the tank accurately. It is also critical to use LES model in order to simulate the advective diffusion of the tracer with the turbulent flow. Numerical simulations in which the RANS based turbulence models are used could not detect the recirculation zones near the inlet of the chambers and the accuracy of the simulation of the tracer with the turbulent flow may reduce as well. Thus, it is suggested to use computational models that can capture the large eddies in the flow field for proper advective dissusion analysis.

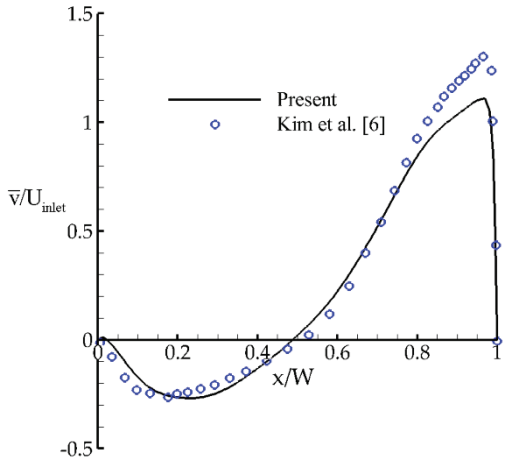

Figure 4. Variation of the time-averaged vertical velocity ($\overline{v}$) along the chamber width (W)

Variation of the time-averaged vertical velocity is compared with the numerical results in the literature at the elevation y/H=0.27 in the third chamber in Figure 4. Negative vertical velocities between the baffle and the center of the chamber indicate a large recirculation zone inside the chamber. The present computational model could detect this recirculation zone accurately. The magnitude of the velocity in the jet zone is underestimated in comparison to the previous numerical results. This could be due to time averaging that was not performed for a long time in the literature since the flow velocities are high at the initial stage of the simulation and magnitude of the velocity in the jet zone is reduced during the simulation.

Thus, the magnitude of the velocity is reduced in the jet zone when time averaging is performed for a long time, as previously reported in [13].

4. TRANSPORT MODEL AND VALIDATION

The transport of concentration of disinfectant injected at the inlet is traced using the following advection-diffusion equation:

$$\frac{\partial \overline{C}}{\partial t} + \overline{u_j} \frac{\partial \overline{C}}{\partial x_j} = \frac{\partial}{\partial x_j}\left((D + D_t) \frac{\partial \overline{C}}{\partial x_j} \right) \tag{1}$$

Here u_j is the velocity component along the *j*-direction (*x, y* and *z*), *t* is time, x_i and x_j are Cartesian coordinates, $\overline{C}$ is filtered concentration, *D* is molecular diffusion, D_t is turbulent diffusion, which can be calculated as $D_t = \nu_t / Sc$. Here ν_t is turbulent viscosity which is calculated during simulation and Sc is the Schmidt number which is set to 1000 in order to be consistent with the numerical studies conducted in the literature [6, 9].

"*Frozen flow*" approach has been extensively used in the tracer studies conducted in the literature. In this approach, steady state flow field is obtained first, then Equation (1) is solved using the steady state flow field. In this approach, interaction of the disinfectant and the turbulent flow cannot be simulated realistically since advection-diffusion equation and flow equations are not solved simultaneously. In the present study, the aim is to simulate the turbulence induced mixing of the disinfectant by solving the advection-diffusion equation with the flow equations simultaneously. In order to achieve this, standard solver *pimpleFoam* that is available in OpenFOAM is modified to include the solution of the advection-diffusion equation with the flow equations for a new variable of concentration $\overline{C}$. Employing an open source computer code in the present study allows us to modify the standard solver depending on the properties of the problem.

In order to validate the solution of the tracer study, tracer is injected at the inlet of the tank shown in Figure 1 during 2.5 *s* and variation of the concentration at the outlet is monitored during the numerical simulation. Concentration of the tracer is non-dimensionalized in the following form in order to be consistent with the previous studies reported in the literature and to satisfy the volume conservation of the injected concentration [2, 6, 9]:

$$E(\theta) = \frac{\overline{C}}{\dfrac{\overline{C}_{initial} T_{injection}}{\tau}} \tag{2}$$

Here $T_{injection}$ is the duration of injection (2.5 *s*), $\overline{C}_{initial}$ is the tracer concentration at the inlet ($\overline{C}_{initial} = 1$), τ is the theoretical residence time. Theoretical residence time is defined for the plug-flow as $\tau = \forall / Q$ [2, 6]. Here $\forall$ is the volume of the tank (m^3) and *Q* is the flow rate in the tank (m^3/s). Theoretical residence time is calculated as 109.2 *s* for the present problem.

RTD and cumulative RTD plots are compared with the results reported in the literature in Figure 5a and Figure 5b, respectively. Time axis is non-dimensionalized with respect to the theoretical residence time as $\theta = t/\tau$.

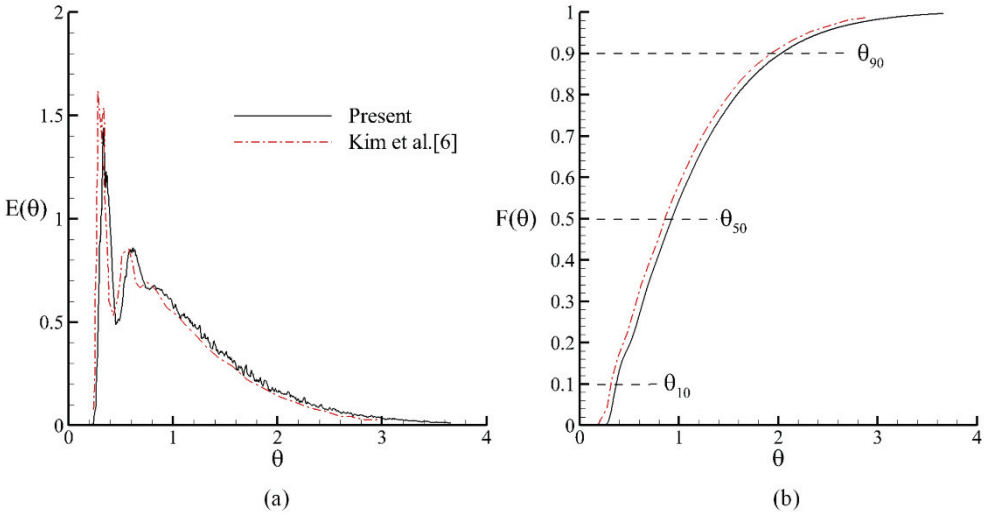

Figure 5. Comparison of the dimensionless concentration of disinfectant at the outlet with the literature: (a) RTD plot; (b) cumulative RTD plot

The first peak in Figure 5a indicates the tracer concentration that is transported by the high velocity parcels in the jet zone and leaves the contact tank after a short time without effective disinfection. Some part of the injected concentration is transported by the jet zone and the remaining part of the concentration is trapped in the reciurculation zones as shown in Figure 3 for a time duration. The trapped volume of the concentration emerges from the recirculation zones and leaves the contact tank at a later time, which is indicated by the second peak observed in Figure 5a. The time value at which the tracer concentration first observed at the outlet indicates that the short-circuiting effects are significant. Short-circuiting reduces the efficiency of the contact tank and causes more disinfectant to be used for effective disinfection and this increases the energy consumption rates during treatment. As seen in Figure 5b, total injected concentration leaves the contact tank at about $\theta = 3.66$. Tracer results are in good agreement with the previous results showing that the present computational model could accurately calculate the turbulence induced mixing in the tank. The small differences observed may be associated with the resolution of the computational mesh since the RTD and cumulative RTD plots shift to the left when the resolution of the mesh reduces. It should be noted that the present mesh is finer than the mesh used in the literature [6].

Indexes are obtained from the cumulative RTD plot to evaluate the hydraulic and mixing efficiencies of the contact tank. The most common index used for the hydraulic efficiency of

the contact tank is θ_{10}, which can be defined as the time required for 10% of the injected tracer to pass at the outlet. This index is also called the "baffle factor." According to the EPA [14] regulations, a contact tank is classified as "poor" for $\theta_{10}<0.3$, "compromising" for $0.3<\theta_{10}<0.5$, "good" for $0.5<\theta_{10}<0.7$ and "excellent" for $0.7<\theta_{10}<1.0$. The baffle factor becomes unity for ideal plug-flow conditions. The present contact tank is classified as compromising since the baffle factor is determined to be 0.369 from Figure 5b. Another type of efficiency index for a contact system is the "mixing efficiency," which is associated with the degree of the mixing of disinfectant with the water. The most common index for the evaluation of the mixing efficiency is the Morrill (Mo) index [14]. The Mo index is defined as the ratio of the time to pass the 90% of the injected concentration to the time to pass 10% of the injected concentration $(Mo = \theta_{90} / \theta_{10})$. The Mo index is unity for the ideal plug-flow and it takes the maximum value 21.9 [14]. EPA regulations suggest that $Mo \approx 2$ for an ideal contact tank. Dispersion index is the other index for the evaluation of mixing efficiency of contact tank, which is defined as [15]:

$$\overline{\sigma} = \frac{\sigma_\theta^2}{\theta_m^2} \tag{3}$$

Here σ_θ^2 is the variance of the RTD plot and θ_m is the mean of the RTD plot, which are defined as:

$$\sigma_\theta^2 = \frac{\int_0^\infty \theta^2 E(\theta) d\theta}{\int_0^\infty E(\theta) d\theta} - \theta_m^2 \tag{4}$$

$$\theta_m = \frac{\int_0^\infty \theta E(\theta) d\theta}{\int_0^\infty E(\theta) d\theta} \tag{5}$$

Dispersion index is a statistical definition associated with the dispersion of the RTD data around the mean of the RTD plot. Dispersion index takes values between 0 and 1 and it approaches 0 when the mixing in the tank increases. The aforementioned indexes are determined from Figure 5b for the contact tank shown in Figure 1 and these indexes are listed in Table 1. A Matlab program is developed for the calculation of the dispersion index based on the discrete RTD data.

Table 1. Efficiency indexes of the contact tank.

θ_{10}	θ_{90}	Mo	$\overline{\sigma}$
0.369	2.027	5.493	0.369

The baffle factor θ_{10} in Table 1 indicates that the short circuiting effects in the contact tank are severe and the hydraulic efficiency is also low. Mixing efficiency of the contact tank is low since the value of Mo index is not close to 2. The design considered in this study should increase both hydraulic and mixing efficiency of the contact system. The energy requirement to drive the flow from the inlet to outlet can be estimated from the following equation [8]:

$$P_f = \Delta p Q / e \tag{6}$$

Here Δp is the pressure drop between the inlet and outlet, Q is the flow rate passing at the contact tank, and e is the coefficient of mechanical efficiency of the pump, which can be taken as 50%. The pressure drop is calculated for the present tank as $\Delta p = 9.45 kPa$. Previous studies in the literature reported that the energy consumed by the pumps is significant in water treatment plants [15]. Energy losses in a contact tank are associated with the friction effects between the baffles and the flow. Previous studies in the literature suggested the use of additional baffles or turning vanes near the corner of the chambers to dissipate the energy of the recirculation zones and to increase the efficiency of the contact system. The use of additional solid regions located inside the tank reduces the effective volume of the contact system and causes extra energy losses. The proposed design that will be discussed next not only increases the hydraulic and mixing efficiency of the contact system but also reduces the friction induced energy losses.

5. SLOT-BAFFLE DESIGN

Aral and Demirel [17] proposed a novel baffle design to increase the efficiency of the contact system and this design is patented [18]. Three-slotted configuration of baffle design is depicted in Figure 6. Geometrical properties of the slots such as location, width, height and the numbers significantly affect the flow structure and efficiency of the contact system. The most efficienct configuration is investigated based on the successive numerical simulations and given in Figure 6. The main difference between the present and previous study [17] is that LES is used for the accurate simulation of the penetrating of the jets to the adjacent chambers. As discussed at the previous part of the study, realistic simulation of mixing of the disinfectant with the turbulence could be peformed using LES since the flow equations and advection-diffusion equation are solved simultaneously.

Averaged and instantenous velocity vectors for the slot-baffle design are shown in Figure 7. The jets emerging from the slots to the adjacent chamber reduce the momentum of the main jet which is the source of the short-circuiting and those jets imping to the neighboring dead zones also increase the mixing in the chamber and turn the dead zones into active mixing zones. Thus, the proposed slot-baffle design not only decreases the short-circuiting but also increases mixing in the contact tank. The main idea of the slot-baffle design is to reduce the friction losses and to increase the mixing efficiency while increasing the surface area between the fluid-fluid interfaces instead of increasing fluid-solid layers. Turning vanes were used and additional horizontal baffles were located on the vertical baffles in order to

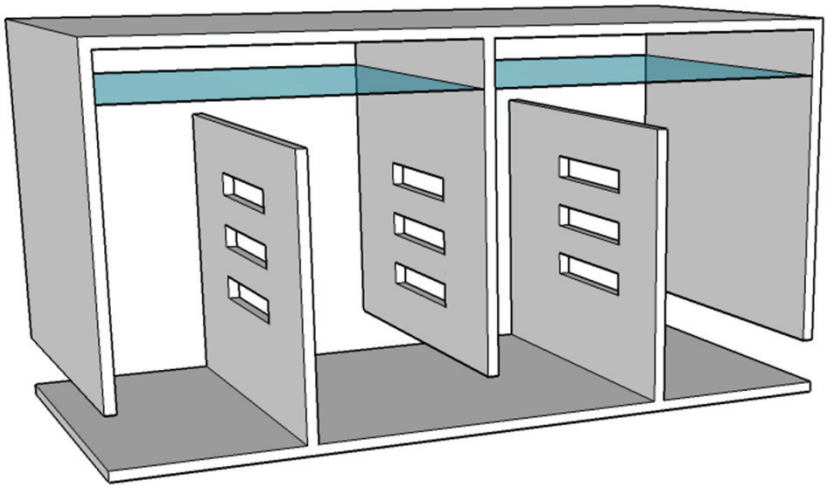

Figure 6. Implemantation of the slot-baffle design

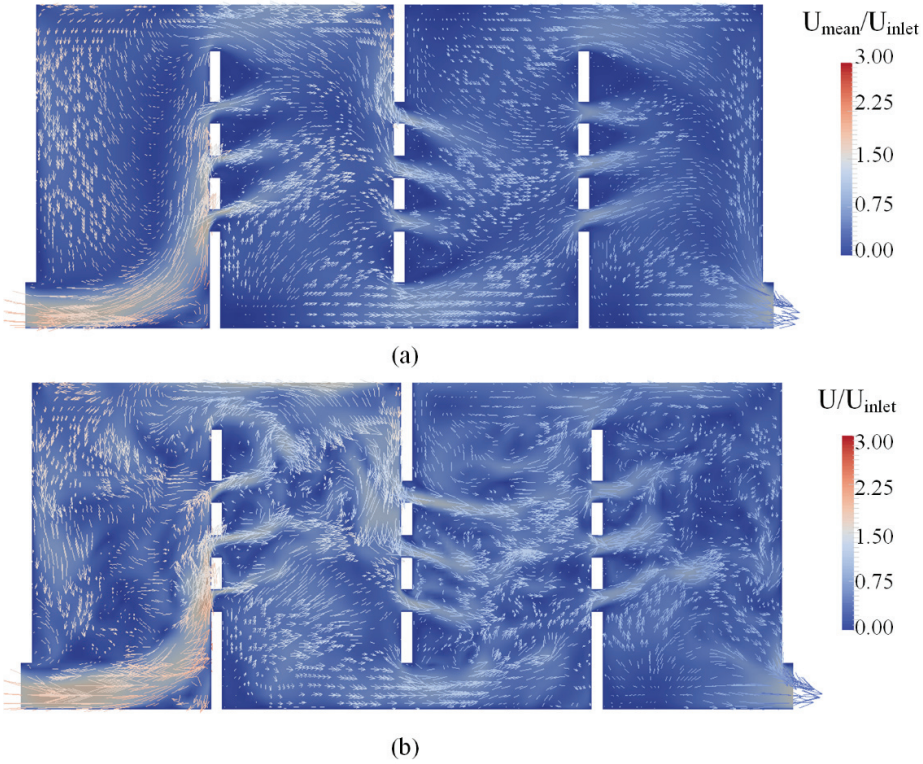

Figure 7. Flow field for the slot-baffle design; (a) Time-averaged flow field; (b) Instantenous flow field at z=b/2

turn the low mixing zones to active mixing zones in the literature [8; 19]. However, those types of tank designs increases the energy requirements to drive the flow through the system since the energy losses increase due to the wall effects. The slot-baffle design reduces the energy losses that occur in the convetional baffle design. As seen in Figure 7b, the flow emerging from the slots significantly altered the instantenous flow field to increase the mixing phenomenon in the tank as well. This will be seen in the results of the tracer study.

Tracer study is performed for the slot-baffle design using the same methodology mentioned in the previous part and the results of the tracer study are given in Figure 8. The first peak in the RTD plot is reduced indicating that the hydraulic efficiency of the contact tank is increased since short-circuiting effects are significantly reduced. The second peak observed in the results of conventional baffle design is not seen in the slot-baffle design, which is another indication of turning low mixing zones into active zones. Shifting of the peak of the RTD plot to the right indicates increasing of the contact time in the tank.

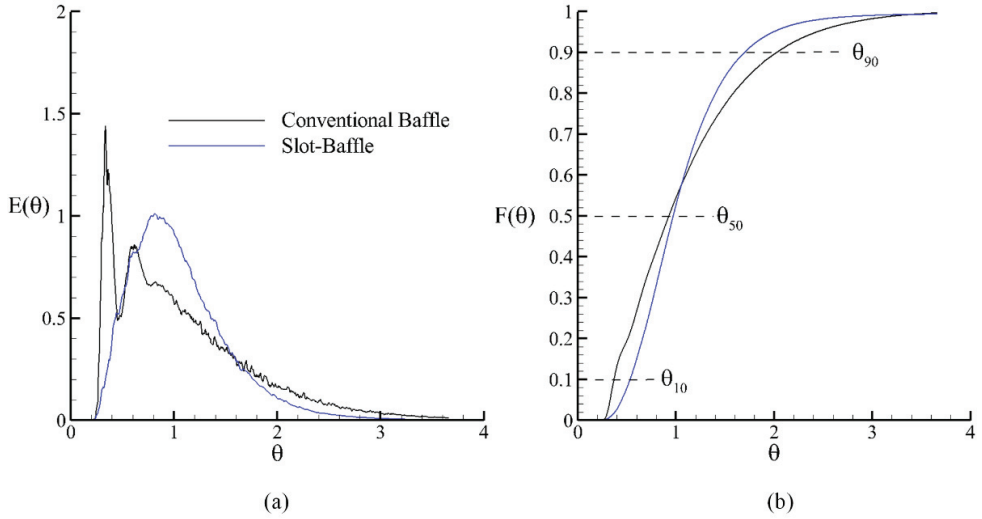

Figure 8. Comparison of tracer results of conventional and slot-baffle design; (a) RTD; (b) Cumulative RTD

As can be seen in the cumulative RTD plot in Figure 8b, the slot-baffle design altered the mixing indexes significantly. Efficiency indexes are determined from Figure 8b for the slot-baffle design and compared with the convetional baffle design in Table 2. Hydraulic efficiency of the contact tank has increased about by 44% reducing the short-circuiting effects. Mixing efficiency of the contact tank has increased by 42% according to the Mo index and 46% according to the dispersion index. Increasing the hydraulic and mixing efficiencies will reduce the required dosage of chlorine to be used in the disinfection process and will also reduce the cost of disinfection as well as the health risk of the chlorine usage. This will also reduce the energy consumed in ozone treatment plants significantly since energy requirement is more pronounced when ozone is used. Comparison of the pressure drops at the last column of the table indicates that the slot-baffle design reduces the energy

losses by 43%. Thus, the energy requirements of the pump to drive the flow through the system will also be reduced.

Table 2. Efficieny indexes of conventional baffle and slot-baffle designs

Baffle design	θ_{10}	Mo	$\overline{\sigma}$	$\Delta p/\rho$ (m^2/s^2)
Conventional baffle	0.369	5.493	0.369	9.45
Slot-baffle	0.532	3.192	0.201	5.41
Improvement (%)	44.17	41.89	45.53	42.75

6. CONCLUSIONS

Turbulent flow in a contact tank is simulated using a second order accurate computational model in this study. LES turbulence approach is employed in order to calculate the effect of time varying turbulent eddies on both flow field and the mixing of the disinfectant with water. A new computational model is developed to determine the efficiency indexes based on the tracer study. Numerical results are compared with the previous results in order to show the accuracy and reliability of the present numerical model.

Tracer studies show that the conventional tank designs suffer from high short-circuiting and low mixing. The proposed novel baffle design improves the hydraulic efficiency by 44% and mixing efficiency by 42%. The proposed baffle design reduces high cholorine dosage used in traditional cholorine treatment plants, which may be risky for human and public health. Increasing hydraulic and mixing efficiency in the contact tank reduces the energy consumption rates in ozone treatment plants. Energy requirements of the pumps to drive the flow through the system are also reduced by the proposed baffle design since energy losses have been reduced by 43%.

Short-circuiting effects cannot be predicted in the contact tanks when plug-flow assumption is used for the design. Viscous and turbulence effects significanlty alter the flow field inside the tank reducing the efficiency of the contact tank. It is recommended that the contact tanks should be designed using CFD methods as demonstrated in this study.

Acknowledgements

The numerical calculations reported in this paper were fully performed at TUBITAK ULAKBIM, High Performance and Grid Computing Center (TRUBA resources).

References

[1] Çakmakçı, M., Özkaya, B., Yetilmezsoy, K. ve Demir, S. Su Arıtma Tesislerinin Tasarım ve İşletme Esasları, İstanbul, 2013.

[2] Zhang, J., Martinez, A. E. T. and Zhang, Q., Hydraulic Efficiency in RANS of the Flow in Multi-chambered Contactors, Journal of Hydraulic Engineering, 139, 1150-1157, 2013.

[3] Angeloudis, A., Stoesser, T., Falconer, R.A. and Kim,D.J., Flow, Transport and Disinfection Performance in Small –and Full-Scale Contact Tanks, Journal of Hydro-Environment Research, 9, 15-27, 2015.

[4] Rauen, W.B., Lin, B., Falconer, R.A. and Teixeira, E.C., CFD and Experimental Model Studies for Water Disinfection Tanks with Low Reynolds Number Flows, Chemical Engineering Journal, 137, 550-600, 2008.

[5] Angeloudis, A., Stoesser, T., and Falconer, R.A., Predicting the Disnfection Efficiency Range in Chlorine Contact Tanks Through a CFD-Based Approach, Water Research, 60, 118-129, 2014.

[6] Kim, D., Kim, D.I., Kim, J.H., and Stoesser, T., Large Eddy Simulation of Flow and Tracer Transport in Multichamber Ozone Contactors, Journal of Environmental Engineering, 136, 1, 22-31, 2010.

[7] Wols, B.A., Hofman, J.A.M.H., Uijttewaal, W.S.J., Rietveld, L.C. and Dijk, J.C., Evaluation of Different Disinfection Calculation Methods using CFD, Environmental Modelling & Software, 25, 573-582, 2010.

[8] Zhang, J., Martinez, A.E.T., Lei, H. and Zhang, Q., Indicators for Technological, Environmental and Economic Sustainablity of Ozone Contactors, Water Research, 101, 606-616, 2016.

[9] Zhang, J., Martinez, A.E.T., and Zhang, Q., Evaluation of Large Eddy Simulation and RANS for Determining Hydraulic Performance of Disinfection Systems for Water Treatment, Journal of Fluids Engineering, 136, 121102-121102-9, 2014.

[10] Kim, D., Elovitz, M., Roberts, P.J.W. and Kim, J.H., Using 3D LIF to Investigate and Improve Performance of a Multichamber Ozone Contactor, Americal Water Works Association Journal, 102, 61-70, 2010.

[11] Zhang, Y., Street, R.L. and Koseff, J.R., A Dynamic Mixed Subgrid-Scale Model and Its Application to Turbulent Recirculating Flows, Physics of Fluids, 5, 3186-3196, 1993.

[12] OpenFOAM, The OpenFOAM Foundation; OpenCFD Ltd.: Bracknell, UK, 2015.

[13] Demirel, E. and Aral, M.M., Unified Analysis of Multi-chamber Contact Tanks and Mixing Efficiency Based on Vorticity Field. Part I: Hydrodynamic Analysis, Water, 8, 495-505, 2016.

[14] U.S. EPA. , Disinfection Profiling and Benchmarking Guidance Manual, Appendix A. Rep. No. EPA-815-R-99-013, 1999, U.S. EPA, Washington, D.C

[15] Demirel, E. and Aral, M.M., Unified Analysis of Multi-Chamber Contact Tanks and Mixing Efficiency Based on Vorticity Field. Part II: Transport Analysis, Water, 8, 537-554, 2016.

[16] Elliot, T., Zeier, B., Xagoraraki, I. and Harrington, G. W., Energy Use at Wisconsin's Drinking Water Facilities, Rep. 2003, 222-1, Energy Center of Wisconsin, Madison, WI.

[17] Aral, M.M. and Demirel, E., Novel Slot-Baffle Design to Improve Mixing Efficiency and Reduce Cost of Disinfection in Drinking Water Treatment, Journal of Environmental Engineering ASCE, 143, 9, 1-5, 2017.

[18] Aral, M.M. and Demirel, E., A New Baffle Design to Improve Mixing and Reduce the Flow Through Energy Requirements in Chlorine and Ozone Contact Tanks, Patent # 62/498,260, 10 January 2017.

[19] Angeloudis, A., Stoesser, T., Gualtieri, C. and Falconer, R.A., Contact Tanks Design Impact on Process performance, Environ. Model. Assess. 21, 563-576, 2016.

İMO Teknik Dergi, 2018 8295-8316, Paper 500

Classification of Construction Accidents in Northern Cyprus

Kemal D. TÖZER[1]
Tahir ÇELİK[2]
G. Emre GÜRCANLI[3]

ABSTRACT

This study, carried out in northern Cyprus, encompasses construction accidents occurred between the years 1994 and 2004 and recorded in the archives of the Ministry of Labor and Social Security. Within the scope of the study, victims were classified according to their industrial brunches firstly and it was established that 793 (26.40%) of total 3004 victims worked in the Construction industry. These 793 construction accidents were classified according to date, hour of the accident, type of accident, result of accident, loss of workday, type and place of injury, age, profession, experience and so on. Results reveal that fall from height (37.70%), crashed by an object (10.97%) and struck by an object (10.84%) are most frequent accident types. However, in case of fatal accidents falls again rank first but electrocutions rank second and crashed, jammed in or between objects and traffic accidents share third place. The results are compared with accidents occurred in Turkey and similarities are observed. Unskilled workers are the most frequent victims (34.40%) of these accidents. At observing the frequency of accidents throughout the year, spring and summer appeared to be the periods in which accidents, and deaths resulting from accidents, were most frequent. It is considered that research findings will provide a broad and beneficiary source for the occupational health and safety studies and would aid policy makers in developing countries especially in Turkey and northern Cyprus.

Keywords: Construction industry, occupational health and safety, classification of occupational accidents, Turkey and Northern Cyprus.

1. INTRODUCTION

Construction industry is one of the largest industry globally in providing employment capacity, productivity, and contributing to the economy (ILO, 2015). At the same time, it is

Note:
- This paper has been received on July 03, 2017 and accepted for publication by the Editorial Board on December 27, 2017.
- Discussions on this paper will be accepted by May 31, 2018.

- DOI: 10.18400/tekderg.325546

1 Eastern Mediterranean University, Department of Civil Engineering, Turkish Republic of Northern Cyprus (TRNC) - kemal.tozer@cc.emu.edu.tr
2 International Cyprus University, Department of Civil Engineering, Turkish Republic of Northern Cyprus (TRNC) - tcelik@ciu.edu.tr
3 Istanbul Technical University, Department of Civil Engineering, İstanbul - gurcanlig@itu.edu.tr

among those industries in which occupational accidents occur most frequently, in almost every country (EASHW, 2003; Eurostat, 2009; HSE, 2009; Reyes et al., 2014). Around 30% of occupational accidents worldwide, resulting in death, take place in construction works (Fang et al., 2004; Gürcanlı & Müngen, 2013). Construction industry is a project based industry, different job activities exist, each activity creates different risks and each project has its own characteristics as well as risks. Moreover, contingent forms of contracting exist and coordination of subcontractors as well as main contractors is usually difficult (Çelik & Tözer, 2014; HSE, 2005). According to International Labour Organisation (ILO) data, it can be seen that the probability of fatal accidents of construction workers is 3-4 times higher than other industries in many coutries (ILO, 2015).

In the USA, 20% of fatal accidents and 9% of occupational injuries take place in the construction industry where its share in total employment is between 6 to 7% (Gürcanlı & Müngen, 2013). It was observed that 32% of occupational deaths in the UK, during 2013-2014 period were in the construction industry (HSE, 2014). About 25% of all occupational accidents in Finland are in the construction industry (Nenonen, 2013). Looking at Singapore, it can be seen that construction industry offers employment to 29% of the work force of the country, meanwhile being the cause of 40% of occupational accidents (Chua & Goh, 2004; Feng et al., 2015).

Prevalent construction types, construction methods and techniques, the work force and their culture in construction industry are almost the same in both Turkey and Northern Cyprus (Kıvrak et al., 2014). Therefore, there are similarities in construction works accidents as well. When Turkey is examined for occupational accidents, it shows similarities with the Northern part of Cyprus. 30.5% of all occupational deaths in Turkey are in the Construction industry (Gürcanlı & Müngen, 2013; Çelik & Tözer, 2014; Gürcanlı, 2013; Akboğa & Baradan, 2015; Baradan et al., 2016).

As in all other fields, the existence of statistical data provides strong evidence in Occupational Health and Safety, and works as a guiding tool (Doguwa, 2010). Occupational accidents are being archived in the Northern Cyprus for the last 20 years by the Labor Directorate disorderly. First, the whole archive was transferred to a digital environment, and all of the data was classified to be used effectively to develop countrywide O&H policies.

2. AIM OF THE STUDY

As mentioned above, the presence and quality of statistical data – as in all other fields – presents very strong evidence to experts in the Occupational Health and Safety field, and serves as a tool of direction (Doguwa, 2010). Thus, the aim of this study carried out in the northern part of Cyprus, is to provide a scientific basis to the investigations on occupational accidents and diseases, carried out by the Labor Directorate, and aid to record them in the literature.

In addition, the main goal of this study is to,

- Provide data on past accidents to the technical personnel, working at construction sites, who are responsible for work safety, ,
- Present data to labor inspectors to guide them for a sound inspection,

- Provide the data needed for creating severity indexes and construction accident likelihood for the risk analysis, which will be established through scientific approacheses

by making a detailed analysis of the recorded accidents in the northern part of Cyprus.

3. METHODOLOGY

Firstly, industrial distribution of occupational accidents was established, working on the digital environment. After that, the study focused on accidents in the Construction Industry. During the study, it became essential to re-arrange accident records compatible with the International Classification of Diseases (ICD-10) format.

In the final stage of the study, findings were interpreted and statistical data on occupational accidents, which took place in the Construction Industry, were presented for the use of the industry and experts. In addition to this, suggestions for technical and administrative arrangements towards controlling occupational accidents in the Construction industry and achieving a sustainable improvement were made, and expert views were also provided.

4. RESULTS

In the year 2013, the ratio of workers subjected to occupational accidents in the south of Cyprus was 985.2 out of 100,000 workers (Bruch, 2014). Having a ratio of 6.6 deaths for 100,000 workers in the EU in general, the Construction industry is the most fatal one after the mining and quarrying industry, which has a 10.9 ratio. Moreover, looking into EU countries, it can be seen that South Cyprus is at the top of the scale with the rate of 4.9 deaths out of 100,000 workers (Eurostat, 2013). However, 10-year data of the South of Cyprus shows that, due to gaining of EU membership, a considerable decrease occurred in occupational accidents in the Construction industry (Eurostat, 2014). However, there was a decline in the economy of South Cyprus, which was directly affected by the economic crisis in Greece. As a result of this decline, a decrease of employment was seen in the narrowing Construction Industry, therefore, a more significant decrease in occupational accidents was also observed.

Looking at the Northern part of Cyprus, it can be seen that the population is around 313,000, and 12.6% of the employment is in the Construction Industry (SPO, 2015). The industry is by far leading in occupational deaths. 48% of occupational deaths in the country take place in the construction sites (Çelik & Tözer, 2014).

4.1. Accident Data according to the Industrials

One of the first findings reached through studies on records is about the industrial distribution of occupational accidents. It can be seen that 793 occupational injuries and deaths of a total of 3004 accidents, investigated by the Directorate of Labor for the twenty-year period 1994-2014, took place in the Construction industry. This figure shows that almost a quarter of all casualties are construction workers, or those from or around constructions. The Construction industry is followed by the Manufacturing industry, with 444 casualties (Table 1). A total of

722 accidents, of which 12 are deaths and 710 are injuries, are provided under the heading of 'other industries', which include agriculture & plantation, financial services, education, public services and hotel, tourism & catering services.

Each industry is also examined for the ratio of deaths originating from work, and the Construction industry was found to have the highest death rate after the mining (quarrying) industry (Table 1).

4.2. Construction Industry and Occupational Accidents in this Industry

4.2.1. Economic Development, Industrial Development, and Occupational Accident Relationship:

Northern Cyprus Construction industry is at the top of the industries considerably contributing to economic growth of the country, and according to the data by SPO, it affects 27 sub industries, thus the state of the economy, directly. Therefore, developments in the Construction industry run parallel with economic growth. While the average growth of the industry was 6.8% during the years 2000-2012, general economic growth average was around 4.9%. The Construction industry grew above the general growth rate during the years of economic development, and showed a sharp decline during periods of economic shrinkage. While the industrial growth peaked during the 2004-2005 period, it went into a sharp decline right after those years (SPO, 2012).

Construction industry is a field in which labor is used intensely. Although various construction methods are used, it is estimated that cost of labor for the most widely used construction methods in the country is 40-50% of the total cost (SPO, 2012). With this aspect, the Construction industry is one that creates most of the employment opportunities. The ratio of employment the industry creates among overall employment shows variations in time. The construction employment rate that was 5-6% in the 70's rose up to 19-20% after 2003. However, in parallel with economic fluctuations, the shrinkage in the industry brought this rate under 10% again (SPO, 2015; SPO, 2012).

Unable to achieve a planned and sustainable growth from the point of employment and economic growth, the industry went through sharp declines because of the dead - ends. Parallel to this, unplanned development there resulted Occupational Health and Safety problems which were growing exponentially. This made the Occupational Health and Safety field a problem increasingly difficult to manage. This situation can be observed clearly, when the number of occupational accidents and employment rate are compared year by year. Analysing results of the study, reveals the changing employment capacity of the construction industry throughout years. Moreover, the industry achieved a very rapid growth and development during the 2004-2005 period, right after the years 2001, 2002, and 2003, during which the state economy was revitalized. In parallel, the Construction industry reached its highest levels of employment. The employment rate of Construction industry, which was around 14% during the 90's, rose up to 18% in early 2000's, when an economic and industrial revival was seen. As stated above, this unplanned development in the Construction industry and unusual increase in employment capacity also caused a rise in occupational accidents.

Table 1. Distribution of occupational accidents in the Northern Cyprus during 1994-2014, distribution of the number of deaths and injuries, death rates within industries.

Industry	Death	Injured	Total	(%)	Death Rate Within the Industry (%)
Construction	42	751	793	26.40	5.30
Carpentry	1	190	191	6.36	0.52
Manufacturing	7	437	444	14.78	1.58
Public Service	7	350	357	11.88	1.96
Finance	5	238	243	8.09	2.06
Costal & harbor works	5	117	122	4.06	4.10
Transportation	2	84	86	2.86	2.33
Mining (Quarries)	5	41	46	1.53	10.87
Other industries	12	710	722	24.03	1.66
Total	86	2918	3004	100.00	2.86

Table 2. Employment capacity of the Construction industry in the northern part of Cyprus, its share in total employment, and distribution of fatal accidents in the Construction industry through years, and the comparison of this with South Cyprus and Turkey.

Years	Northern Part of Cyprus			Rep. of Cyprus (Southern Part of Cyprus)			Turkey		
	1	2	3	1	2	3	1	2	3
2000	6199	16.46	50.00	27400	8.52	21.22	761452	3.50	32.30
2001	6038	17.54	80.00	28800	8.72	21.81	681882	3.20	33.80
2002	6521	18.62	0.00	30400	9.04	22.20	713629	3.30	36.60
2003	7071	19.70	33.30	32400	9.43	22.68	685902	3.20	33.80
2004	6953	17.78	37.50	34100	9.63	23.36	752136	3.80	31.30
2005	7467	15.86	66.67	35700	9.88	23.85	933498	4.70	27.10
2006	9157	13.94	57.14	37300	10.11	24.35	1185728	5.80	24.90
2007	8701	12.02	85.71	39400	10.39	25.02	1247970	6.00	34.40
2008	7367	10.10	50.00	40500	10.41	25.68	1238888	5.80	34.30
2009	6356	9.54	16.67	38600	9.99	25.50	1227698	5.80	13.30
2010	6316	8.98	0.00	36300	9.38	25.56	1431000	6.30	33.10

1-Employment in Construction industry (registered)
2-Share (%) of Const Employ. in Total
3-Share (%) of Fatal Const. Accidents

The economic crisis during 2005-2006, and the decline in the Construction industry in the following years, resulted in a decline in the industrial employment capacity. As the employment capacity average of the industry went down to 8.34% during the 10-year period after the economic crisis, the number of occupational accidents also declined.

Comparing Northern Cyprus to the EU member Republic of Cyprus and to Turkey, the first thing that is noticed is that employment capacity of the Construction industry in Northern Cyprus is much higher (in percentage) that South Cyprus and Turkey. Table 2 examines the data of the three neighboring countries during the years 2000-2010. According to the data, Northern Cyprus is far ahead in fatal accidents in the Construction industry. However, the levels of the other two countries are also considerably high.

4.2.2. Distribution of Accidents According to Time of Day:

Examining through time, it can be seen that the number of annual investigations between 1994 and 2004 is quite low. For the first 11-year period of the 20 years under study, average annual investigations were found to be 9.36. The main result of this is that most of the occupational accidents during those years were not reported to the Labor Directorate. For the second half of the 20-year period, however, the average annual investigation figure rose up to 68.6. It is assumed that this increase is the result of coordination between the Labor Directorate and Social Security Office and Department of Health. In addition to this, it is also thought that another reason for the rising number of accidents can be the fact that there was a serious growth in the Construction industry during that period, resulting in an increase in the number of constructions and workers.

A decline is seen in construction works in the Northern Cyprus during summer and winter months because of the effect of the climate (Department Of Meteorology, Republic of Cyprus). Spring and autumn months, on the other hand, are perfectly suitable to carry out construction works. However, autumn being towards the end of the year, usually discourages investors. Therefore, autumn months (September, October, and November), or in other words, last months of the year, are the months with the least activity in construction works, hence the lowest number of occupational accidents. Spring months, being the beginning of the new year, and having suitable weather conditions are preferred by both investors and other stakeholders. Therefore, during the spring months of March, April, and May, more construction works, and more occupational accidents are observed. The weather being very hot in summer months leads to a decrease in construction works, but at the same time, unusual climatic conditions push the limits of workers and increase the risk of accidents. Especially people working in open air, directly subjected to the effects of the sun, can suffer of loss of concentration, difficulty in breathing, dizziness, extreme loss of body fluids, and similar ailments, and consequently face the risk of accidents. Data obtained through the study shows that although construction works are less in summer, the number of accidents comes second after spring. The summer period is followed by autumn, and finally by winter, which is at the end of the year.

In their study, Akboğa and Baradan (2015) focused on the 94 fatal construction accidents in the city of İzmir, in Turkey, during the years 2007-2011. Through their analyses, they established a concentration of fatal accidents on Mondays and Thursdays. Pointing to the fact that workers could have a difficulty in focusing on work during the first day of the week,

and this lack of attention being the cause of accidents on Mondays, however they could not point to any cause for accidents happening on Thursdays. This study established that construction accidents mostly happened at the start of the week, on Mondays and Tuesdays, and the number dwindled towards the end of the week.

Gürcanlı and Müngen (2013), in the study they carried out in Turkey, pointed to the fact that most accidents in constructions took place between 15:00-17:00 hours (right before the end of work), between 10:00-12:00 (right before lunch time), and between 13:00-14:00 (right after lunch), and they interpreted this as hunger, weakness after a meal, and end of day fatigue being the reason for accidents. Findings obtained as a result of this study showed that accidents mostly took place right before and after lunch break, which is in parallel with the findings of Gürcanlı and Müngen. This fact points out that hunger and after meal fatigue can trigger2 accidents (Table 3).

Table 3. Distribution of work-based injuries and deaths in the construction industry by time of the day.

Time Interval	**Death**		**Injured**		**Total**	
	No.	%	No.	%	No	%
4.00 and 7.00	0	0.00 (0.6%)*	3	0.40 (0.4%)	3	0.38 (0.5%)
07:00<t≤08:00	4	9.52 (1.2%)	41	5.46 (0.6%)	45	5.67 (0.8%)
08:00<t≤09:00	4	9.52 (9.3%)	66	8.79 (13.1%)	70	8.83 (11.6%)
09:00<t≤10:00	1	2.38 (11.1%)	71	9.45 (12.5%)	72	9.08 (12.0%)
10:00<t≤11:00	2	4.76 (12.2%)	66	8.79 (13.7%)	68	8.58 (13.1%)
11:00<t≤12:00	1	2.38 (12.3%)	47	6.26 (12.7%)	48	6.05 (12.6%)
12:00<t≤13:00	1	2.38 (2.3%)	30	3.99 (1.4%)	31	3.91 (1.7%)
13:00<t≤14:00	4	9.52 (8.5%)	60	7.99 (8.4%)	64	8.07 (8.4%)
14:00<t≤15:00	5	11.90 (10.5%)	63	8.39 (11.2%)	68	8.58 (10.9%)
15:00<t≤16:00	5	11.90 (12.7%)	71	9.45 (10.4%)	76	9.58 (11.3%)
16:00<t≤17:00	1	2.38 (13.3%)	32	4.26 (12.1%)	33	4.16 (12.6%)
17:00<t≤18:00	3	7.14 (2.5%)	17	2.26 (1.6%)	20	2.52 (1.9%)
18:00<t≤19:00	0	0.00 (1.3%)	12	1.60 (0.6%)	12	1.51 (0.9%)
19:00<t≤20:00	0	0.00 (0.6%)	6	0.80 (0.4%)	6	0.76 (0.5%)
After 8.00 PM	0	0.00 (1.6%)	10	1.33 (0.8%)	10	1.26 (1.1%)
Unknown	11	26.19	156	20.77	167	21.06
Total	42	100,00	751	100,00	793	100,00

*Numbers in the parentheses reveal percentages for Turkey from Gurcanli and Mungen, (2013)

4.2.3. Classification of Construction Accidents:

First of all, as stated earlier, accident records in the study were converted to ICD-10 format, and classified per causes of accidents. According to this, 'falls' type of accidents take the

first place in terms of frequency, and those resulting in death and injury. Looking at accidents resulting in injuries, 'falls' is followed by 'struck by thrown objects'or by a 'projected object', 'crashed, jammed in or between objects', 'sharp object injury', 'falls on the same level', 'injured by falling objects', 'traffic accidents', 'contact with heat or with hot substances', and 'exposure to electricity' type accidents, similar to the study by Akboğa and Baradan (2015). In fatal accidents, 'falls' is followed by 'exposure to electricity', 'crashed, jammed in or between objects', 'traffic accident', 'falling objects', and 'building and construction collapse' type accidents, in that order (Table 4).

Table 4. Causes of Construction accidents with ICD-10 Codes

Causes	Death		Injured		Total	
	No.	%	No.	%	No.	%
Falls (W12, W13)	21	50 (43.7)*	278	37.02 (33.3)	299	37.7
Exposure to electricity (W85, W86)	10	23.81 (11.8)	9	1.2 (2.9)	19	2.4
Crashed, jammed in or between objects (W23)	3	7.14	84	11.19	87	10.97
Trafic Accidents (V00 - V60)	3	7.14 (6.7)	54	7.19 (1.4)	57	7.19
Falling objects (W20)	2	4.76	57	7.59	59	7.44
Building or Construction Collapse (W20)	2	4.76 (6.8)	4	0.53 (3.1)	6	0.76
Cave-ins (while or after excavation) (W20)	1	2.38 (5.5)	5	0.67 (1.9)	6	0.76
Struck by thrown, projected object (W20)	0	0	86	11.45	86	10.84
Sharp object injury (W24 - W29)	0	0 (8.9)	63	8.39 (3.9)	63	7.94
Fall on same level (W01, W03, W10)	0	0	62	8.26	62	7.82
Contact with heat or hot substances (X10 - X19)	0	0 (2.1)	23	3.06 (2.9)	23	2.9
Stricking against or struck by objects (W22)	0	0 (10.5)	8	1.07 (10.7)	8	1.01
Explosins (W36 - W40)	0	0	6	0.8	6	0.76
Contact with chemical Substances (T52 - T59)	0	0	4	0.53	4	0.5
Other	0	0	4	0.53	4	0.5
Unidentified	0	0	4	0.53	4	0.5
Total	42	100	751	100	793	100

*Numbers in the parentheses reveal percentages for Turkey from Gurcanli and Mungen, (2013)

Gürcanlı and Müngen (2013) in the study they carried out in Turkey, rerached similar results. Their findings have been given in parantheses in Table 4. Data in Tablo 4 has been sorted out according to number of fatalities. As the labor office and all other responsible parties have followed and recorded all fatal accidents meticulously, one cannot claim the same same for non-fatal accidents. In Table 5, falls type accidents are examined in detail and divided into three groups such as, 'falls from scaffolds', 'falls from structural elements' and 'other type of falls'. A total of 86 accidents of falls from scaffoldings (of which 5 died) have been recorded. 59 accidents of falls from structural elements have been recorded with 7 deaths. In addition, it was observed that 58 accidents due to falls from movable ladders, or others group, were recorded, with 4 deaths. These facts show that the most frequent type of fall are falls from scaffoldings, but the most fatal fall type are falls from structural elements.

Table 5. Detailed classification of falls

Type of Falls (W12, W13)	Death	Injured	Total
Falls from scaffoldings			
Scaffold failing-breaking-falling	3	24	27
On the scaffold (loosing footing)	1	9	10
On the scaffold (while going up-down)	0	7	7
On the scaffold (erecting-dismantling)	0	5	5
On the scaffold (slipping, loss of balance etc.)	1	36	37
Sub. Total	5	81	86
Falls from structural elements			
Falls from structural element (from the roof)	0	10	10
Falls from structural element (from edges of the slabs)	3	28	31
Falls from structural element (flight of stairs)	1	6	7
Falls from structural element giving in	1	1	2
Falling down through opening on the floor	2	7	9
Sub. Total	7	52	59
Other type of falls			
Moving ladder	4	54	58
From the molds	2	18	20
Into a canal, hole etc.	0	13	13
From a vehicle, machine	2	35	37
Going up on unsuitable object	1	14	15
Other	0	11	11
Sub. Total	9	145	154
Total	21	278	299

Table 6 examines other fatal accident types besides falls, in detail. As shown in the table, exposure to electricity accidents were recorded 19 times, and 10 of these resulted in deaths. These point to the fact that electrical accidents are more deadly than falls from structural elements. Again, in Table 6, 'crashed, jammed in or between' type of accidents are grouped under five sub-headings, and 5 of the 145 victims lost their lives.

Table 6. Detailed classification of other type of accidents

Type of other Fatal Accidents	Death	Injured	Total
Exposure to Electric (W85, W86)			
Contact with live electricity	4	3	7
Contacting aerial electric cable	2	3	5
Contacting electric cable in the open	1	2	3
Contacting cable placed in the wall-floor	1	1	2
Electric shock of other types	2	0	2
Sub.Total	10	9	19
Other type of fatal accidents			
Crushed between a stationary and a moving object (W23)	2	48	50
Crushed under a fallen object (W20)	2	60	62
Crushed between moving objects (W23)	0	4	4
An organ getting jammed in a machine (W23)	0	15	15
Crushed under a load (W23)	1	13	14
Traffic Accidents (V00-V60)	3	54	57
Building & Construction Collapse (W20)	2	4	6
cave-ins (W20)	1	5	6
Other	0	1	1
Sub.Total	11	204	215
Total	21	213	234

4.2.4. Facts About Victims:

In this study, construction workers, who suffered an accident, are divided into groups according to the kind of work they were doing on the construction site. In other words, they are divided into groups based on their vocation. As it can easily be understood, the group mostly affected by accidents is the group of 'unskilled workers' (Table 7). It is assumed that, this arises from the fact that a great number in the work force in the Construction industry is made up of 'unskilled workers'. Another reason is the fact that the 'unskilled workers' group

has the least work experience and training in the industry (Çelik et al. 2012). In underdeveloped countries, and in developing countries, like in Northern part of Cyprus, most of the employers refrain from providing vocational training to new workers.

Instead of giving them vocational training, inexperienced workers are forced to start from the lowest level of work at the site, and expected to learn the job by themselves in time and without help or supervision. Inexperienced workers pay for this faulty attitude of employers – which has become habitual due to the local conditions – by getting injured, and sometimes even by losing their lives. New and untrained workers in the Construction industry go through their training process in the field, as 'unskilled workers'. Given the situation as it is, 'unskilled workers' turn out to be the group suffering from most accidents, with 30.09% injury, and 28.57% death rates. 'Unskilled workers' group is followed by 'formwork skilled workers', with 14.29% death and 11.58% injury rate, and 'paint/plaster skilled workers' with 10.29% death and 11.58% injury rate. Rates regarding 'Operators', 'welders', 'electricians', and 'steel fixers' job type groups are shown in Table 7.

Accident victims were later examined by dividing them into 7 groups according to their field titles, and their ages. After establishing 6 age groups, as shown in Table 8, the number of victims in each group was figured out. According to this, a total of 23 victims (of which 4 were deaths) were collected in 7 different title groups within the under 20 year old designation. In the 20+ group, a total of 275 victims were established, of which 9 lost their lives. These figures place the 20+ group in the first place regarding their exposure to accidents, but behind the 30+ group in deaths. While at least 1 death or injury was registered in the 20's group, except for the 'employer' designation. 'Unskilled worker' designation group had the most death and injury incidents recorded within the 20's group. The age group with the highest number of deaths (13) is the 30's age group, with a total of 271 accident victims. At least 1 death or injury was recorded in the other 6 groups within the 30's designation, except for the '3rd party' and 'secretary' groups. 'Unskilled worker' group is again at the top for deaths and injuries, within the 30's age group. 40's age group is in the 3rd place with a total of 154 victims, 6 of which are deaths. While at least 1 death or injury was recorded in the 40's age group except for the 'employer' and 'secretary' title designations, 'unskilled worker' group is again at the top of the count regarding deaths and injuries. A total of 51 accidents were recorded for the 50's age group, of which 6 were deaths, and 1 death and 4 injuries were recorded for the 60's age group. As stated above, the 'unskilled worker' group for all age ranges rank at the top in terms of accidents.

Later, it was attempted to establish how often each job type group encountered any type of accident. According to this, as it is shown in Table 9, the most frequent accident type, which is the 'falls' type, is a great risk for almost all job type groups. As for the 'unskilled workers', who encounter the highest number of accidents, it can be seen that they are prone to all types of accidents. It is assumed that this arises from the fact that 'unskilled workers' are used in all activities and levels of the construction. Another reason is that 'unskilled workers' group is frequent in the field. It is also observed that 'paint/plaster skilled workers' are affected from 'falls' type of accidents most frequently, and they encounter more often the 'fall on same level' and 'falling object' type of accident risks in that order. Looking at 'steel fixers', it can be seen that after 'falls' accidents, they encounter 'crashed, jammed between objects' accidents more frequently.

Table 7. Distribution of fatal and non-fatal accidents according to job types

Job Types	Death	Injured	Total
	No.	No.	No.
3rd Party	1	3	4
Alum. PVC Skilled Worker	0	15	15
Asphalt Skilled Workers	1	5	6
Assembly Personnel	0	17	17
Carpenter	0	21	21
Ceramic Skilled Worker	2	23	25
Concrete Skilled Worker	0	9	9
Electrician	3	31	34
Employer	2	4	6
Eng. / Arch. / Mng.	1	5	6
Foreman	0	18	18
Formwork Skilled Workers	6	87	93
Gatekeeper	0	4	4
Insulation Works	0	11	11
Mechanics	0	11	11
Operators	3	68	71
Paint/Plaster Skilled Worker	6	82	88
Plumber / Pipe Fitter	1	21	22
Roofer	0	5	5
Secretary	0	2	2
Steel Fixer	2	31	33
Unskilled Workers	12	226	238
Wall Works Skilled Worker	0	9	9
Welders	1	39	40
Unknown	1	4	5
Total	42	751	793

The reason for this is that, besides working at heights, they do works like hand, carrying of objects, shaping materials by applying power, or using powerful mechanical tools. This increases the risk of getting jammed between the material and the power tool . 'Electricians' working at construction sites also suffer 'falls' type accidents because they work at heights (Table 9). However, another increased risk for 'electricians' is their working with electricity,

which is reflected in the consequences. After the 'unskilled workers' group, 'formwork skilled workers' encounter the most accidents at construction sites. Besides being victims of 'falls' type accidents often, because they work at heights and mostly close vicinity to the edges, they also face accidents like 'fall on same level' and 'falling object'. 'Operators' use vehicles, and therefore work at ground level; but operators who use large work machines can also suffer injuries from 'falls' (from machine) while servicing the machines and doing maintenance work. However, the most frequent accidents facing operators are 'falls, 'traffic accidents, and 'crashed, jammed between objects', in that order.

At a later stage, it was examined whether workers who encounter accidents had received any training about the work they did or not. This examination showed that a great number of accident victims did not receive any occupational training (Table 10). As stated previously, most of the employers in Northern Cyprus refrain from providing occupational training to new workers, and they leave them to learn the work on the site by themselves. Moreover, at the beginning of this study, no licensed institution was found in the Northern Cyprus providing Occupational Health and Safety training. The only educational work done for the industry in the field of Occupational Health and Safety in Northern Cyprus was the Occupational Health and Safety Expertise education, which was initiated in 2014 by the Labor Office.

Figures given in Table 10 show the graveness of the problem with the training status of the employees. According to these figures, only 21 out of 793 victims, that is 2.6% had training prior to beginning work. A survey by Çelik et al. (2012) on the training level of Construction industry workers in northern part of Cyprus, arrived at a similar conclusion. Again, in Table 11, it can be seen that the job type group with the least vocational training is 'unskilled laborers'.

First thing that is noticeable in Table 10 is that a large part of the victims (16.9%), especially those losing their lives, is the ones whose vocational experience were not established, or somehow not registered. In addition, it was established that 27.59% of accident victims were injured during their first month at work, and 5.93% lost their lives during the 1-6 months at work. On the other hand, the death rate of all accidents was 5.3%. Hence, the conclusion that accidents resulting in deaths are related to experience at work.

Analysis of the place of injuries on bodies of the accident victims are given in detail in Table 11. Looking at the analysis results, place of wounds on the body parts of most of the victims registered (98.36%) have been recorded. According to this, 40.86% of the victims received wounds in 'hands and arms', but these wounds did not cause deaths. Similarly, 24.97% of the victims received wounds in 'legs and feet', and these also were not deadly. 'Innards and torso' wounds were seen in 3.40% of injuries and these also did not cause deaths. On the other hand, injuries in the 'waist, neck, and spinal column' region made up 4.04% of accidents and 3.13% of these resulted in deaths. Similarly, injuries in the 'face, head, and skull' region amounted to 10.34% of the accidents, and 8.54% of these caused deaths. In some accidents, victims were injured in more than one part of the body. This type of injuries (different parts of the body) made up 9.46% of all accidents, and 4% of these resulted in deaths. The most dramatic result noticeable in Table 11 is that a great part of those victims who lost their lives received wounds comprising the whole of the body (all body). While almost all of such accidents are referred to as serious accidents, and make up 5.30% of all accidents, the death rate of these was established as 69.05%.

Table 8. Distribution of Victims in the Construction industry among Age Groups and Job Types

	≤19		20≤x≤29		30≤x≤39		40≤x≤49		50≤x≤59		≥60		Unknown		Total		
Job Types	Death	Injured	Death	Injured	Death	Injured	Death	Injured	Death	Injured	Death	Injured	Death	Injured	Death	Injured	Total
3rd Party	1			1		1						1			1	3	4
Alum. PVC Skilled Worker		2		5		2		4		1				1		15	15
Asphalt Skilled Workers				2		2	1			1					1	5	6
Assem bly Perso nnel				8		8		1								17	17
Carpe nter				5		9		3		4						21	21
Ceramic Skilled Worker	1	2		11		6	1	2						2	2	23	25
Concrete Skilled Worker				4		3		2								9	9
Electri cian			1	12	2	12		4		1		1		1	3	31	34
Employ er							1	2	1	2					2	4	6
Eng. / Arch. / Mng.				3	1	1		1							1	5	6
Foreman				2		6		5		4		1				18	18
Formwo rk Skilled Workers		3	2	29	1	33	1	15	2	5				2	6	87	93
Gatekee per				1		1		2								4	4
Insulati on Works				4		5		1		1						11	11
Mecha nics				6		5										11	11
Opera tors			2	14		25		25	1	4					3	68	71
Paint/ Plaster Skilled Worker	1		1	29	1	31		18	2	3	1			1	6	82	88
Plumber / Pipe Fitter				9	1	7		3		2					1	21	22
Roofer				2		3										5	5
Secretary				2												2	2
Steel Fixer		2		10	2	11		5		2				1	2	31	33
Un- skilled Workers	1	8	3	91	4	66	2	48		11		1	2	1	12	226	238
Wall Works Skilled Worker				2		3		3		1						9	9
Welders		2		13	1	17		4		3					1	39	40
Un- known				1		1							1	2	1	4	5
Total	4	19	9	266	13	258	6	148	6	45	1	4	3	11	42	751	793

All the details of analyses carried out in relation to the type of injuries that victims received are shown in Table 12. Looking at analysis results, injury types of most of the victims registered (98.61%) have been established. According to this, 1.64% of the victims had 'trauma', 2.90% 'loss of limbs', and 0.25% 'contact with chemicals' type of injuries, but these did not cause death. The ratio of victims who received 'fracture' type wounds is 41.87%, and such injuries caused deaths at the rate of 0.30%. Although causing deaths at a rather low ratio, 'fracture' type injuries have been the most frequently encountered injuries. It was established that 'burn' type injuries were seen in 3.15% of accidents, and they caused deaths at the rate of 4.00%.

Table 9. Distribution of Accidents according to Job Type versus Accident Type

Job Type	Building & Construction Collapse	Cave-in	Contact with Chemical Substances	Contact with heat or hot substances	Crashed, Jammed Between Objects	Explosives	Exposure to Electricity	Fall on Same Level	Falling Objects	Falls	Sharp Object İnjury	Striking against or struck by objects	Struck by thrown, projected object	Traffic Accident	Unknown
3rd Party		1								3					
Alum. PVC Skilled Wo.								2	1	5	5		2		
Asphalt Skilled Wor.				2	2					1				1	
Asse mbly Perso nnel					1			2	1	10	2		1		
Carp enter								3	1	8	7	1	1		
Ceramic Skilled Wor.					3		2	1	2	7	4		6		
Concrete Skilled Wor.	4									2				3	
Electri cian				1	5		5	3	2	7	4		4	2	1
Emp loyer					1		1			4					
Eng. / Arch. / Mng.					1	1				3	1				
Foreman					2	1		2	1	7	2		1	2	
Form work Skilled Wor.		2			5		1	9	5	49	7		12	3	
Gate keeper								1	1	1				1	
Insul ation Works					1	1		1	1	6	1				
Mecha nics			1	1	1	1		1	3	1	2				
Opera tors		1		7	9		1	2	3	19		3	8	18	
Paint/ Plaster Skilled W.				1	2		1	10	6	54	3	1	4	2	4

Table 9. Distribution of Accidents according to Job Type versus Accident Type (continue)

Job Type	Building & Construction Collapse	Cave-in	Contact with Chemical Substances	Contact with heat or hot substances	Crashed, Jammed Between Objects	Explosives	Exposure to Electricity	Fall on Same Level	Falling Objects	Falls	Sharp Object İnjury	Striking against or struck by objects	Struck by thrown, projected object	Traffic Accident	Unknown
Plumb er / Pipe Fitter					1				3	13	3		2		
Roofer										3			2		
Secretary								1						1	
Steel Fixer					9		1	1	2	10	1		4	5	
Un-skilled Wor kers	2	2	2	9	37	1	5	19	22	68	16	3	32	18	2
Wall Works Skilled W.					3			2	1	1	1		1		
Wel ders			1	1	4	1	2	1	4	16	4		6		
Un-known				1				1		1				1	1
Total	6	6	4	23	87	6	19	62	59	299	63	8	86	57	8

Table 10. Experience and Vocational Training Status of Workers according to Job Types

Job Type	**Working Experience (Months)**									**Training**			
	0	**1<x<6**	**7<x<12**	**13<x<36**	**37<x<72**	**73<x<108**	**>108**	**Unknown**	**Total**	**Unknown**	**Trained**	**Not Trained**	**Total**
3rd Party	4								4	2		2	4
Alum. PVC Skilled Wor.		3	3	1	2	1		5	15	4		11	15
Asphalt Skilled Workers				1	1		4		6	2		4	6
Assembly Personnel	1	2	1	4	1	2	1	5	17	6	1	10	17
Carpenter			6	6		1	4	4	21	5		16	21
Ceramic Skilled Worker	1	2	7	2	2	4	1	6	25	11		14	25
Concrete Skilled Worker		2	2	3		1	1		9	3		6	9
Electrician	1	6	7	4	5	3	3	5	34	8	8	18	34
Employer				1	2		1	2	6	1		5	6
Eng. / Arch. / Mng.	1	1		2		1	1		6		6		6
Foreman		3	2	3	3	3	4		18	4	1	13	18

Table 10. Experience and Vocational Training Status of Workers according to Job Types (continue)

Job Type	Working Experience (Months)									Training			
	0	1<x<6	7<x<12	13<x<36	37<x<72	73<x<108	>108	Unknown	Total	Unknown	Trained	Not Trained	Total
Formwork Skilled Wor.	3	13	26	9	7	5	4	26	93	28		65	93
Gatekeeper		1			2		1		4	1		3	4
Insulation Works		2	1	2	2	1		3	11	3		8	11
Mechanics				8	1		1	1	11	3		8	11
Operators		15	14	14	5	3	13	7	71	17	3	51	71
Paint/ Plaster Skilled Wo.	2	16	17	18	10	8	7	10	88	24		64	88
Plumber / Pipe Fitter		3	2	8	4		3	2	22	8		14	22
Roofer		2	1	1				1	5	3		2	5
Secretary		1	1						2		1	1	2
Steel Fixer	2	4	6	6	2		1	12	33	8		25	33
Unskilled Workers	13	40	57	45	27	3	17	36	238	79		159	238
Wall Works Skilled Wor.			5	2			1	1	9	2		7	9
Welders	1	2	2	9	11	4	6	5	40	12	1	27	40
Unknown			1		1			3	5	5			5
Total	29	118	161	149	88	40	74	134	793	239	21	533	793

Table 11. Job types vs. place of injuries on the body

Injured Part of the Body									
Job Type	**All Body**	**Different Parts**	**Face, Head & Skull**	**Hands and Arms**	**Innards and Torso**	**Legs and feet**	**Unknown**	**Waist, Neck & S.Column**	**Total**
3rd Party	1					2	1		4
Alum. PVC Skilled Wor.		3		9		3			15
Asphalt Skilled Workers	1	1		2		2			6
Assembly Personnel		2	1	9		5			17
Carpenter			2	12	1	5		1	21
Ceramic Skilled Worker	2		1	13		7		2	25
Concrete Skilled Worker		2		1	1	5			9

Table 11. Job types vs. place of injuries on the body (continue)

Injured Part of the Body									
Job Type	**All Body**	**Different Parts**	**Face, Head & Skull**	**Hands and Arms**	**Innards and Torso**	**Legs and feet**	**Unknown**	**Waist, Neck & S.Column**	**Total**
Electrician	3	3	2	16	1	7		2	34
Employer	1	1	1	1	1	1			6
Eng. / Arch. / Mng.	1	2		3					6
Foreman		3	1	8	2	4			18
Formwork Skilled Wor.	5	15	7	42	6	13		5	93
Gatekeeper		1				3			4
Insulation Works	1	1		3	1	4		1	11
Mechanics	1	2		6		1		1	11
Operators	4	7	9	25	3	16	3	4	71
Paint/Plaster Skilled Wo.	5	3	12	30	2	23	4	9	88
Plumber / Pipe Fitter	1	2	3	9	1	6			22
Roofer		1	2	1		1			5
Secretary		1						1	2
Steel Fixer	2	3	3	15	3	5	1	1	33
Unskilled Workers	12	19	30	97	3	72	2	3	238
Wall Works Skilled Wor.			2	3		4			9
Welders	1	3	6	19	2	8		1	40
Unknown	1					1	2	1	5
Total	42	75	82	324	27	198	13	32	793

It was also seen that ‘interior organs’ type injuries made up 16.02% of the accidents and 7.87% of those resulted in deaths. On the other hand, ‘open wound injury’ type accidents made up 21.56% of all accidents, and 0.58% of these resulted in deaths. It was also seen that these types of injuries (different types of injuries) are 11.22% of all accidents, but 32.58% of them caused deaths. This situation shows that in accidents, where different types of injuries are seen at the same time, count at the top of fatal incidents.

Table 12. job types vs type of the injuries

Type of the injuries										
Job Type	**Burns**	**Closed Iniury**	**Contact with Chemicals**	**Diferent type of iniures**	**Fracture**	**Loss of limbs**	**Open İnjury**	**Trauma**	**Unknown**	**Total**
3rd Party				1	2				1	4
Alum. PVC Skilled Wor.		2		1	4		8			15
Asphalt Skilled Workers	2	1		1	2					6
Assembly Personnel		5			7		4	1		17
Carpenter		2			8	2	7	2		21
Ceramic Skilled Worker		4		2	10		9			25
Concrete Skilled Worker		3		2	2		2			9
Electrician	3	6		2	13	1	8	1		34
Employer		1		2	3					6
Eng. / Arch. / Mng.				2	2	1	1			6
Foreman				3	9		6			18
Formwork Skilled Wor.		22		14	38	2	17			93
Gatekeeper		2			2					4
Insulation Works	1	2			6		1	1		11
Mechanics	1	2		1	2	1	4			11
Operators	7	9		8	32	2	11		2	71
Paint/Plaster Skilled Wo.	1	15		9	43	2	13	1	4	88
Plumber / Pipe Fitter		1		2	15		4			22
Roofer		1		1	1		1	1		5
Secretary				1				1		2
Steel Fixer		5		9	7	1	11			33
Unskilled Workers	8	37	1	24	103	10	51	2	2	238
Wall Works Skilled Wor.		1			4		4			9
Welders	2	6	1	3	15	1	9	3		40
Unknown				1	2				2	5
Total	25	127	2	89	332	23	171	13	11	793

5. CONCLUSION

Detailed analysis of the construction accidents occurred in Northern Cyprus between 1994 and 2014, reveals the alarming situation of the industry. As stated at the beginning of this study, high risks present in the nature of this industry. However, employers have not realized the importance of safety management as well as implementing very basic preventive measures yet. Of course the secondary factors may be stated as the unconsciousness of workers and employers, who have to work face to face with these risks. As it is clearly pointed out in the study, training level of workers in the Construction industry, and their awareness of Occupational Health and Safety are quite low. Additionally, a great number of construction companies did not provide any training for their employees in the field of Occupational Health and Safety. This is another element contributing to the dramatic situation of the industry.

Learning from past experience, in other words historical records that include types of accident, work type, activity at time of accident, and so on is important for accident prevention because every construction projects may have some similarities with the past projects. For establishment and implementation of safety management on the construction site, these kinds of past data may provide necessary background knowledge. If we focus on the accidents in the industry, it can be seen that falls type accidents leads first and these accidents, mostly resulting in deaths, which generally took place in multi-story buildings, and on scaffoldings. In addition, the work type that is most prone to accidents, injuries, and deaths, is the unskilled workers group.

Projects run by the EU on the island, recently, and support programs, have paved the way for some serious developments in the field of Occupational Health and Safety. However, the works and encouragements of the EU in the field are not sufficient for needed improvements by themselves. The economic, political, and legal problems in the field of Occupational Health and Safety in the country need to be taken into consideration systematically by the political and legal institutions of the country.

Acknowledgements

Authors of this study would like to thank Director, Vice-Director and all the personnel of the Labor Office of the Northern Cyprus for their contributions.

References

[1] Akboğa Ö., Baradan S., (2015). An Examination of the Characteristics of Fatal Accidents in the Construction industry: Izmir Field Study. *Proceeding of the 5th Symposium on Worker Health and Work Safety Presentations, Chamber of Civil Engineers Izmir Branch, Turkey*, Vol.1 pp. 215-224.

[2] Baradan S. Akboğa Ö. Çetinkaya U. Usmen MA. (2016) Univariate and Cross tabulation Analysis of Construction Accidents in the Aegean Region.*Teknik Dergi.* 27(1), 7345-7370.

[3] Bruch E., (2014). *International Safety and Health Construction Co-coordinators Organizations, Evaluation of the EU Occupational Safety and Health Directives,* Construction Sites – 92/57/EEC.

[4] Chua, D.K.H., Goh, Y.M., (2004). Incident causation model for improving feedback of safety knowledge. *J. Constr. Eng. Manage.* 130 (4), 542–551.

[5] Çelik. T., Tözer. KD, İlter O., Köseoğlu O., (2012). Training Work within the scope of Occupational Safety and Health Administration System and the Effects of this Application on Workers. *Proceedings of the PYYK 2012, Izmir Higher Technological Institute, Izmir.*

[6] Çelik. T., Tözer. K.D., (2014). General Analysis of Occupational Accidents in the TRNC, and the Situation in the Construction industry: Effects of the Workers' Level of Education and Culture on Occupational Accidents, *Proceedings of the PYYK 2014, Akdeniz University, Antalya.*

[7] Doguwa S.I., (2010). Statistics for National Development, *Journal of Applied Statistics* Vol.1 No.1, 99-106.

[8] European Agency for Safety and Health at Work -EASHW-, (2003). *Facts: Accident Prevention in the Construction industry*. European Commission Senior Labour Inspectors' Committee, Belgium.

[9] European Commission. Eurostat (2009). *European Statistics in Focus 63/2009: Population and Social Conditions.* European Communities. Luxembourg.

[10] European Commission. Eurostat (2013). *European Social Statistics*. Luxembourg.

[11] European Commission. Eurostat (2014). *International Safety and Health Construction Coordinators Organization - Evaluation of the EU Occupational Safety and Health Directives,* Construction Site - 92/57/EEC. Luxembourg.

[12] Fang D.P., Huang X.Y., Hinze J., (2004). Benchmarking studies on construction safety management in China, *J Cons. Eng. Man*, 130, 424-32.

[13] Feng Y. Zhang S. Peng W., (2015). Factors influencing workplace accident costs of building projects, *Safety Science* 72, 97-104.

[14] Gürcanlı G. E., (2013). An Analysis of Deaths and Injuries in the Construction industry, Turkish Medical Doctors Union, *Journal of Occupational Health and Safety*, Vol. 2013/2, 20-29.

[15] Gürcanlı G. E., Müngen U., (2013). Analysis of Construction Accidents in Turkey and Responsible Parties, *Industrial Health*, Vol.51, 581-595.

[16] Health and Safety Executive, (2005). *Health and Safety Induction for Smaller Construction Companies Site Safety* - Scotland, UK.

[17] Health and safety Executive, (2010). *2009/2010 Health and Safety Executive Statistics* (INDG345), UK.

[18] Health and safety Executive, (2014). *Health and Safety in Construction in Great Britain,* UK.

[19] International Labour Organization, (2015). *Construction: a hazardous work*, Available: http://www.ilo.org/safework/areasofwork/hazardous-work/WCMS_356576/lang--en/index.htm.

[20] Kıvrak S., Arslan G., Tuncan M., Bingönül M.T., (2014). Impact of national culture on knowledge sharing in international construction projects, *Canadian Journal of Civil Engineering*, 2014, Vol.41 (7): 642-649.

[21] Leung, C.W., Chow, W.K., (2002). A brief review on construction safety in some Southeast Asian countries, *Fire Science and Technology,* Vol.45, 39–49.

[22] Nenonen N., (2013). The Finnish Occupational Accidents and Diseases Statistics Database Employed for Safety Promotion, *Tampere University of Technology.*

[23] Reyes J.P., San-Jose J.T., Cuadrado J., Sancibrian R., (2014). Health & Safety Criteria for determining the sustainable value of construction projects, *Safety Science*, vol.62, pp 221-232.

[24] State Planning Organization, (2012). *Macroeconomic and Industrial Developments in 2009*, SPO-MSG 2012-6, State Printing Office, TRNC.

[25] State Planning Organization, (2015). *Macroeconomic and Industrial Developments 2010-2013*, SPO-MSG 2013-7, State Printing Office, TRNC.

[26] ICD-10, International Statistical Classification of Diseases and Related Health Problems 10th Revision, WEB: http://apps.who.int/classifications/icd10/browse/2016/en. Date:17/03/16.

[27] Department Of Meteorology, Republic of Cyprus. The Climate of Cyprus.

[28] http://www.moa.gov.cy/moa/ms/ms.nsf/DMLcyclimate_en/DMLcyclimate_en?Open Document

İMO Teknik Dergi, 2018 8317-8338, Paper 501

Modeling Laminated Orthotropic Plate-Foundation Interaction Subjected to Moving Load Using Vlasov Model

Korhan ÖZGAN[1]

ABSTRACT

In this study, dynamic behavior of laminated orthotropic plates on elastic foundation is investigated adapting the three-parameter subsoil model. Analysis of the system is performed by using the software SAP2000 combining with MATLAB code for calculation of soil parameters for modified Vlasov model. A computing tool is coded in MATLAB for the purpose, allowing data exchange between SAP2000 and MATLAB via Open Application Programming Interface (OAPI) feature. The consistency of the proposed model is shown by a numerical example taken from the literature. Subsequently, the effects of lamination scheme, various lamination angles, lamination number, subsoil depth, elasticity modulus of subsoil, plate thickness and the velocity of moving load on the behavior of laminated orthotropic plates on elastic foundation are investigated. It is concluded that it is a convenient approach to use OAPI feature of SAP2000 to model the complex behavior of laminated orthotropic plates on elastic soil, under moving loads.

Keywords: Moving load, elastic foundation, laminated orthotropic plate, OAPI.

1. INTRODUCTION

The analysis of engineering structures in contact with subsoil is still important today. Especially in recent years, rapid developments in the industry and use of composites in the sector caused an increase in the studies on soil-structure interaction. For years, the relationship between soil and structure is investigated by modeling as plate or beam on elastic foundation. Beams or plates on elastic foundation are used in many engineering areas such as aerospace industry, mechanical engineering, dentistry, liquid and gas transmission lines, aircraft hangars, airfields, highway and railway pavements. Railways, highways and airfield pavements are usually subjected to traversing moving loads such as wheel loads from moving vehicles and planes. It is therefore interesting and important for engineers to understand the dynamic behavior of the plates or beams on elastic foundations before their structural design.

Not: Bu yazı
- This paper has been received on September 21, 2017 and accepted for publication by the Editorial Board on February 07, 2018.
- Discussions on this paper will be accepted by May 31, 2018.

• DOI: 10.18400/tekderg.339219

1 Karadeniz Technical University, Dep. of Civil Engineering, Trabzon, Turkey - korhanozgan@yahoo.com

Dynamic behavior of plates resting on elastic foundations subjected to moving loads has been studied by researchers for many years incorporating various types of soil models. Kim and Roesset [1] investigated the dynamic response of an infinite plate on Winkler-type elastic foundation subjected to constant amplitude or harmonic moving loads. Huang and Thambiratnam [2] developed a procedure incorporating the finite strip method and a spring system for the dynamic response of plate resting on an elastic foundation, subjected to moving loads. Kim [3] investigated the stability and dynamic displacement response of an infinite thin plate resting on a Winkler-type or a two parameter elastic foundation subjected to in-plane static compressive forces and a distributed moving load with a constant velocity. Lu et al. [4] examined vibration behavior of a plate on a two-parameter foundation subjected to moving rectangular loads of varying velocities.

On the other hand, composite materials are widely used in various fields of engineering like aerospace, naval, automotive and civil, owing to high strength or stiffness sections for lower weight using various fiber orientations and lamination schemes. Accordingly, studies on laminated orthotropic plates subjected to moving load had been carried out by many authors. Wang [5] developed a mixed finite element formulation based on the Mindlin-Reissner plate theory for a moving orthotropic thin plate. Zhu and Law [6] analyzed the dynamic behavior of an orthotropic plate under moving load using Lagrange equation and modal superposition. Alisjahbana [7] presented an approximate method for determination of the natural frequencies and mode shapes of rectangular clamped orthotropic plates subjected to dynamic moving loads. Lee and Yhim [8] performed dynamic analysis of single and two-span continuous composite plate structures subjected to multi-moving loads. Law et al. [9] investigated the problems of identification of moving loads on a three-dimensional bridge deck. Hatami et al. [10] studied free vibration of axially moving symmetrically laminated plates subjected to in-plan forces using the classical plate theory. Ghafoori and Asghari [11] investigated the dynamic response of angle-ply laminated composite plates traversed by a moving mass or a moving force. Malekzadeh et al. [12] presented a solution procedure based on the three-dimensional elasticity theory for the dynamic response of cross-ply laminated thick plates subjected to moving load. Thai et al. [13] investigated static, free vibration, and buckling behavior of laminated composite plates using the first-order shear deformation theory. Chen et al. [14] studied the dynamic instability of laminated composite plates under thermal and arbitrary in-plane periodic loads using first-order shear deformation plate theory. Patel [15] studied the geometric nonlinear bending behavior of laminated composite stiffened plates subjected to uniform transverse loading.

However, combination of laminated orthotropic material properties with subsoil effects at the same time in a study is very rarely found. Özçelikörs et al. [16] presented new functional and finite elements for interaction of orthotropic plate-foundation using the Gateaux differential and Pasternak type elastic foundation model. Pradhan and Kumar [17] studied vibration of orthotropic single layered graphene sheets embedded in Winkler-type and Pasternak-type elastic medium using nonlocal elasticity theory and differential quadrature method. Akgoz and Civalek [18] performed geometrically nonlinear free vibration analysis of thin laminated plates resting on non-linear elastic foundations. Vosoughi et al. [19] investigated dynamic response of moderately thick antisymmetric cross-ply laminated rectangular plates on Pasternak type elastic foundation using higher order shear deformation theory. Afsharmanesh et al. [20] solved buckling and vibration characteristics of circular laminated plates under in-plane edge loads and resting on Winkler-type foundation by the

Ritz method. Mantari et al. [21] presented a free vibration analysis for functionally graded plates resting on Pasternak type elastic foundation using a quasi-3D hybrid type HSDT with 5 unknowns. Alipour [22] developed a new analytical approach for bending and stress analysis of angle-ply laminated composite and sandwich plates on non-uniform elastic foundation. Studies on laminated orthotropic plates on three parameter elastic foundation subjected to moving load have not been encountered yet in the literature.

As the first attempt, dynamic response of laminated orthotropic plates on elastic foundation under moving load is studied by using modified Vlasov foundation model. SAP2000 [23] software for the finite element analysis of soil-structure system with MATLAB [24] software for the calculation of soil parameters according to modified Vlasov model were used simultaneously. A computing tool was developed to provide two-way data exchange between SAP2000 and MATLAB by employing Open Application Programming Interface (OAPI) feature of SAP2000 software. Further, the effects of lamination scheme, various lamination angles, lamination number, subsoil depth, elasticity modulus of subsoil, plate thickness and velocity of moving load on the behavior of laminated orthotropic plates on elastic foundation were examined.

2. SAP2000 OPEN APPLICATION PROGRAMMING INTERFACE

With OAPI feature, the user is able to access SAP2000 by an external application with help of any supporting programming language such as Visual Basic, Microsoft Excel and MATLAB. It also allows users to build, analyze and design and to obtain analysis and design results. Structural model may be created via SAP2000 software. Any information for the structural model may be sent to SAP2000 with OAPI using a programming language. The desired features of SAP2000 may be accessed and performed for analysis or design. Analysis or design results of SAP2000 into any application may be transferred. In other words, finite element analysis is performed by SAP2000 and the results can be utilized by an external application [23].

In this study, SAP2000 was used interactively with a computing tool coded in MATLAB using OAPI functions for the analysis of laminated orthotropic plates on elastic foundation according to the modified Vlasov model.

3. THEORETICAL FORMULATION AND FEM MODEL

If modified Vlasov model is used to model soil structure interaction, the dynamic equation of the plate receiving vertical reaction of the subsoil into account without damping can be written as,

$$D\nabla^4 w(x,y,t) - 2t\nabla^2 w(x,y,t) + kw(x,y,t) + m\frac{\partial^2 w(x,y,t)}{\partial t^2} = p(x,y,t) \quad (1)$$

where w, m and p denote vertical displacement of the plate, mass density and the magnitude moving load respectively. k and $2t$ depict subgrade reaction modulus and shear deformation

parameter of the subsoil. Value of γ and β coefficient for Newmark-β method used for time integration of Eq.(1) are taken as 0.5 and 0.25 respectively [25].

If $P(x,y,t)$ is zero in Eq.(1), free vibration equation of a plate on elastic foundation is obtained.

Subsoil reactions of elastic foundation to a plate may be given by equation below depending on the displacement function *w* of the subsoil surface when modified Vlasov model is considered.

$$q_z = kw(x,y,t) - 2t\left(\frac{\partial^2 w(x,y,t)}{\partial x^2} + \frac{\partial^2 w(x,y,t)}{\partial y^2}\right) \tag{2}$$

Subgrade reaction modulus (*k*) and shear deformation parameter (2*t*) of subsoil for modified Vlasov model in above expression may be defined as

$$k = \int_0^{H_s} \frac{E_s(1-\nu_s)}{(1+\nu_s)(1-2\nu_s)}\left(\frac{\partial\varphi(z)}{\partial z}\right)^2 dz \tag{3}$$

$$2t = \int_0^{H_s} \frac{E_s}{2(1+\nu_s)}\varphi(z)^2\, dz \tag{4}$$

where H_s, E_s and ν_s are depth, elasticity modulus and Poisson's ratio of the subsoil respectively.

If shear deformation parameter of subsoil, *2t*, is taken as equal to zero, Eq.(1) returns to dynamic governing equation for plate on Winkler type elastic foundation. Although it is the most preferred and very easy to apply, Winkler model ignores interaction and shear deformation within the subsoil assuming subsoil under the plate to be independent, closely spaced, discrete and linearly elastic springs. In reality, soil is a continuous medium and this assumption is seen as a deficiency of the model. For elimination of the deficiency in the Winkler model, researchers have endeavored developing a new two-parameter foundation models such as Pasternak Model, Hetenyi Model and Vlasov model. But they failed to establish any relationship between the soil parameters and soil types. Vallabhan et al. [26] have focused on this problem and have introduced a new third parameter, γ, as a function of the vertical deformation profile within the subsoil to use for the calculation of soil parameters. The necessity to determine the values of soil parameters, *k* and 2*t*, arbitrarily is eliminated by computing these values as a function of a new third parameter, γ, using an iterative procedure in their model called the modified Vlasov model.

The mode shape function, $\varphi(z)$, in Eq.3-4 describes the relationship between vertical displacement throughout subsoil and surface vertical displacement of plate. Mode shape function depends on the subsoil surface vertical deformation parameter, γ, and may be given as below, Fig.1.

$$\varphi(z)=\frac{sinh\ \gamma\left(1-\dfrac{z}{H_s}\right)}{sinh\ \gamma} \tag{5}$$

where γ is calculated using the equation shown below.

$$\left(\frac{\gamma}{H_s}\right)^2=\frac{(1-2\nu_s)}{2(1-\nu_s)}\frac{\int_{-\infty}^{+\infty}\int_{-\infty}^{+\infty}(\nabla w)^2\,dxdy}{\int_{-\infty}^{+\infty}\int_{-\infty}^{+\infty}w^2dxdy} \tag{6}$$

As can be seen in Eq.(5) above, displacements of the plate must be known to calculate the γ parameter. For this, the analysis of the soil-structure system must be performed. But it is necessary to know the values of soil parameters, k and $2t$ before the analysis, and soil parameters vary depending on mode shape function, $\varphi(z)$. At the same time, mode shape function is dependent on the vertical deformation parameter, γ. Therefore, the solution of this complex soil-structure interaction problem must be performed using an iterative technique.

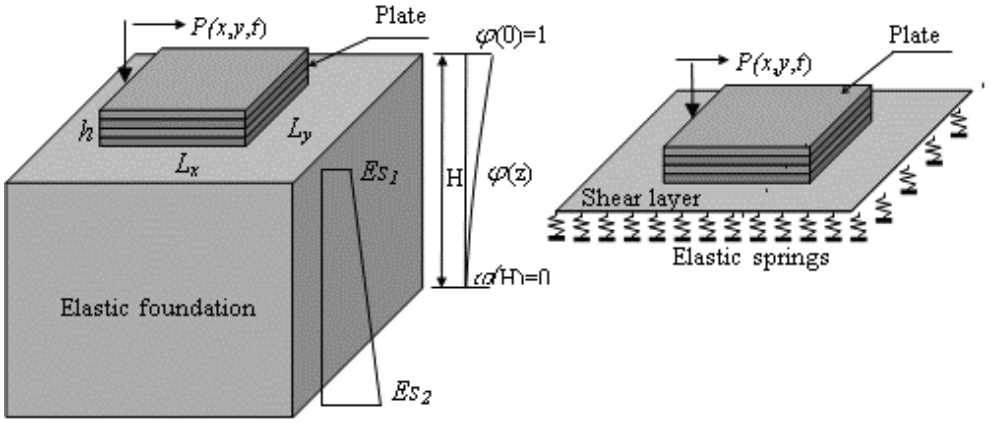

a) 3D plate on elastic subsoil *b) Mathematical model*

Fig.1 A plate on three parameter elastic foundation

For the analysis of mathematical model shown in Fig.1(b), finite element model of the laminated orthotropic plate on elastic foundation is developed initially by the use of SAP2000 software. Plate is defined as an area element and the shear layer is defined as a shell-layered/nonlinear element with unit thickness. Elastic area springs are then assigned at the

bottom of the shell-layered/nonlinear element. After the finite element model is completed in SAP2000, a computing tool developed in MATLAB is used to allow two-way data flow with SAP2000 simultaneously. Soil parameters calculated in MATLAB are supplied as input data to SAP2000 via OAPI functions. Subsequently the structure-soil system is analyzed and the surface displacements of the foundation are sent to MATLAB code. Soil parameters are re-calculated. The process is repeated until the difference between the new value of γ_{i+1} and the previously calculated γ_i attains a prescribed tolerance. The flow chart for the solution is given in Fig.2.

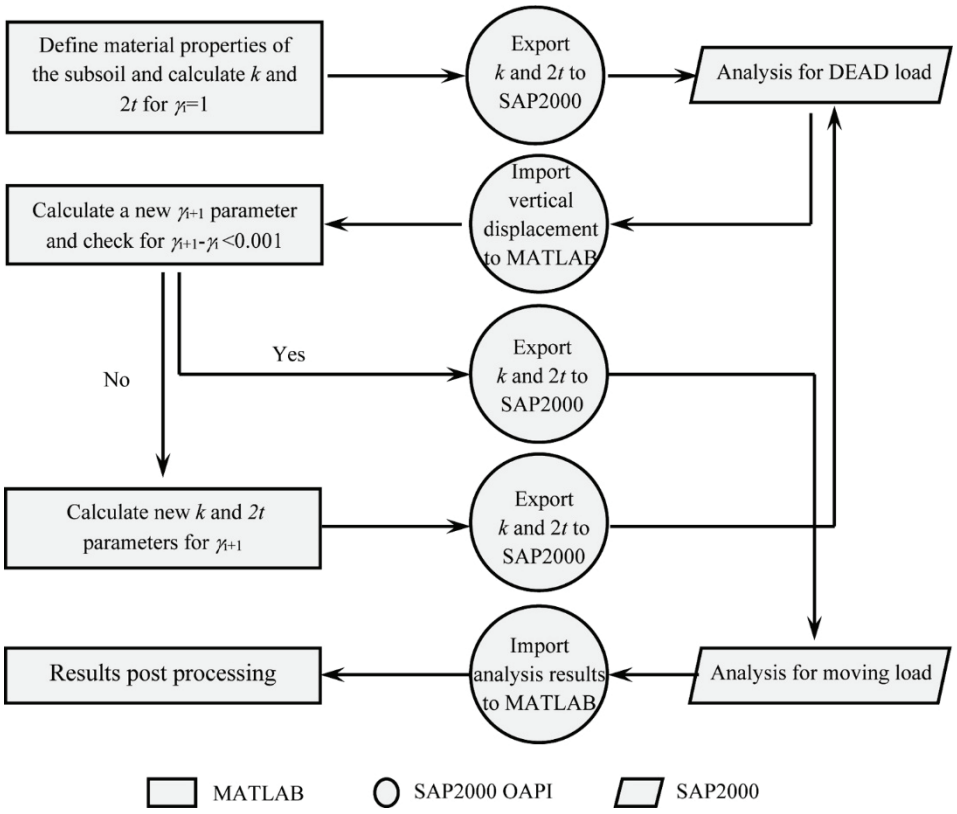

Fig.2 Flowchart for analysis of plates on elastic foundation by OAPI

4. NUMERICAL VERIFICATION

An orthotropic laminated beam with different boundary conditions solved by Kahya [27], Shi and Lam [28], Aydogdu [29] and Jun et al. [30] was selected to validate the presented consistent model, and non-dimensional fundamental frequencies were compared. Properties of the material used in the analysis are as follows:

E_1=144.8×10^6 kN/m^2, E_2=9.65×10^6 kN/m^2

G_{12}= 4.14×10^6 kN/m^2, ν_{12}=0.30, ρ=1389.23 kg/m^3

Comparison of non-dimensional fundamental frequencies of laminated orthotropic beams for different boundary conditions are made in Table 1. Ratio of beam span to beam thickness (L/h) was taken as 15 and non-dimensional frequency parameter was calculated with the equation $\widehat{\omega}_1 = \omega_1(L^2/h)\sqrt{\rho/E_1}$. Based on the results obtained, it can be concluded that four different solutions are in good agreement with each other and the presented model provides results with sufficient accuracy.

Table 1. Nondimensional fundamental frequencies ($\widehat{\omega}_1$) for various laminated beams

Beam	*Ref.*	Boundary conditions			
		SS	CC	CS	CF
[0/90]	Kahya [27]	2.4850	4.6011	3.5241	0.9218
	Shi and Lam [28][a]	2.4979	4.6194	3.5264	0.9199
	Aydogdu [29][b,c]	2.5015[b]	4.6531	3.5474	0.9251
		2.5036[c]	4.6685	3.5543	0.9255
	Present study	2.5010	4.5772	3.5179	0.9232
[0/90/0/90]	Kahya [27]	1.8329	3.6017	2.6784	0.6707
	Shi and Lam [28]	1.9619	3.6994	–	–
	Jun et al. [30][d]	1.9658	3.7086	2.7607	0.6746
	Present study	1.9683	3.7058	2.7619	0.6751

[a] FEM based on higher-order beam theory
[b] Ritz method based on parabolic shear deformation beam theory
[c] Ritz method based on exponential shear deformation beam theory
[d] Dynamic FEM based on first-order beam theory

5. LAMINATED ORTHOTROPIC PLATES ON THREE PARAMETER ELASTIC FOUNDATION

A parametric study was performed on a square laminated orthotropic plate resting on modified Vlasov type elastic foundation subjected to a moving concentrated load with a magnitude of 500 kN. When the load is acting on the plate, the plate makes a forced vibration motion and the motion returns to free vibration when the load leaves the plate. Dimensions of the plate are 1000 mm × 1000 mm. Thickness is taken as 150 mm. Elasticity modulus of subsoil (E_{s1}= E_{s2}) is 68950 kN/m^2, Poisson's ratio of the subsoil (ν_s) is 0.25 and subsoil depth (H_s) under the plate is taken as 10 m. The plate is considered to have four layers having the same thickness. The laminates are arranged by the following material properties:

E_1=172.5×10^6 kN/m^2, E_2=6.9×10^6 kN/m^2, G_{12}= 3.45×10^6 kN/m^2, ν_{12}=0.25, ρ=1578 kg/m^3

Effects of lamination schemes

Firstly, effects of lamination scheme on the behavior of plates on elastic foundations are investigated using material and geometrical properties given above. Four different lamination schemes are examined such as $[0/90]_s$, $[0/90/0/90]_s$, $[90/0]_s$, and $[45/-45]_s$. Soil parameters

evaluated for centrally concentrated static load are presented in Table 2. Moving load analysis was performed using these soil parameters. Furthermore, frequencies of the plate for each lamination scheme were calculated.

Table 2 Soil parameters for various lamination schemes

Lamination schemes	γ	k (kN/m^3)	$2t$ (kN/m)
$[0/45]_s$	4.50610	18687.24	30543.18
$[0/90]_s$	4.37260	18145.62	31459.46
[0/90/0/90]	4.00798	16679.80	34246.83
[0/45/0/45]	3.86610	16116.65	35458.20

Different soil parameters were obtained for various lamination schemes. This is to be expected because the vertical displacement of plate changes depending on the lamination schemes. While subgrade reaction modulus decreases from $[0/45]_s$ lamination scheme to [0/45/0/45] lamination scheme, shear deformation parameter increases in the same order.

The first six frequencies of plate on elastic foundation are evaluated for each lamination schemes and presented in Table 3 and Fig.3 by using soil parameters obtained above.

Table 3 First six frequencies for various lamination schemes

Lamination schemes	Frequencies (Hertz)					
	f_1	f_2	f_3	f_4	f_5	f_6
$[0/45]_s$	16.69	18.94	19.61	21.72	22.44	24.85
$[0/90]_s$	16.52	18.90	19.46	21.66	22.77	24.71
[0/90/0/90]	16.05	18.92	18.92	21.59	23.85	23.93
[0/45/0/45]	15.88	18.56	18.99	21.53	22.94	24.30

It can be seen from the table and the accompanying figure that the natural frequency increases as the mode number increases. The first and fourth frequencies decrease from $[0/45]_s$ lamination scheme to [0/45/0/45] lamination scheme. The same trend in the second and third frequency is observed. However irregular ups and downs are seen in the fifth and sixth frequencies.

Mode shapes of the plate on elastic foundation were also obtained for all lamination schemes. But since the presentation of all mode shapes would take up excessive space, only mode shapes corresponding to six lowest frequency for $[0/90]_s$ are presented in Fig. 4.

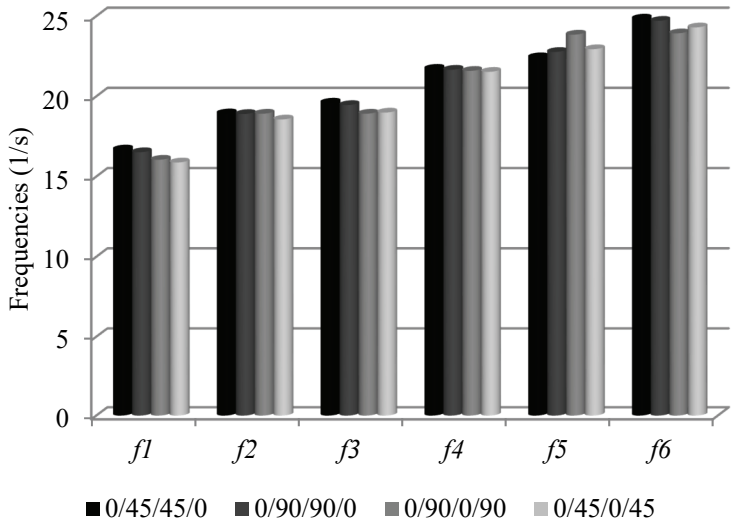

Fig.3 Comparison of first six frequencies for various lamination schemes

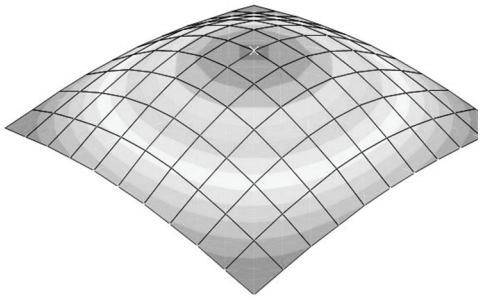

a) Mode 1

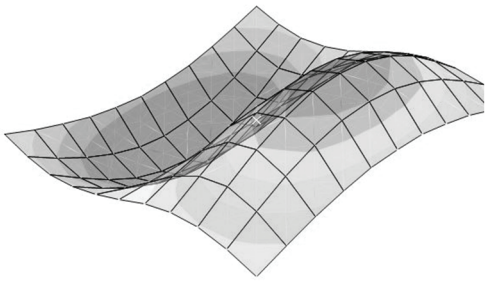

b) Mode 2

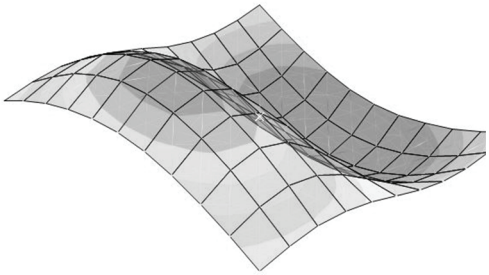

c) Mode 3

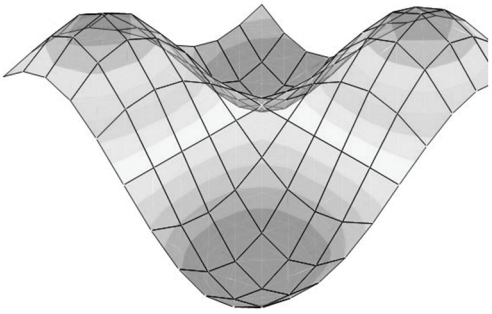

d) Mode 4

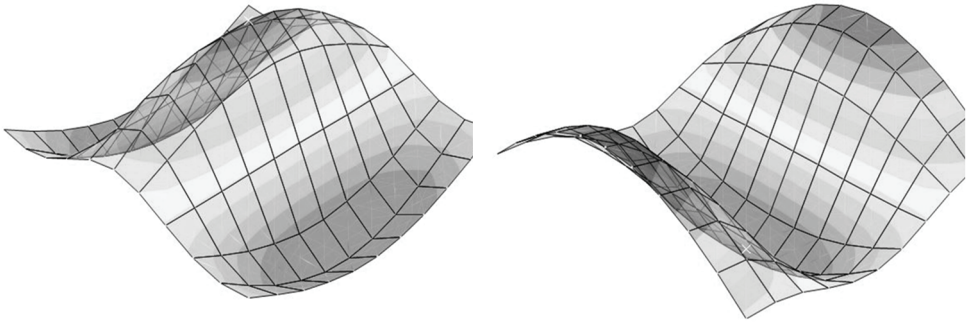

e) Mode 5 f) Mode 6

Fig. 4 First six mode shapes for $[0/90]_s$ laminated orthotropic plate on elastic foundation

Effects of moving load on the behavior of laminated orthotropic plate regarding lamination schemes were investigated considering soil-structure interaction. For the analysis, non-dimensional velocity (α) defined as the ratio of velocity to critical velocity ($\alpha=c/c_{cr}$) was used. The critical velocity is calculated depending on the first frequency of plate with the formulation of $c_{cr}=2\times f_1\times L$. Here, the average of the first frequencies corresponding to each lamination schemes has been used as f_1 which has been taken as nearly 16.5. $\alpha=0$ indicates the state where the plate is subjected to a centrally concentrated load. Midpoint displacements obtained from the analysis are presented in Table 4 and Fig.5.

As seen from Table 4 and Fig.5, as the velocity of moving load increases, the midpoint displacement increases until the velocity reaches the value of $\alpha=0.6$, after which it decreases again. The effects of lamination schemes on the displacement of plate are seen more clearly as the load velocity increases. Midpoint displacements decrease from $[0/45]_s$ lamination to [0/90/0/90] lamination for each velocity of moving load. It has also been said that the effects of the lamination scheme are more effective for the moving load as compared with the static centrally concentrated load.

Effects of lamination angles (0/θ/θ/0)

Here, the influence of lamination angles on the behavior of the plate was investigated. For this purpose, a four-layer plate was considered. Each layer has equal thickness. Angles of top and bottom layer are kept at 0^o and middle layers are changed as 0^o, 30^o, 45^o, 60^o and 90^o. Soil parameters obtained for various lamination angles are given in Table 5.

As middle lamination angle (θ) increases, modulus of subgrade reaction decreases and shear deformation parameter increases.

The first six frequencies of plate on elastic foundation are presented in Fig.6 using these soil parameters. As seen from the figure, the first four frequencies of the plate tend to decrease as lamination angle (θ) increases. Furthermore, effects of lamination angles on the frequencies of plate decrease for the frequencies corresponding to large modes.

Table 4 Midpoint vertical displacement of plate for various lamination schemes

Lamination schemes	w (mm)					
	α=0.0	α=0.2	α=0.4	α=0.6	α=0.8	α=1.0
$[0/45]_s$	2.59	3.04	4.02	4.76	4.38	3.43
$[0/90]_s$	2.48	2.80	3.93	4.46	4.12	3.16
[0/45/0/45]	2.47	2.59	3.91	4.46	3.77	2.93
[0/90/0/90]	2.34	2.53	3.86	4.03	3.49	2.57

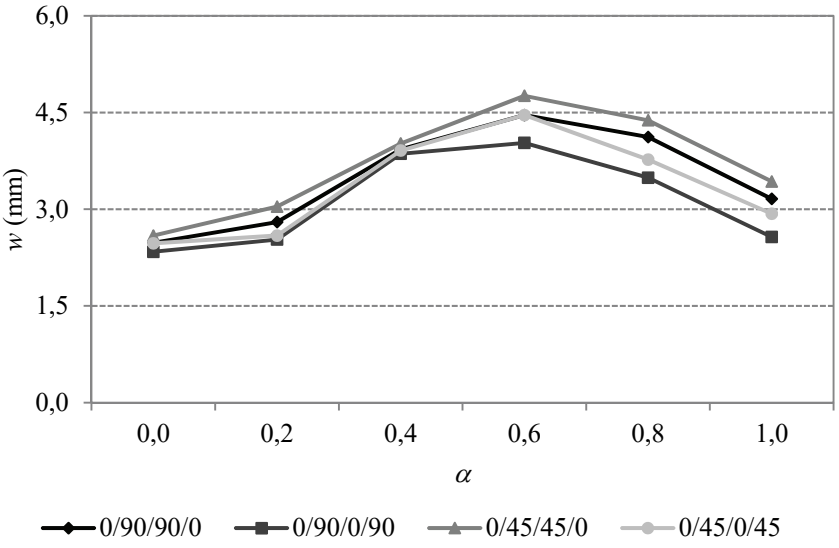

Fig.5 Comparison of midpoint displacement of plate for various lamination schemes

Table 5 Soil parameters for various lamination angles (0/θ/θ/0)

Lamination schemes	γ	k (kN/m^3)	$2t$ (kN/m)
$[0/0]_s$	5.09986	21115.69	27021.45
$[0/30]_s$	4.74592	19664.96	29019.29
$[0/45]_s$	4.50610	18687.24	30543.18
$[0/60]_s$	4.34213	18022.29	31675.97
$[0/90]_s$	4.37226	18145.62	31459.46

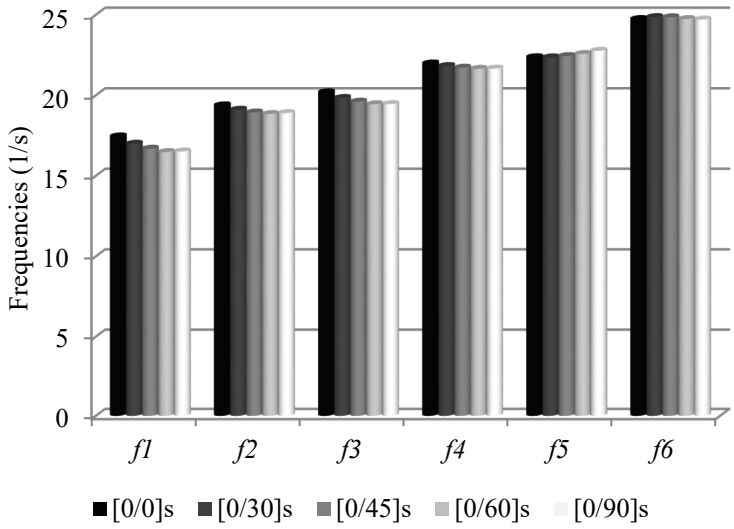

Fig.6 Comparison of first six frequencies for various lamination angles

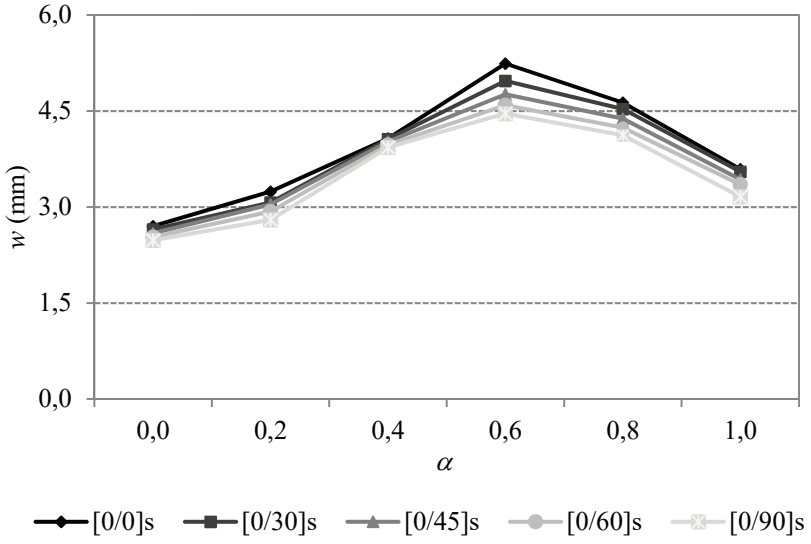

Fig.7 Comparison of midpoint displacement of plate for various lamination angles

Midpoint displacement of the plate for various lamination angles is plotted in Fig.7. The smallest vertical displacement is obtained for $[0/90]_s$ in comparison to other lamination

schemes. The displacement increases with decreasing middle lamination angle (θ) for all non-dimensional velocities of moving load. The largest value of midpoint displacement is obtained for α=0.6 as before. The lamination angles effect on the displacement for α=0.6 is much higher than that of other non-dimensional velocities. Further, displacement order for various lamination angles considered is as follows $[0/0]_s$ > $[0/30]_s$ > $[0/45]_s$ > $[0/60]_s$ > $[0/90]_s$.

Effects of layer number

Here, keeping the plate thickness constant, the plate is considered as 3-layered, 4-layered, 5-layered and 6-layered to demonstrate the effects of number of layers on the behavior of the plate. Table 6 shows that modulus of subgrade reaction decreases with increasing number of layers. But, shear deformation parameter increases as the number of layer increases.

Table 6 Soil parameters for various layer numbers

Lamination schemes	γ	k (kN/m^3)	$2t$ (kN/m)
[0/90/0]	4.75291	19693.56	28977.04
$[0/90]_s$	4.37226	18145.62	31459.46
[0/90/0/90/0]	4.19780	17440.05	32740.72
$[0/90/0]_s$	4.12921	17164.52	33270.57

Fig. 8 displays the variation of first six frequencies with the numbers of layers of the plate. Frequencies decrease from 3-layered plate to 6-layered plate except for fifth frequencies.

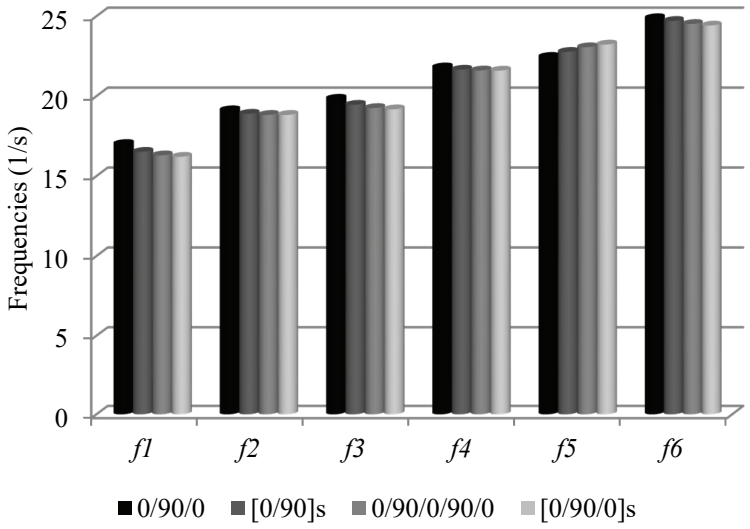

Fig.8 Comparison of first six frequencies for various layer numbers

Midpoint displacements(w) of the plate for various layer numbers are plotted in Fig.9. It is also seen that the central displacement increases up to α=0.6 and decreases for the larger values of α. It is also observed that the curves approach each other as the number of layers increases. So, it can be said that an increase in the number of layers does not cause any significant change on the results beyond a certain value.

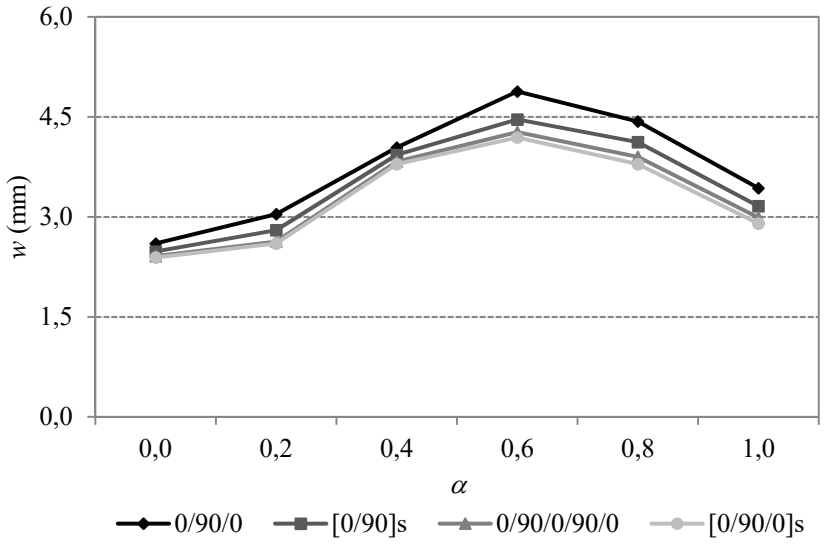

Fig.9 Comparison of midpoint displacement of plate for various lamination numbers

Effects of subsoil depth

The plate on elastic foundation with $[0/90]_s$ lamination is chosen to indicate the effects of subsoil depth on the responses. Analyses were performed for five different subsoil depths of 2, 4, 6, 8 and 10 m. Soil parameters under a central concentrated load are tabulated in Table 7. As the subsoil depth increases, subgrade reaction modulus decreases while shear deformation modulus increases because deeper rigid base makes soil stratum more flexible.

Table 7 Soil parameters for various subsoil depth

Subsoil Depth (m)	γ	k (kN/m^3)	$2t$ (kN/m)
2	1.16488	42700.44	15605.36
4	1.94472	24289.08	24844.61
6	2.70872	19749.34	29336.09
8	3.25181	18468.33	30993.67
10	4.37226	18145.62	31459.46

Frequencies of the plate on elastic foundation are plotted in Fig.10. As seen from the figure, frequencies of the plate decrease when soil stratum is more flexible. But changes in the frequencies decrease with increasing subsoil depth. This means that subsoil depth does not affect the frequencies considerably after a certain value of subsoil depth.

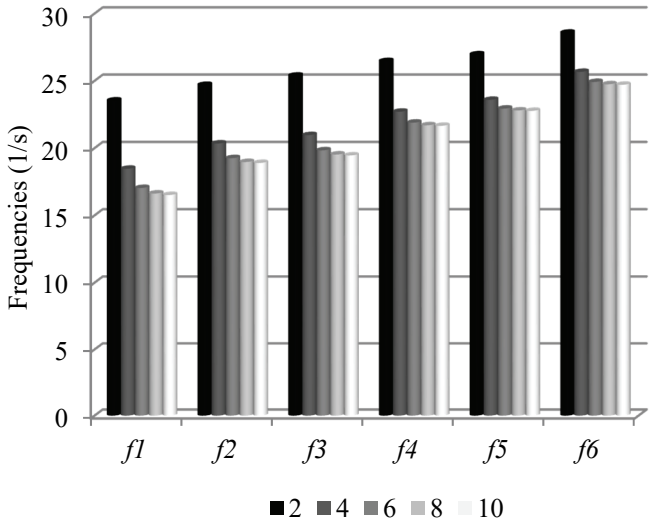

Fig.10 Comparison of first six frequencies for various subsoil depth

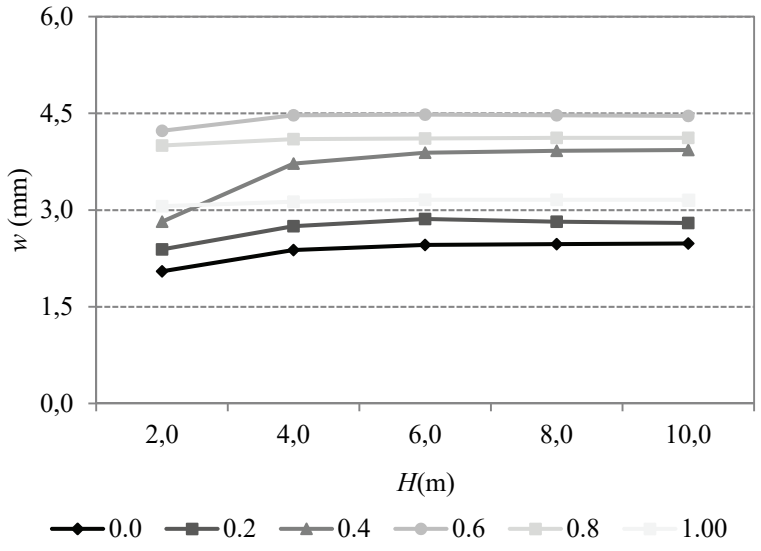

Fig.11 Comparison of central displacement of plate for various subsoil depth

It is observed that the central displacement is maximum for H =10 m, and minimum for H=2 m. That is because, as the depth of the soil stratum decreases, the central displacement decreases as well. The displacement increases with the decreasing modulus of subgrade reaction and increasing shear deformation parameter. All these findings suggest that the effects of soil parameters on the displacement are quite significant but the same cannot be claimed for the soil depth. Studying Fig.11, it is easy to see that the effect of subsoil depth on the plate displacement vanishes as the soil gets deeper. This means that subsoil depth does not affect the results considerably after a certain value; namely 6 m for α=0.0, 0.2 and 0.4, 4 m for α=0.6 and, 2 m for α=0.8 and 1.0.

Effects of subsoil elasticity modulus

Various values of subsoil modulus of elasticity at the bottom have been considered to display the effects of changes of subsoil elasticity modulus through the depth on the behavior of plate for $[0/90]_s$ lamination schemes. Subsoil elasticity modulus at the bottom, E_{s2}, was changed for the ratios of E_{s2}/E_{s1}=1, 2, 3 and 4, keeping subsoil elasticity modulus at the top constant at E_{s1}=68950 kN/m^2. Table 8 demonstrates soil parameters for various ratio of E_{s2}/E_{s1}. Table 8 shows that the subgrade reaction modulus increases while shear deformation parameter decreases as the ratio of E_{s2}/E_{s1} increases that is, as the subsoil becomes stiffer.

Table 8 Soil parameters for various ratio of bottom to top elasticity modulus of subsoil

E_{s2}/E_{s1}	γ	k (kN/m^3)	$2t$ (kN/m)
1	4.37226	18145.62	31459.46
2	4.52411	20848.92	33759.70
3	4.65731	23472.46	35872.88
4	4.77701	26037.75	37838.20

Comparison of the first six frequencies for various ratios of E_{s2}/E_{s1} is presented in Fig.12. It is seen that all frequencies increase with the increasing ratio of E_{s2}/E_{s1} and the increases are quite similar for the frequencies corresponding to the first six modes.

Comparison of the midpoint displacement of plate for various ratios of Es_2/Es_1 is given in Fig.13. Results show that the central displacements of the plate decrease as the subsoil elasticity modulus at the bottom increases. As the foundation becomes stiffer by increasing the subsoil elasticity modulus at the bottom, the midpoint displacement of the plate continues to drop. But the effects of subsoil elasticity modulus on the displacement of the plate loses its importance for a large velocity moving load, especially for α=0.8.

Effects of plate thickness

Herein, effects of the plate thickness on the behavior of plate are investigated. For this purpose, the various thickness to length ratio is used taking h/L=0.015, 0.030, 0.045 and 0.060 keeping the span of plate constant at 10 m. The plate has 4 layers of equal thickness and its lamination scheme is $[0/90]_s$. It is seen from Table 9 that subgrade reaction modulus decreases while shear deformation modulus increases as h/L ratio increases.

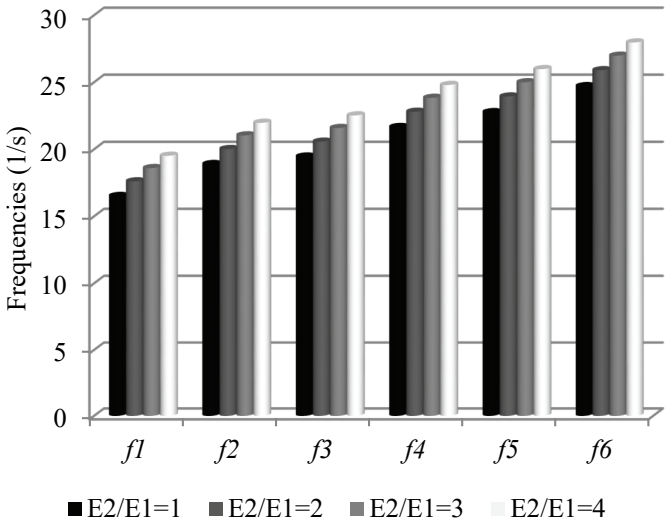

Fig.12 Comparison of first six frequencies for various ratio of bottom to top elasticity modulus of subsoil

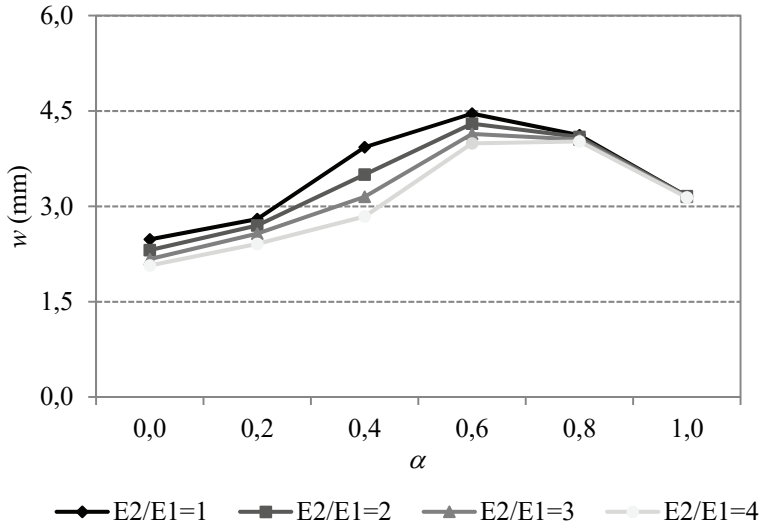

Fig.13 Comparison of midpoint displacement of plate for various ratio of E_2/E_1

Table 9 Soil parameters for various plate thicknesses

h/*L*	γ	*k* (kN/m^3)	2*t* (kN/m)
0.015	4.37226	18145.62	31459.46
0.030	2.57224	11412.20	50985.25
0.045	1.96482	9760.53	61719.86
0.060	1.65983	9156.86	67841.71

Fig.14 demonstrates comparison of first six frequencies for various plate thicknesses. Frequencies decrease with increasing plate thickness. But the drops in the frequencies for large values of plate thickness are less.

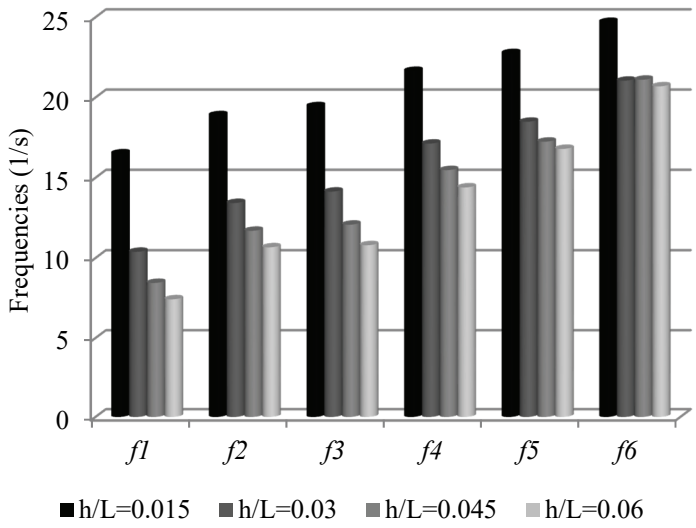

Fig.14 Comparison of first six frequencies for various plate thicknesses

As seen from Fig.15, displacements decrease with increasing plate thickness. This is because bending rigidity of the plate increases as the plate thickness increases hence, the decrease in vertical displacement of the plate. It can also be observed that for large values of the ratio *h*/*L*, the midpoint displacement does not vary significantly. Furthermore, the effect of plate thickness on the displacement of plate is lost after a certain value of plate thickness.

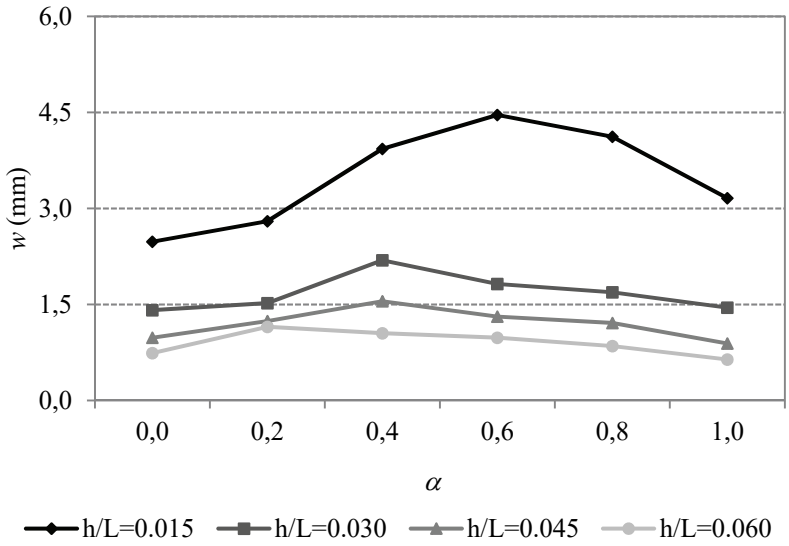

Fig.15 Comparison of midpoint displacement of plate for various plate thicknesses

The variation of midpoint displacement with non-dimensional time for 0/90/90/0 symmetric laminated plate and various velocities of moving load and for various laminated plates and α=0.6 values are shown at Fig.16a and Fig.16b.

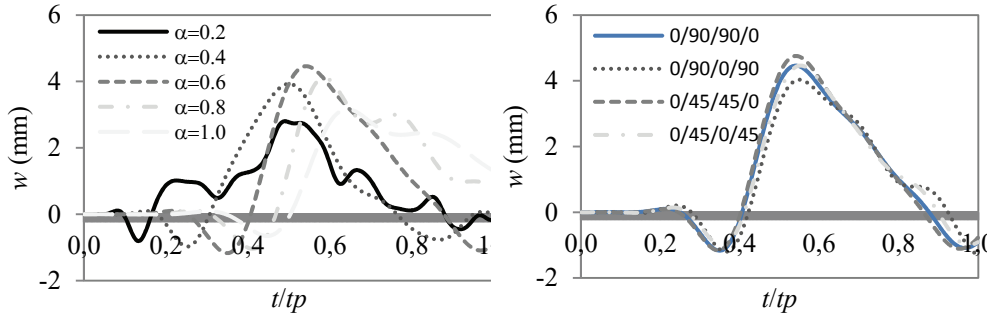

a) b)

Fig.16 Variation of midpoint displacement with non-dimensional time

6. CONCLUSIONS

In this study, the behavior of laminated orthotropic plates on an elastic foundation subjected to moving load was studied using the modified Vlasov model. For this purpose, a computer

tool was developed to make two-way data exchange between SAP2000 and MATLAB using OAPI functions. First the accuracy of the proposed model was verified and the effects of the lamination scheme, various lamination angles, lamination number, subsoil depth, elasticity modulus of subsoil, plate thickness and velocity of moving load on the behavior of laminated orthotropic plates on elastic foundation were discussed. The conclusions drawn from the study are summarized below.

- The results from the solution procedure presented in the study show good agreement with those of the numerical analyses in the literature. The solution procedure may be effectively used for the analysis of laminated composite plates on elastic foundations. The main advantage of the solution procedure developed is that it is a powerful tool to handle and solve various situations with various boundary conditions, orientation angles, lamination schemes and load types.
- Plate thickness, subsoil depth and elasticity modulus have important influence on the behavior of the plate.
- Midpoint displacement of the plate for all lamination schemes increases as the velocity of moving load increases up to a certain value. The displacements decrease with increasing velocity of the moving load.
- The effects of lamination schemes on the displacement of plate are seen more clearly as the load velocity increases.
- The effect of the layer number on the results decreases as the number of layers increases.
- Subsoil depth does not affect the results considerably after a certain value.
- The effect of subsoil elasticity modulus on the results loses its importance for large velocities of moving load.
- The effect of the plate thickness on the results decreases as the thickness of plate increases.

References

[1] Kim, S.M., Roesset, J.M., Moving loads on a plate on elastic foundation. Journal of Engineering Mechanics-Asce. 124(9), 1010-1017, 1998.

[2] Huang, M.H., Thambiratnam, D.P., Dynamic response of plates on elastic foundation to moving loads. Journal of Engineering Mechanics. 128(9, 1016-1022, 2002.

[3] Kim, S.M., Buckling and vibration of a plate on elastic foundation subjected to in-plane compression and moving loads. International Journal of Solids and Structures. 41(20), 5647-5661, 2004.

[4] Lu, Z., Yao, H.L., Zhan, Y.X., Hu, Z., Vibrations of a plate on a two-parameter foundation subjected to moving rectangular loads of varying velocities. Journal of Vibroengineering. 16(3), 1543-1554, 2014.

[5] Wang, X.D., Numerical analysis of moving orthotropic thin plates. Computers & Structures. 70(4), 467-486, 1999.

[6] Zhu, X.Q., Law, S.S., Dynamic behavior of orthotropic rectangular plates under moving loads. Journal of Engineering Mechanics-Asce. 129(1), 79-87, 2003.

[7] Alisjahbana, S.W., Dynamic Response of Clamped Orthotropic Plates to Dynamic Moving Loads in 13th World Conference on Earthquake Engineering. Vancouver, B.C., Canada, 2004.

[8] Lee, S.Y., Yhim, S.S., Dynamic analysis of composite plates subjected to multi-moving loads based on a third order theory. International Journal of Solids and Structures. 41(16-17), 4457-4472, 2004.

[9] Law, S.S., Bu, J.Q., Zhu, X.Q., Chan, S.L., Moving load identification on a simply supported orthotropic plate. International Journal of Mechanical Sciences. 49(11), 1262-1275, 2007.

[10] Hatami, S., Azhari, M., Saadatpour M.M., Free vibration of moving laminated composite plates. Composite Structures. 80(4), 609-620, 2007.

[11] Ghafoori, E., Asghari, M., Dynamic analysis of laminated composite plates traversed by a moving mass based on a first-order theory. Composite Structures. 92(8), 1865-1876, 2010.

[12] Malekzadeh, P., Fiouz A.R., Razi, H., Three-dimensional dynamic analysis of laminated composite plates subjected to moving load. Composite Structures. 90(2), 105-114, 2009.

[13] Thai, C.H., Nguyen-Xuan, H., Nguyen-Thanh, N., Le, T.H., Nguyen-Thoi, T., Rabczuk T., Static, free vibration, and buckling analysis of laminated composite Reissner-Mindlin plates using NURBS-based isogeometric approach. International Journal for Numerical Methods in Engineering. 91(6), 571-603, 2012.

[14] Chen, C.S., Tsai, T.C., Chen, W.R., Wei, C.L., Dynamic stability analysis of laminated composite plates in thermal environments. Steel and Composite Structures. 15(1), 57-79, 2013.

[15] Patel, S.N., Nonlinear bending analysis of laminated composite stiffened plates. Steel and Composite Structures. 17(6), 867-890, 2014.

[16] Ozcelikors, Y., Omurtag, M.H., Demir, H., Analysis of orthotropic plate-foundation interaction by mixed finite element formulation using Gateaux differential. Computers & Structures. 62(1), 93-106, 1997.

[17] Pradhan, S.C., Kumar, A., Vibration analysis of orthotropic graphene sheets embedded in Pasternak elastic medium using nonlocal elasticity theory and differential quadrature method. Computational Materials Science. 50(1), 239-245, 2010.

[18] Akgoz, B., Civalek, O., Nonlinear vibration analysis of laminated plates resting on nonlinear two-parameters elastic foundations. Steel and Composite Structures. 11(5), 403-421, 2011.

[19] Vosoughi, A.R., Malekzadeh, P., Razi, H., Response of moderately thick laminated composite plates on elastic foundation subjected to moving load. Composite Structures. 97, 286-295, 2013.

[20] Afsharmanesh, B., Ghaheri, A., Taheri-Behrooz, T., Buckling and vibration of laminated composite circular plate on winkler-type foundation. Steel and Composite Structures. 17(1), 1-19, 2014.

[21] Mantari, J.L., Granados, E.V., Hinostroza, M.A., Soares, C.G., Modelling advanced composite plates resting on elastic foundation by using a quasi-3D hybrid type HSDT. Composite Structures. 118, 455-471, 2014.

[22] Alipour, M.M., An analytical approach for bending and stress analysis of cross/angle-ply laminated composite plates under arbitrary non-uniform loads and elastic foundations. Archives of Civil and Mechanical Engineering. 16(2), 193-210, 2016.

[23] SAP2000, Integrated Finite Elements Analysis and Design of Structures. Computers and Structures. p. Inc, Berkeley, CA, 2008.

[24] MATLAB, The language of technical computing. The Mathworks. p. Natick, MA, 2009.

[25] Humar. J.L., Dynamic of Structures, Englewood Cliffs, NJ, Prentice-Hall, 1990.

[26] Vallabhan, C.V.G., Straughan, W.T., Das, Y.C., Refined Model for Analysis of Plates on Elastic Foundations. Journal of Engineering Mechanics-Asce. 117(12), 2830-2844, 1991.

[27] Kahya, V., Dynamic analysis of laminated composite beams under moving loads using finite element method. Nuclear Engineering and Design. 243, 41-48, 2012.

[28] Shi, G., Lam, K.Y., Finite element vibration analysis of composite beams based on higher-order beam theory. Journal of Sound and Vibration. 219(4), 707-721, 1999.

[29] Aydogdu, M., Vibration analysis of cross-ply laminated beams with general boundary conditions by Ritz method. International Journal of Mechanical Sciences. 47(11), 1740-1755, 2005.

[30] Jun, L.H., H.; Rongying, S., Dynamic finite element method for generally laminated composite beams. International Journal of Mechanical Sciences. 50, 466-480, 2008.

TEKNİK DERGİ MANUSCRIPT DRAFTING RULES

1. The whole manuscript (text, charts, equations, drawings etc.) should be arranged in Word and submitted in ready to print format. The article should be typed on A4 (210 x 297 mm) size paper using 10 pt (main title 15 pt) Times New Roman font, single spacing. Margins should be 40 mm on the left and right sides and 52.5 mm at the top and bottom of the page.
2. Including drawings and tables, articles should not exceed 25 pages, technical notes 6 pages.
3. The manuscript, along with a hardcopy, must be electronically sent (CD or e-mail attachment).
4. The text must be written in a clear and understandable language, conform to the grammar rules. Third singular person and passive tense must be used, and no inverted sentences should be contained.
5. Title must be short (10 words maximum) and clear, and reflect the content of the paper.
6. Sections should be arranged as: (i) abstract and keywords, (ii) title, abstract and keywords in the other language, (iii) main text, (iv) symbols, (v) acknowledgements (if required) and (vi) references.
7. Both abstracts should briefly describe the object, scope, method and conclusions of the work and should not exceed 100 words. If necessary, abstracts may be re-written without consulting the author. At least three keywords must be given. Titles, abstracts and keywords must be fitted in the first page leaving ten line space at the bottom of the first page and the main text must start in the second page.
8. Section and sub-section titles must be numbered complying with the standard TS1212.
9. Symbols must conform to the international rules; each symbol must be defined where it appears first, additionally, a list of symbols must be given in alphabetic order (first Latin, then Greek alphabets) at the end of the text (before References).
10. Equations must be numbered and these numbers must be shown in brackets at the end of the line.
11. Tables, drawings and photographs must be placed inside the text, each one should have a number and title and titles should be written above the tables and below the drawings and photographs.
12. Only SI units must be used in the manuscripts.
13. Quotes must be given in inverted commas and the source must be indicated with a reference number.
14. Acknowledgement must be short and mention the people/ institutions contributed or assisted the study.
15. References must be numbered (in brackets) in the text referring to the reference list arranged in the order of appearance in the text. References must include the following information:

    If the reference is an article: Author's surname, his/her initials, other authors, full title of the article, name of the journal, volume, issue, starting and ending pages, year of publication.

    Example : Naghdi, P. M., Kalnins, A., On Vibrations of Elastic Spherical Shells. J. Appl. Mech., 29, 65-72, 1962.

    If the reference is a book: Author's surname, his/her initials, other authors, title of the book, volume number, editor if available, place of publication, year of publication.

    Example : Kraus. H., Thin Elastic Shells, New York. Wiley, 1967.

    If the reference is a conference paper: Author's surname, his/her initials, other authors, title of the paper, title of the conference, location and year.

    If the source is a thesis: Author's surname, his/her initials, thesis title, level, university, year.

    If the source is a report: Author's surname, his/her initials, other authors, title of the report, type, number, institution it is submitted to, publication place, year.
16. Discussions to an article published in Teknik Dergi should not exceed two pages, must briefly express the addressed points, must criticize the content, not the author and must be written in a polite language. Authors' closing remarks must also follow the above rules.
17. A separate note should accompany the manuscript. The note should include, (i) authors' names, business and home addresses and phone numbers, (ii) brief resumes of the authors and (iii) a statement "I declare in honesty that this article is the product of a genuinely original study and that a similar version of the article has not been previously published anywhere else" signed by all authors.

CONTENTS

Comparison of Blast Analysis Methods for Modular Steel Structures 8253
Bülent ERKMEN

An Efficient Contact Tank Design for Potable Water Treatment 8279
Ender DEMİREL, Mustafa M. ARAL

Classification of Construction Accidents in Northern Cyprus 8295
Kemal D. TÖZER, Tahir ÇELİK, G. Emre GÜRCANLI

Modeling Laminated Orthotropic Plate-Foundation Interaction Subjected to Moving Load Using Vlasov Model 8317
Korhan ÖZGAN

ISSN: 1300-3453